



Title	PREPARATIONS AND PROPERTIES OF INTERCALATION COMPOUNDS DERIVED FROM FeOCl AND Mg(OH) <sub>2</sub>
Author(s)	Kikkawa, Shinichi
Citation	大阪大学, 1979, 博士論文
Version Type	VoR
URL	<a href="https://hdl.handle.net/11094/24580">https://hdl.handle.net/11094/24580</a>
rights	
Note	

*The University of Osaka Institutional Knowledge Archive : OUKA*

<https://ir.library.osaka-u.ac.jp/>

The University of Osaka

PREPARATIONS AND PROPERTIES OF INTERCALATION  
COMPOUNDS DERIVED FROM  $\text{FeOCl}$  AND  $\text{Mg}(\text{OH})_2$

Shinichi Kikkawa

80SC00376

## CONTENTS

CHAPTER 1.	GENERAL INTRODUCTION .....	1
CHAPTER 2.	KINETIC STUDY ON THE INTERCALATION IN A SYSTEM OF FeOCl AND PYRIDINE .....	14
	2 - 1. Introduction .....	15
	2 - 2. Experimental Section .....	18
	2 - 3. Results .....	20
	2 - 4. Discussion .....	29
CHAPTER 3.	PREPARATIONS AND PROPERTIES OF CHARGE TRANSFER TYPE INTERCALATION COMPOUNDS ----- FeOCl(organic compound) <sub>1/n</sub> .....	40
	3 - 1. Introduction .....	41
	3 - 2. Organic Intercalations on MOCl (M = Ti, V, Cr, Fe, and In) .....	43
	3 - 3. Intercalation Compounds FeOCl (pyridine derivative) <sub>1/n</sub> and FeOCl(n-propylamine) <sub>1/4</sub> .....	49
CHAPTER 4.	PREPARATIONS AND PROPERTIES OF GRAFT TYPE INTERCALATION COMPOUNDS ----- FeOOCH <sub>3</sub> and FeO(O <sub>2</sub> C <sub>2</sub> H <sub>4</sub> ) <sub>1/2</sub> .....	66
	4 - 1. Introduction .....	67
	4 - 2. Graft Type Intercalation Compound ----- FeOOCH <sub>3</sub> .....	69
	4 - 3. Graft Type Intercalation Compound ----- FeO(O <sub>2</sub> C <sub>2</sub> H <sub>4</sub> ) <sub>1/2</sub> .....	82

CHAPTER 5.	PREPARATIONS AND PROPERTIES OF ANION EXCHANGE TYPE INTERCALATION COMPOUNDS	
	----- $\text{Mg}_6\text{Al}_2(\text{OH})_{16}\text{CO}_3 \cdot n\text{H}_2\text{O}$ .....	97
5 - 1.	Introduction .....	98
5 - 2.	Crystal-chemical Properties of Mg,Al and Ni,Al Hydroxy-perchlorate and Hydroxy-carbonate .....	102
CHAPTER 6.	TOTAL DISCUSSION .....	123
ACKNOWLEDGEMENT	.....	140
REFERENCES	.....	141

CHAPTER 1.

GENERAL INTRODUCTION

Some kinds of layered inorganic compounds take up organic molecules, inorganic ions and so on in their interlayer space accompanying changes of their interlayer distances. This peculiar phenomenon is generally called as an intercalation, although an absorption of inorganic compounds is sometimes named as an intersalation. The study of materials with layer structures --- their interesting anisotropic behavior attracts ever increasing attention --- has made considerable progress in the past years. The most exciting development in this field of layered compounds during the last decade has been the study of intercalated solids (1,2).

One of the popular intercalations has been observed in clay minerals such as smectite and vermiculite (3,4). Montmorillonite belongs to smectite group and it is composed of units made up of two silica tetrahedral sheets with a central alumina octahedral sheet as shown in Fig.1. These units have negative charge because the aluminum is partly substituted with magnesium. Exchangeable cations, e.g.  $\text{Na}^+$ ,  $\text{K}^+$ ,  $\text{Ca}^{2+}$ , go into the interlayer region with some amounts of water molecules. These cations balance the remained charges in the host alumino-silicate layers and they link together these layers. Electrostatic force is the main interaction between the exchangeable cations and the host layers. These situations are represented as  $(x/n)\text{R}^{n+}(\text{Mg}_x\text{Al}_{2-x})(\text{Si}_4\text{O}_{10})(\text{OH})_2 \cdot m\text{H}_2\text{O}$  where  $\text{R}^{n+}$  is an exchangeable cation, and  $x$  is less than 0.33. The interlayer cations can be substituted with organic cations such as  $\text{CH}_3(\text{CH}_2)_n\text{NH}_3^+$ . This is

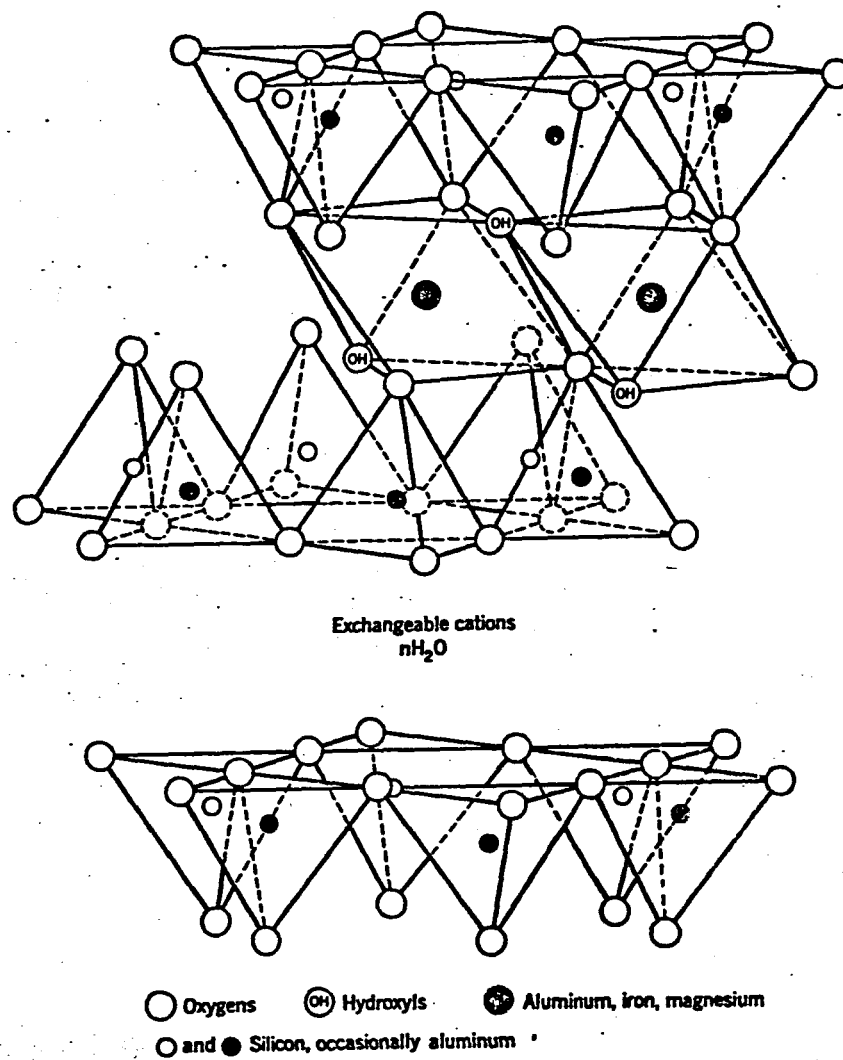


Fig.1. Diagrammatic sketch of the structure of smectite (3).

a kind of intercalation called as an ion-exchange type. The interlayer water molecules are kept between the alumino-silicate layers by the interaction between exchangeable cations and dipole moments of the water molecules. Hydrogen bond to the alumino-silicate layer also plays an important role to link water molecules to the host layers. Polar organic compounds, e.g. alcohol, can exchange these water molecules and expand the interlayer spacing of the host layers. These molecules easily come out from the interlayer region by heat-treatments because of their weak bondings to the host layer. This kind of intercalation is called as a sorption type.

In vermiculite, the substitution in its host layer occurs not only in the alumina octahedral position just as in the case of montmorillonite but also in the silica tetrahedral position. The composition of vermiculite is represented as  $\{(x+4y)/n\}R^{n+} - \{Mg_x(Al,Fe)_{3-x}\}(Si_{1-y}Al_y)_4O_{10}(OH)_2 \cdot mH_2O$  where  $R^{n+}$  is an exchangeable cation and the amount of the interlayer cation  $(x+4y)/n$  is between 0.22 and 0.36. Vermiculite also forms intercalation compounds both of sorption type and of ion-exchange one.

Organic intercalation in clay minerals has been extensively studied mainly in the fields of earth and soil sciences. Arrangements of absorbed species in interlayer region <sup>and</sup> interactions between intercalated organic molecules and the host silicate layer have been studied from the physico-chemical points of view (5,6). However intercalations on clay minerals are only of the



above mentioned sorption and cation exchanged types. There are another three types of intercalation compounds which have not yet been or which can not be prepared from clay minerals. One is a charge transfer type in which charge transfer interaction plays an important role to keep guest molecules in the interlayer region of host materials. Clay minerals have all of their bonding electrons in their  $\sigma$ -bonds. All components of the host layer have fixed valencies. They have neither the electrons which can be transferred to the intercalated materials nor the character to accept electrons from the guest species. On the other hand, an attempt was made to try to graft organic materials to interlayer surface of clay minerals. The attempt has not yet fully been succeeded because organic molecules were bonded only as silyl derivatives (7,8). Another type of intercalation is an anion exchanged one. Exchanged ions on intercalations have been peculiarly limited to cations (3). Anions can be intercalated in the interlayer region, if host layer has remaining positive charge. Applications of another layer compounds as host materials make it possible to prepare these types of intercalation compounds.

Intercalations on layer compounds except for clay minerals were not well known until Gamble's discovery. Gamble et al. made a comprehensive study on other sorption type compounds introducing a variety of organic molecules between the layers of  $\text{TaS}_2$  and  $\text{NbS}_2$  (9). These group VB metal dichalcogenides are metallic and easily intercalate organic bases. Superconducting transition

temperature  $T_c$  for the pure  $2H-TaS_2$  is about 0.8K.  $T_c$  increases to 3K, when organic molecules are introduced to separate the layers by over  $50\text{\AA}$  (10). Amines and pyridines are used as intercalates. X-ray photo electron measurements revealed a decrease in the electron density at the nitrogen of intercalated organics. Another results on reactivity and properties also suggest the transfer of electronic charge from the organic molecule, particularly the nitrogen atom, to the sheet of transition metal dichalcogenides. Alkyl chains of amines and aromatic plane of pyridine are almost perpendicular to the host's sheets so that nitrogen atoms are as close to the host layer as possible. Charge transfer from the nitrogen atom to the host sheet is easily attained in this orientation.  $6\text{\AA}$  expansion of the interlayer distance also supports this structural model in the intercalation of pyridine. The model originally proposed, however, showed the absorbed organic molecules lie flat along the sheets.

There have been many investigations on the intercalations of dichalcogenides (11,12,13,14). Most of the researches are on  $TaS_2$  and  $NbS_2$ . Among the dichalcogenides shown in Fig.2, group V compound and groups IV and VI ones are respectively metallic and semiconductive (15). It is not so easy to intercalate organic molecules into semiconductive materials. Cyclopropylamine is another organic amine with low ionization potential. Acrivos et al. showed that this amine could be absorbed into  $HfS_2$ ,  $TaS_2$ , and

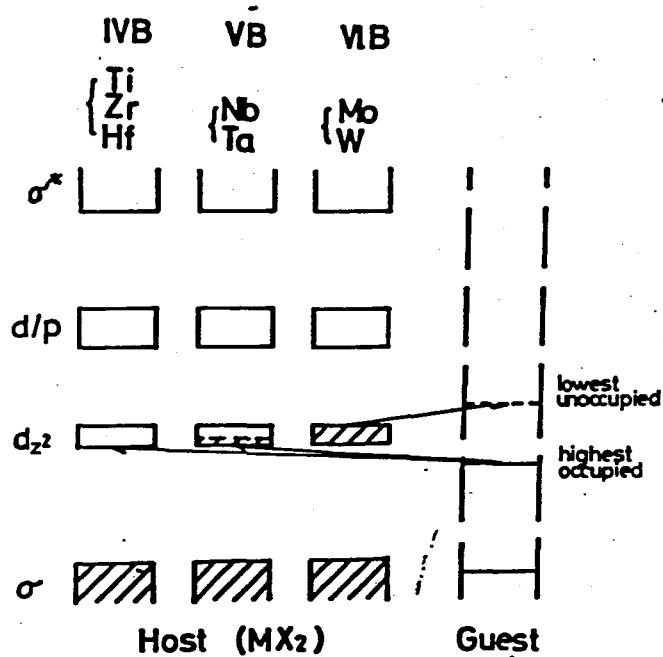
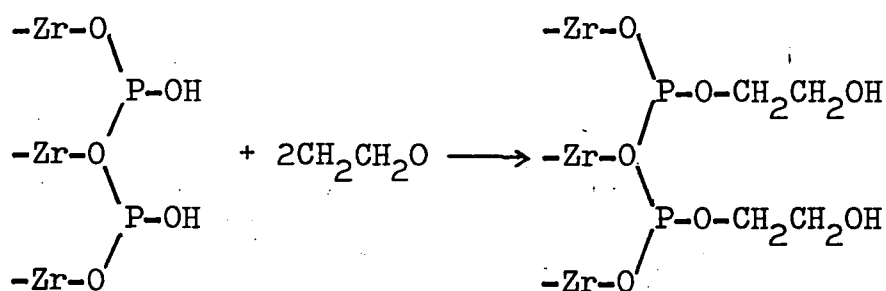


Fig. 2. Schematic representation of electron transfer between transition metal dichalcogenides and organic guest. Shaded orbitals are already occupied with the electrons of  $MX_2$ .

$\text{MoS}_2$  even if they are semiconductive (16). Optical measurements were done on the product. Bathochromic shifts of the Fermi level were observed with the intercalations for groups IV and V dichalcogenides but hypsochromic for group VI. The properties of intercalated transition element dichalcogenides were summarized using the Mulliken's concept of charge transfer (17). As shown in Fig.2,  $d_{z^2}$  orbital is empty for compounds of group IV, partially filled for group V and completely filled for group VI. Electrons transfer from the highest occupied level of the intercalate to the vacant  $d_{z^2}$  orbitals of host materials in the intercalations for group IV and V compounds. In the case of semiconductive group VI such as  $\text{MoS}_2$ , electrons transfer from the filled  $d_{z^2}$  orbital of the host layer to the lowest unoccupied level of the guest cyclopropylamine. Acrivos et al., however, explained the properties of the intercalated compound  $\text{Na-MoS}_2$  in the opposite way in other manuscript (18). They thought that the donated electron from sodium goes into the empty conduction band based on the  $d_{x^2-y^2}$  and  $d_{xy}$  orbitals. Both explanations are reasonable from considerations of the energy level diagram, but the intercalates such as amine and pyridine usually work as electron donors in Mulliken's concept of charge transfer interaction. Intercalations on semiconductive materials must be studied furthermore to solve whether the metallic property is required for the host to form a charge transfer type intercalation compound or not.

Another type of intercalation compound is graft type complex. Intercalated organic molecules are firmly fixed to host layers with covalent or ionic bond in the complex. Both the host layer and the guest molecule are a little modified to ionized states in an early stage of the intercalation, and then they react each other ~~to form~~ <sup>forming</sup> covalent or ionic bonding. Ethylene oxide was grafted to a layer compound of zirconium phosphate  $\text{Zr}(\text{HPO}_4)_2$  as shown in a following equation (19).



Bonding between  $\text{CH}_2\text{CH}_2\text{OH}$  and oxygens on the interlayer surface of zirconium phosphate is mostly covalent. There is no preparation of graft type complex where organic molecules are linked to host layer by ionic bond.

The hydroxide minerals to be called as pyroaurite and sjögrenite group have compositions of  $\left[ \text{M}_{1-x}^{2+} \text{M}_x^{3+} (\text{OH})_2 \right]^{+x} (x/n) \text{R}^{-n} \cdot y\text{H}_2\text{O}$ , where  $\text{M}^{2+}$  and  $\text{M}^{3+}$  are respectively divalent and trivalent cations and  $\text{R}^{-n}$  is an anion (20,21). Hydrotalcite is well known mineral of this kind with  $\text{M}^{2+}$  mainly  $\text{Mg}^{2+}$ ,  $\text{M}^{3+}$  mainly  $\text{Al}^{3+}$ ,  $x \approx 1/4$ ,  $y \approx 1/2$ , and the anion is  $\text{CO}_3^{2-}$ . The formula without using fractions is  $\text{Mg}_6\text{Al}_2(\text{OH})_{16}\text{CO}_3 \cdot 4\text{H}_2\text{O}$ . Many similar minerals are known with  $\text{M}^{2+} = \text{Mg}, \text{Fe}, \text{Ni}, \dots$ ,  $\text{M}^{3+} = \text{Al}, \text{Fe}, \text{Cr}, \dots$ ,  $\text{R}^{-n} = \text{CO}_3, \text{SO}_4, \text{NO}_3, \dots$ . Structural studies were made on natural

minerals of  $M^{2+}/M^{3+} \simeq 3$  containing only carbonate as interlayer anion (22). The structure consists of brucite-like octahedral hydroxide layers with a net positive charge which is neutralized by interlayer anions. Water molecules occupy the remaining interlayer space. This corresponds to the opposite situation of the before mentioned clay minerals. If the interlayer anion is exchangeable, the mixed hydroxide forms a new kind of intercalation compound --- anion exchange type. Gastuche et al. prepared hydrotalcite-like compounds with various ratio of  $Mg^{2+}/Al^{3+}$  containing mainly carbonate using chloride solution of magnesium and aluminum (23,24). They discussed about the range of  $Mg^{2+}/Al^{3+}$  based on the ratio in the initial solution. It should be done on the ratio in solid. The results on x-ray diffraction, DTA, and IR were also presented with the ratios. The height of a carbonate ion in its  $C_3$  axis is about twice of an ionic radius of  $O^{2-}$ . The ionic radii are  $1.4\text{\AA}$  and  $1.8\text{\AA}$  for  $O^{2-}$  and  $Cl^{-}$  respectively. Chloride ion does not have IR absorption above  $600\text{ cm}^{-1}$ . Neither x-ray nor IR showed the coexistence of chloride with carbonate in their results. The observed chloride in their chemical analysis was thought as an impurity. Miyata and his colleague synthesized the system  $M^{2+} - Al^{3+} - R^{n-}$  where  $M^{2+} = Mg^{2+}, Ni^{2+}, Zn^{2+}$  and  $R^{n-} = Cl^{-}, NO_3^{-}, ClO_4^{-}, SO_4^{2-}, CrO_4^{2-}$  (25,26). They tried to obtain each form without carbonate. Their chemical analyses show a presence of carbonate in their samples. IR absorptions of carbonate are not observed on their results.

They did not discuss about how the anions are coexisting in the crystals and how to obtain single anion phase.

All intercalation compounds already prepared are divided mainly into three types such as an ion-exchange, a sorption and a graft type. Although many studies have been performed for each type of intercalation compound, there have been no systematic study on intercalation compounds. Clay mineralogist studied only on clay-organics. People in the field of solid state science did not have much interests in clay-organics.

On the way to extend the investigations on intercalation compounds from clay-organics to many kinds of other complexes, it is an interesting question to examine what factor plays an important role to form each type of intercalation compound and how the mechanism of intercalation is understood. In the present study, following points are studied to obtain answers to these questions.

(1) Kinetics of the Intercalation in a System of FeOCl and Pyridine.

Intercalation is a peculiar reaction because an interlayer distance of the host material extremely expands during the reaction process. There have been few kinetic studies on intercalations. In Chapter 2, the kinetics of intercalation is studied in a case of pyridine into a layer compound FeOCl. A model is proposed for this peculiar reaction.

(2) Preparations and Properties of Charge Transfer Type Intercalation Compound ---  $\text{FeOCl}(\text{organic compound})_{1/n}$

In Chapter 3, charge transfer complexes are synthesized using semiconductive layer compound FeOCl and organic bases. Effects of organic basicity are examined on preparations and properties of the products using organic compounds with various  $\text{pK}_a$  as intercalates.

(3) Preparations and Properties of Graft Type Intercalation Compound ---  $\text{FeOOCH}_3$  and  $\text{FeO}(\text{O}_2\text{C}_2\text{H}_4)_{1/2}$

Iron oxychloride has a layer structure derived from  $\gamma\text{-FeOOH}$ . Alkoxide ion  $\text{RO}^-$  is made from alcohol molecule under an appropriate condition. It has similarities to hydroxyl ion  $\text{OH}^-$  in its structure and properties. These two facts suggest that the chloride ions in FeOCl are possibly substituted with alkoxide  $\text{RO}^-$  forming graft type complexes FeOOR. Chapter 4 deals with the replacements of the chloride ions of FeOCl layer with methanol and with ethylene glycol. Organic derivatives of FeOCl are obtained.

(4) Preparations and Properties of Anion Exchange Type Intercalation Compound ---  $\text{Mg}_6\text{Al}_2(\text{OH})_{16}\text{CO}_3 \cdot n\text{H}_2\text{O}$

The presence of natural hydrotalcite group minerals suggests that anion exchange type intercalation compound is possibly prepared by substitutions of  $\text{Mg}^{2+}$  in  $\text{Mg}(\text{OH})_2$  with  $\text{Al}^{3+}$ . Chapter 5 shows preparations of hydrotalcite-like compounds with various ratios of divalent and trivalent



cations. Mg (or Ni) and Al mixed perchlorate solutions are titrated with NaOH. Host layers with different amounts of remaining charge may have selectivity for the kinds of their interlayer anions. The range of  $M^{2+}/M^{3+}$  in this compound and the behavior of interlayer anion are studied. The exchangeability of interlayer anion is also examined on synthetic and natural products.

(5) Total Discussions

In Chapter 6, intercalation compounds appeared in literatures are again classified including the newly prepared ones in the present investigation. They are grouped mainly into three classes according to their modes of interaction between host and guest. The methods how to synthesize other newly intercalated compounds belonging to these types are discussed summarizing preparation methods, properties of the intercalated compounds in the present study and kinetics of intercalations.

CHAPTER 2.

KINETIC STUDY ON THE INTERCALATION IN A SYSTEM  
OF  $\text{FeOCl}$  AND PYRIDINE

## 2 - 1. Introduction

Some layer compounds such as  $\text{TaS}_2$  absorb many kinds of organic molecules into their van der Waals interlayer gap, and form new layered charge transfer complexes (9). A mechanism for the complete process of intercalation is thought to consist of the following steps. Host materials absorb intercalates to their active centers on their edges at first. And then absorbed intercalates diffuse into the lattice forming a stable intercalation compound. Diffusion and stabilization are often seen in other usual inorganic solid state reactions. Intercalation is peculiarly followed by a large expansion of interlayer distance of host inorganic lattice. In the case of  $\text{TaS}_2$ , the interlayer distance is  $6\text{\AA}$  and the expansion is about  $6\text{\AA}$  for the intercalation of pyridine (9). But there are few kinetic studies on insertion reaction (27,28).

Iron oxychloride belongs to an orthorhombic space group  $P_{mnm}$  with  $a = 3.780$ ,  $b = 7.917$ ,  $c = 3.302\text{\AA}$ , and  $Z = 2$  (33). The crystal structure consists of stack of double layer sheet of  $\text{cis-FeCl}_2\text{O}_4$  octahedra linked together with shared edges as shown in Fig.3. The outermost atoms at each side of the layer are Cl ions. The interlayer bonding between adjacent layers is van der Waals interaction. Pyridine and pyridine derivatives are absorbed into the interlayer van der Waals gap as will be discussed in Chapter 3.



A kinetics of intercalation on FeOCl - pyridine is studied as an example of intercalations. Saturated vapor pressure of pyridine are appropriate for kinetic studies because the duration of the intercalation is not so long. This chapter deals with a kinetics on an intercalation of pyridine (hereafter denoted as Py) into FeOCl. The results are discussed and some mechanisms for this reaction are presented.

## 2 - 2. Experimental Section

Materials. Iron oxychloride was prepared in a temperature gradient 370 °C/400 °C by heating a mixture of  $\alpha\text{-Fe}_2\text{O}_3$  and  $\text{FeCl}_3$  in a sealed Pyrex glass tube. The duration of this reaction was 2 days. Products deposited in a cool zone were washed with water to remove excess  $\text{FeCl}_3$ . The obtained  $\text{FeOCl}$  was sorted out with 100 and 200 meshes. Particle size of the sample is estimated to be between 74 and 149  $\mu\text{m}$ . Pyridine was dried with sodium hydroxide.

Experimental Technique and Apparatus. Isothermal intercalation kinetics were determined by measuring weight gain during reaction using silica spring microbalance as shown in Fig. 4. Silica spring having the sensitivity of 9.62 mm/ 100mg extention was used. Change in weight was determined by measuring change in the spring length with a cathetometer.

Sample of about 30 mg in silica pan was weighed and suspended from the spring. The vacuum system was evacuated for at least 15 hr before an experiment. After the hot zone was heated at desired temperatures, pyridine vapor was put into the system. During an experiment vapor pressure of the whole system was kept at 12 mmHg, a saturated vapor pressure at room temperature. Measurements were made at the following temperatures, 14, 24, 40, 55, 70, 86, 98, 110, 123, and 128 °C.

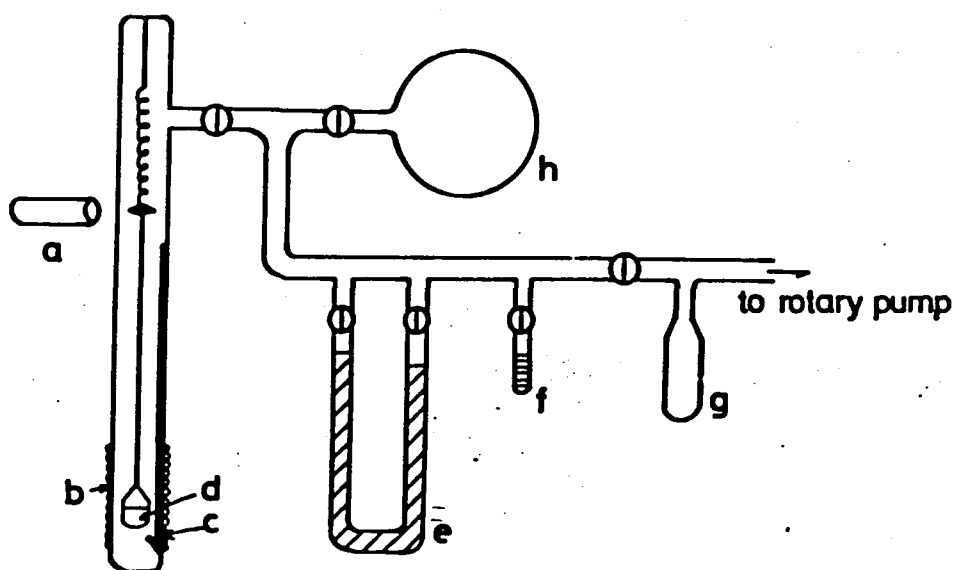


Fig. 4. Schematic representation of intercalation reaction apparatus.

a. cathetometer    b. ribbon heater    c. thermocouple  
d. silica pan    e. pressure gauge    f. pyridine  
reservoir    g. trap    h. gas storage

## 2 - 3. Results

Compositions of the final products were determined by weight gains and chemical analyses. The products were  $\text{FeOCl(Py)}_{1/3}$  and  $\text{FeOCl(Py)}_{1/4}$  respectively at high ( $70\sim 123^\circ\text{C}$ ) and low ( $14\sim 55^\circ\text{C}$ ) temperatures. After a reaction was completed, the reaction vessel was evacuated using mechanical pump for about 1 hr. However a desorption of the intercalated pyridine was not detected.

Isothermal weight gain data were represented using fractional absorptions,  $\alpha$  and  $\beta$ , respectively for the final compositions of  $\text{FeOCl(Py)}_{1/3}$  and  $\text{FeOCl(Py)}_{1/4}$  against time. Examples are shown in Fig. 5. The absorption curves ( $\alpha$  or  $\beta$  vs.  $t$ ) were mainly sigmoid with a short initiation period. Plateau is found around  $\beta \sim 0.4$  obviously in the lower temperatures. Possible reaction processes are discussed below for the intercalation of pyridine into  $\text{FeOCl}$ .

(1) Initial Stage. The results were tried to interpret in terms of kinetics mainly controlled by nucleation, interface reaction, or diffusion. The data were plotted using Sharp's method to judge which of these steps is important (29). As shown in Fig. 6, functions  $\ln[-\ln(1-\alpha)]$  and  $\ln[-\ln(1-\beta)]$  were plotted against  $\ln t$ , where  $\alpha$  and  $\beta$  were fractional absorptions for the final products of  $\text{FeOCl(Py)}_{1/3}$  and  $\text{FeOCl(Py)}_{1/4}$  respectively, and  $t$  was a reaction time in minutes. The data



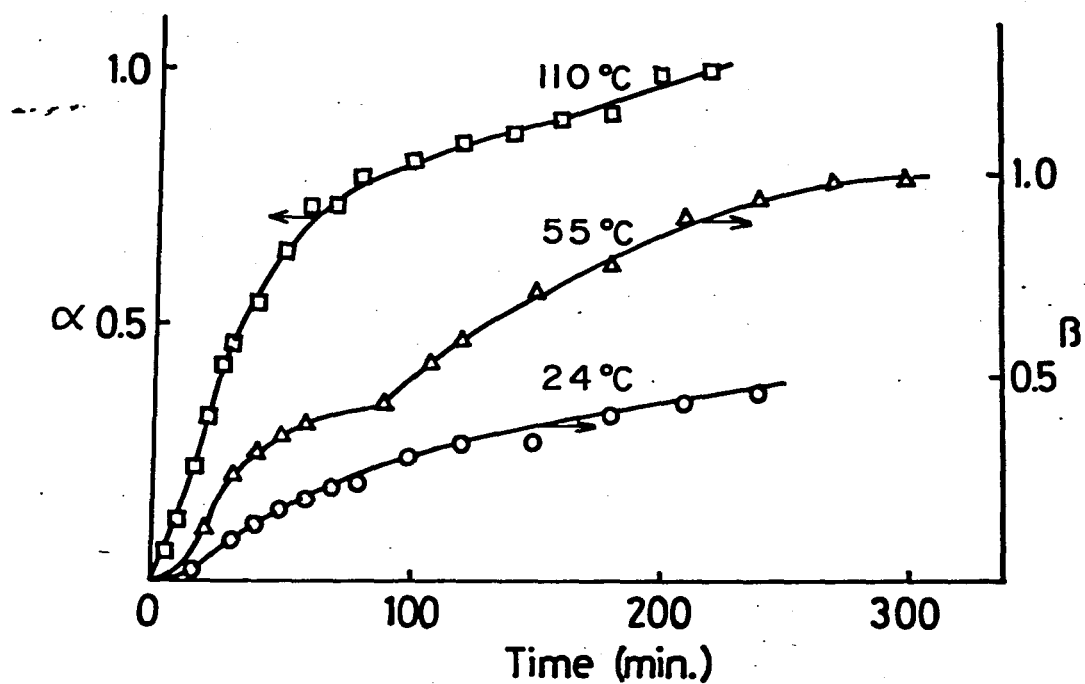
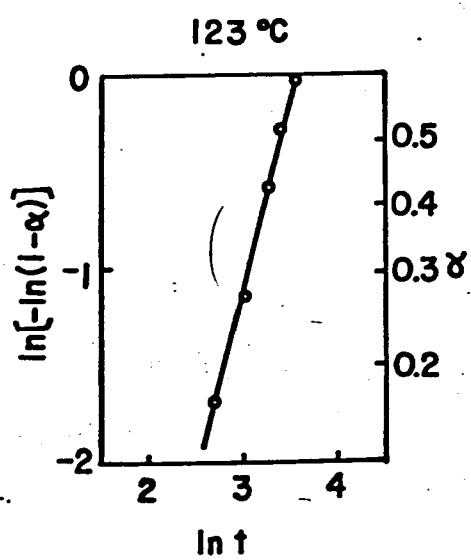
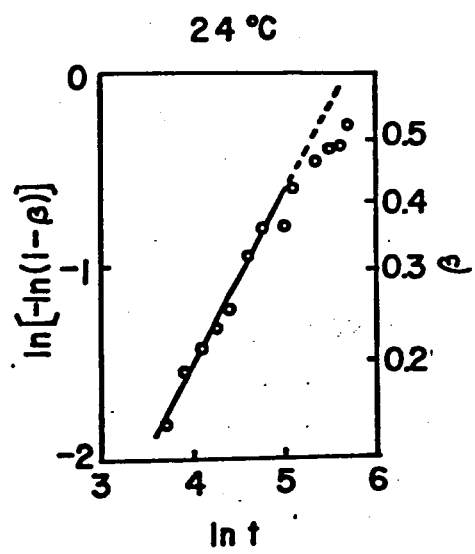


Fig. 5. Examples of isothermal weight gain at 24, 55, and 110 °C.  $\alpha$  and  $\beta$  are respectively fractional absorptions for the compositions of  $\text{FeOCl(Py)}_{1/3}$  and  $\text{FeOCl(Py)}_{1/4}$ .



(a)



(b)

Fig.6. Isothermal weight gain data plotted using Sharp et al.'s method.

points are almost on a straight line up to around  $\alpha \sim 0.5$  and  $\beta \sim 0.4$ . Probable kinetic equations were derived from the gradients of these lines and tested as follows.

At temperatures higher than  $70^\circ\text{C}$ , the gradient is nearly 2 as shown in Fig. 6(a). Sharp's method suggests that the rate-controlling step is a nucleation and it follows Avrami--Erofeev equation modified to two-dimensional case, which is described below.

$$\{-\ln(1-\alpha)\}^{1/2} = kt.$$

Data points are on the lines, as shown in Fig. 7, in the region below  $\alpha = 0.5$ . Deviation from this equation is found above  $\alpha = 0.5$ .

At lower temperatures below  $55^\circ\text{C}$ , gradient is about one as seen in Fig. 6(b). This gradient suggests that the rate-determining step is a two-dimensional interface reaction or a first-order nucleation. Functions of  $\beta$  were plotted versus  $t$  for these two processes. A better fit was obtained for the first-order nucleation process, as indicated in Fig. 8, than for the interface reaction. In this case the reaction follows the equation,

$$-\ln(1-\beta) = kt.$$

This equation also fits only below  $\beta = 0.4$ .

(2) Diffusion Step. Absorbed pyridine molecules diffuse into the inner region of  $\text{FeOCl}$  after the nucleation is over to some extent at the crystal edges. This diffusion makes it possible for  $\text{FeOCl}$  to absorb pyridine molecules successively. Pyridine

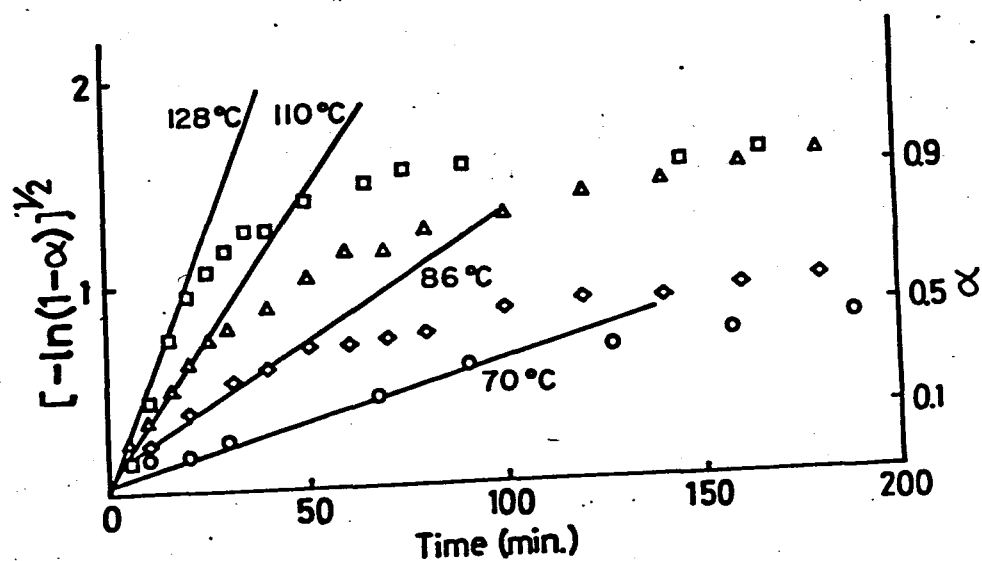


Fig. 7. Typical data plotted using two-dimensional Avrami-Erofeev equation in the higher temperature region.

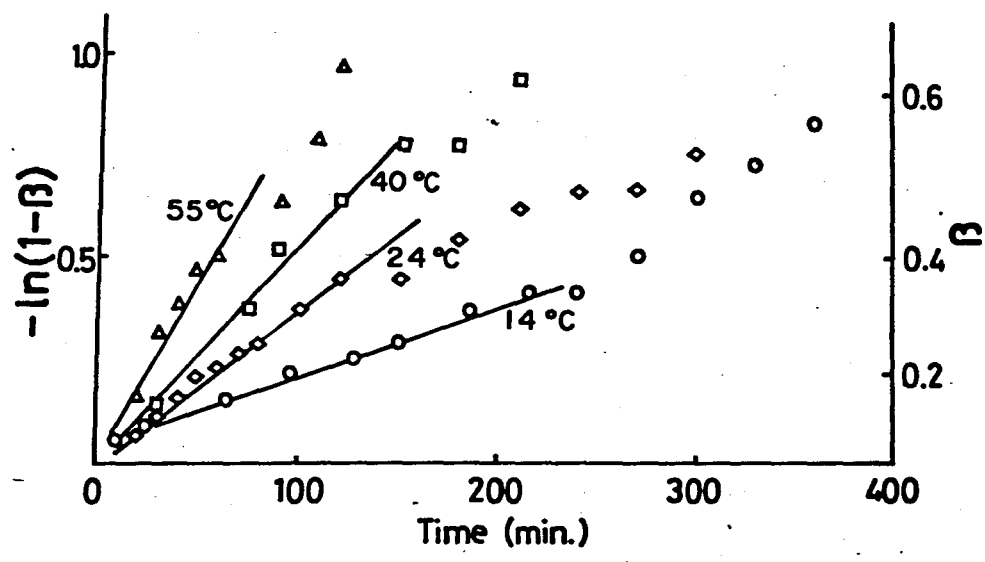


Fig. 8. Test of first-order rate equation for typical data.

molecules drive into the very anisotropic planar spaces of the interlayer region. The famous three-dimensional Jander's diffusion controlled rate equation was modified to two-dimensional case. As shown in Figs. 9 and 10, both  $\alpha$  and  $\beta$  nicely follow the following equations,

$$\{1-(1-\alpha)^{1/2}\}^2 = kt$$

$$\{1-(1-\beta)^{1/2}\}^2 = kt$$

up to where  $\alpha$  and  $\beta$  are about 0.8.

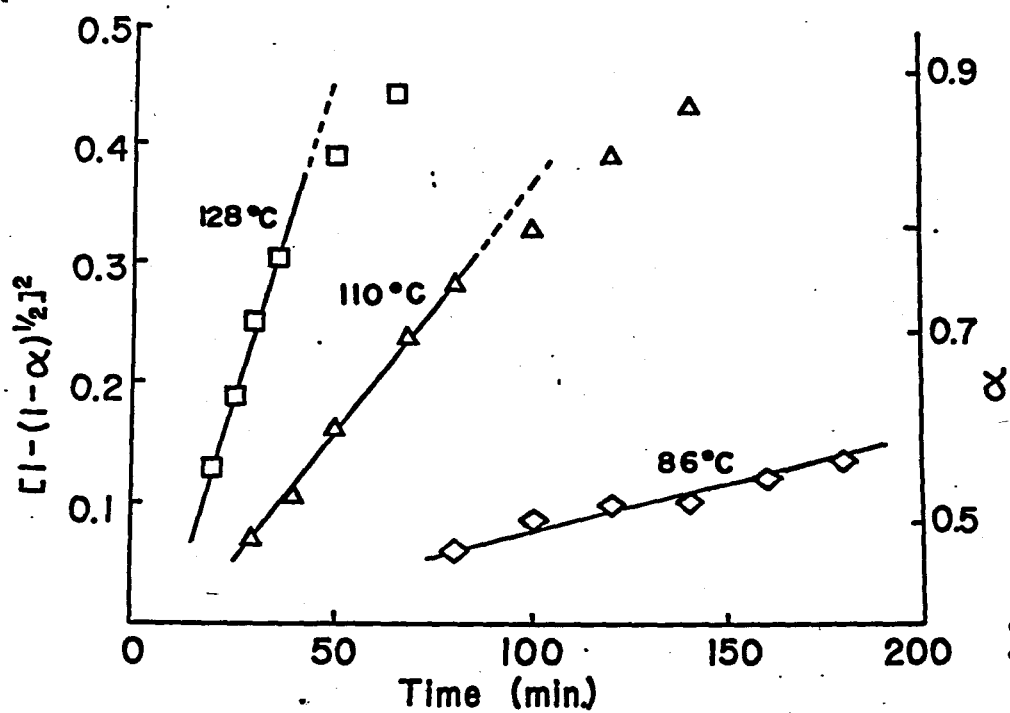


Fig. 9. Two-dimensional Jander's equation in the higher temperature region.

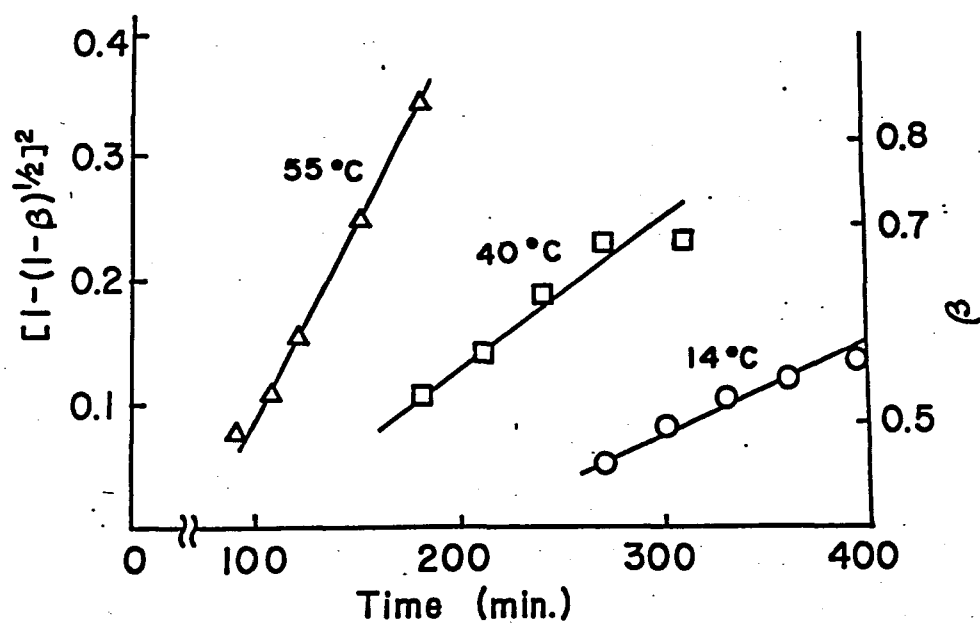


Fig. 10. Data plotted using two-dimensional Jander's equation in the lower temperature region.



## 2 - 4. Discussion

A mechanism for the complete process of intercalation is thought to consist of the following four elementary steps. Step 1, a diffusion of intercalate to the surface of the host material, is the fastest and obviously not rate determining. Step 2 is an adsorption of intercalates on the surface. It seems also unlikely that this will be rate determining step, because this adsorption is only physisorption. Step 3, a formation of the activated complex of the intercalate with the host surface atoms and a concomitant increase of the interlayer distance, however, can be assumed to involve chemisorption. It requires an energy for the activation and most probably is the rate determining step. This is confirmed by the fact that intercalation involves some types of charge transfer from the guest species to the host layers and by the experimental observation that an increase in temperature always leads to an increased rate of intercalation. Step 4 is a diffusion of the intercalate into the host lattice forming a stable intercalation compound. This step is also likely to be rate determining, especially in cases where intercalation has proceeded to a considerable extent.

Subba Rao and Shafer proposed similar mechanisms for the intercalation of metal hydroxide into  $\text{TaS}_2$  (27). The reaction obeyed the first-order rate law only up to

a limited reaction time  $t'$  ( $t' < t_{\text{total}}$ ), and then for the time longer than  $t'$  it exhibited a complicated behavior with a decreasing rate due to the diffusion of intercalate.

In the case of FeOCl-pyridine, the intercalation is understood with a nucleation followed by diffusion. A nucleation process is dominant in the initial stage of the reaction and then a diffusion is in the following step.

Pyridine molecules are only physically adsorbed on the edges of FeOCl layers at first. Because of the basic nature of pyridine, adsorbed molecules react fairly quickly with crystal edges forming a nucleus of the intercalation compound. The interlayer distance of host layers may expand only at edges of the crystals on this stage. The inner region is not yet expanded. In the lower temperature region, the reaction rate of this nucleation is given by the first-order rate equation,

$$-\ln(1-\beta) = kt$$

as in the case of TaS<sub>2</sub>-metal hydroxide (27).

The nucleation in the higher temperature region occurs much quickly on every active sites of the edges. All sites are in planes of the host layers because of the layer structure of FeOCl. The layer structure of host crystals probably affects a dimensionality of the kinetics. The nucleation process follows two-dimensional Avrami-Erofeev equation,

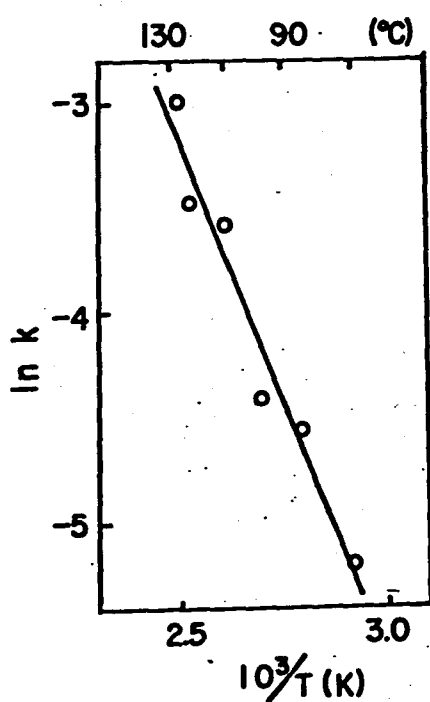
$$\left[-\ln(1-\alpha)\right]^{1/2} = kt.$$

The same equation was applied to the insertions of NH<sub>3</sub> and ND<sub>3</sub> to 2H-TaS<sub>2</sub> (30).

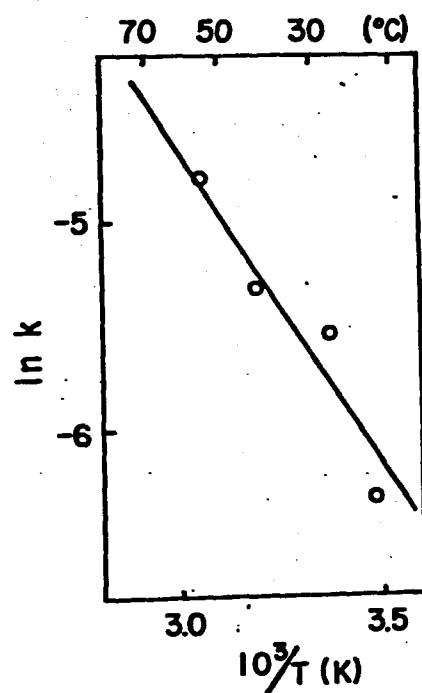
The observed rate constants at various temperatures roughly obey the Arrhenius equation in both higher and lower temperature regions as indicated in Fig. 11. The observed values of activation energies are 6 kcal/mol for the first-order rate law in a lower temperature region, and 10 kcal/mol for the Avrami-nucleation rate law at higher temperatures. These values are in a range of values observed for chemical adsorption.

Nucleations in both temperature regions follow the above mentioned each rate law in the initial stages of the intercalation. But deviations occur around  $\alpha=0.5$  and  $\beta=0.4$ , and thereafter diffusion becomes predominant. The absorbed species at the edges diffuse into the inner region even at the beginning of intercalation. Nucleation is very fast and diffusion is sluggish in this stage. Intercalated pyridine molecules inhibit successive absorption and diffusion becomes important when some amount of pyridine is adsorbed. Rough estimation showed that, at these deviation points from the nucleations, layers of activated complexes have the thickness consisting of at least some ten thousand pyridine molecules from the edge to the center of FeOCl.

A very simple model is used to understand the diffusion process. The FeOCl crystal is thought as a disk and the intercalated pyridine molecules diffuse from the edge to the center of the disk. As illustrated in Fig. 12, the radius of the disk is  $r_0$ . According to an usual Fick's law, a thickness



(a)



(b)

Fig. 11. Temperature dependences of rate-constants  $k$  for Avrami-Erofeev equation (a) and for first-order rate equation (b), respectively.

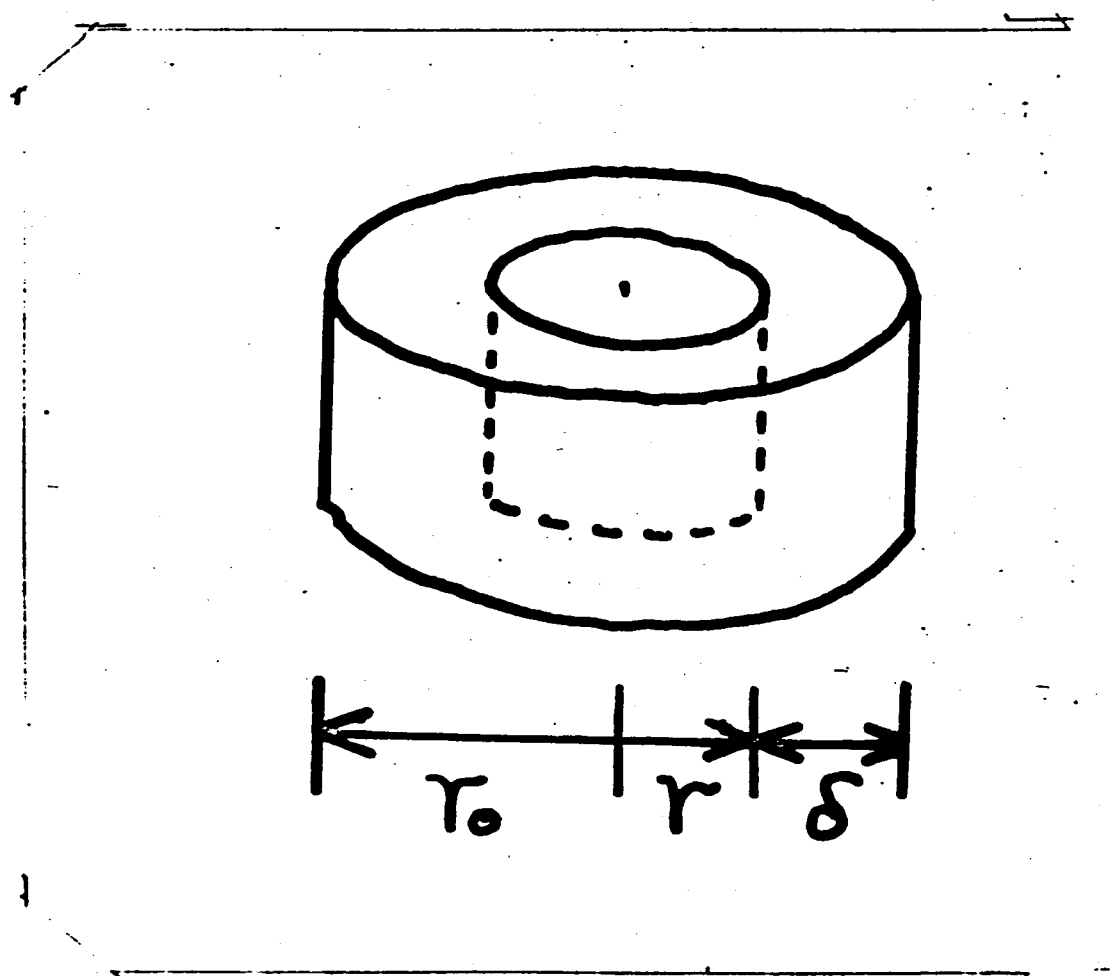


Fig. 12. Disk model of FeOCl.

$r_0$  is the radius of the disk,  $r$  is the radius of unreacted part of FeOCl, and  $\delta$  is the thickness of the product layer.

of the product's layer changes following the next equation.

$$\frac{d\delta}{dt} = \frac{k_1 c}{\delta}$$

where  $\delta$  is a thickness of the product's layer,  $c$  is a concentration of pyridine at the edges of FeOCl,  $t$  is a time, and  $k_1$  is a constant. Assuming that  $\delta=0$  at  $t=0$  and  $c$  is constant, this equation is solved to

$$\delta^2 = 2k_1 ct \quad (1)$$

On the other hand, the radius ( $r$ ) of the unreacted part of FeOCl disk is represented by

$$r = r_0(1-x)^{1/2}$$

where  $x$  is a fractional reaction. Then the thickness of the product's layer is given by

$$\delta = r_0 - r = r_0[1-(1-x)^{1/2}] \quad (2)$$

The equations (1) and (2) are combined to give

$$[1-(1-x)^{1/2}]^2 = k_2 t \quad (3)$$

where  $k_2 = 2k_1 c / r_0^2$ . As mentioned before in Figs. 9 and 10, the diffusion rate law is applicable to the intercalation of pyridine in the range where the fractional absorptions are from 0.4 to 0.8 in both the higher and the lower temperature regions.

To strengthen a validity of the diffusion model, the dependences of the parameter  $k_2$  in Eq.(3) were checked on the particle size ( $r_0$ ) of FeOCl and the pyridine pressure ( $c$ ). FeOCl crystals were sieved with 32, 48, 100, and 200 meshes. The particle size dependence of  $k_2$  was examined at 110°C

under the saturated pressure of pyridine. The particle sizes were 74- 149, 149- 297, and 297- 500  $\mu\text{m}$  in diameter. As shown in Fig. 13, it is expected that  $k_2$  is proportional to  $1/r_o^2$ . The pressure dependance of  $k_2$  was investigated at 110°C using the particle size of 74- 149  $\mu\text{m}$ . The results in Fig. 14 shows that  $k_2$  is proportional to the pyridine pressure, in other word, the concentration (c) of pyridine at edges of FeOCl.

Arrhenius plots are made in Fig. 15 for the observed diffusion rate constants in the both temperature regions. Activation energies are 15 kcal/mol for the higher temperature region and 9 kcal/mol for the lower region. These energies are used to break the bond formed at the initial stage between FeOCl and pyridine and to drive pyridine molecule into inner neighbor in FeOCl lattice. Thus the bonding energy between FeOCl and pyridine is smaller than these values. X-ray diffractometry showed that the phase in diffusion process is still a mixture of two phases - the obtained complex and the pure FeOCl. This observation is considered as follows. A FeOCl disk has two portions. One is the outer part of the obtained complex which has an expanded interlayer distance of 13.54Å, and the other is the inner unreacted part of FeOCl. The edge expanded in the nucleation exerts substantial strain on the inner region of the disk. Intercalated pyridine molecules diffuse from the edge to the center accompanying successive expansion of the interlayer distance of the inner parts. Microscopic observation showed that all

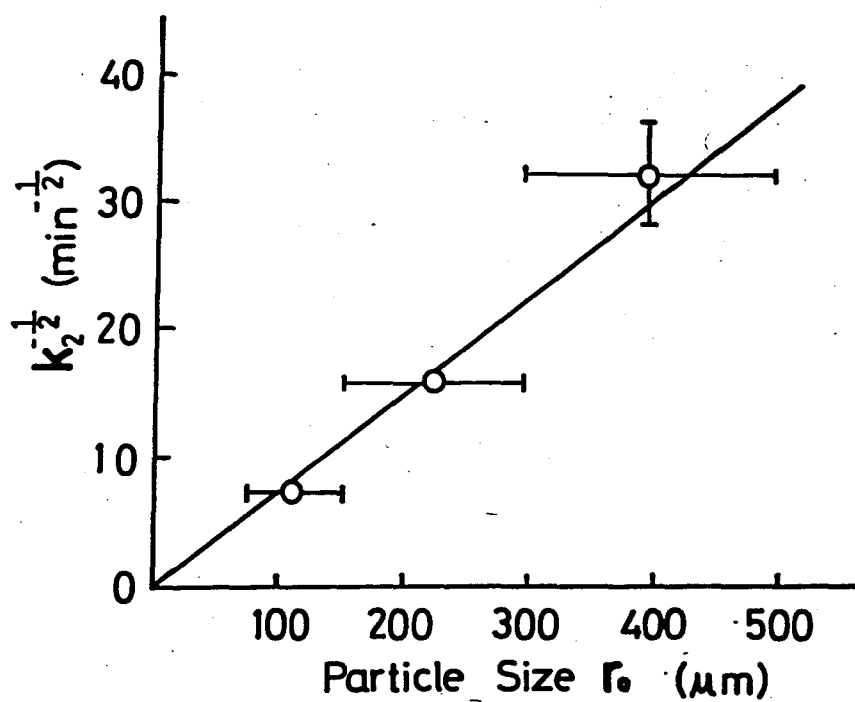


Fig. 13. Particle size dependence of rate constant  $k_2$  of two-dimensional Jander's equation in the higher temperature region.



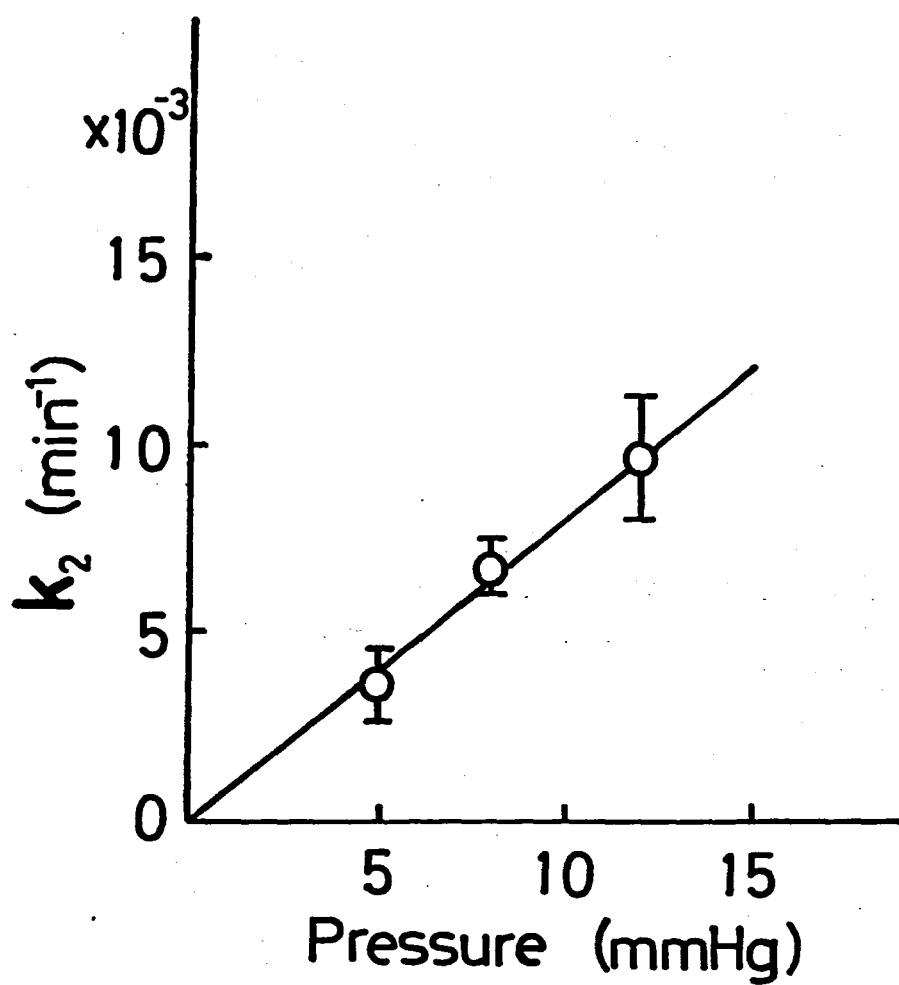


Fig. 14. Pressure dependence of rate constant  $k_2$  of two-dimensional Jander's equation in the higher temperature region.

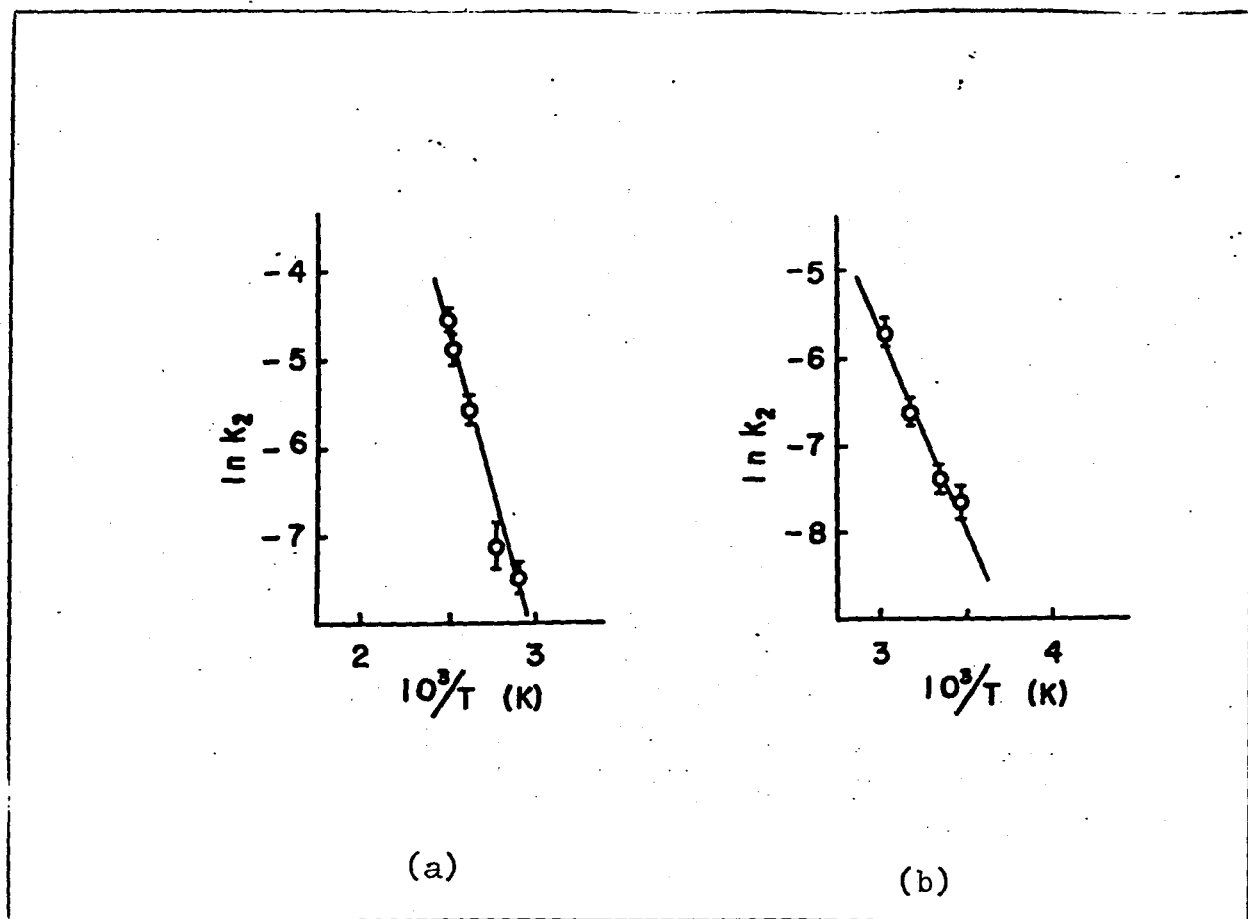


Fig. 15. Arrhenius plots for diffusion processes in the higher (a) and in the lower (b) temperature regions, where  $k_2$  is the rate constant in equation (3).

crystals had fringe of the obtained complex. Similar situation was found in the case of diffusion of interlayer water in vermiculite (31). ✓

In conclusion, the intercalation is understood by a nucleation followed by a diffusion. These reaction processes showed explicitly two-dimensionality due to the layer structure of host FeOCl crystals. Activation energies of all processes were about 10 kcal/mol. These values are reasonable for the formation energy of charge transfer bond between the host FeOCl and the guest pyridine molecules (32). ✓

### CHAPTER 3.

PREPARATIONS AND PROPERTIES OF CHARGE TRANSFER  
TYPE INTERCALATION COMPOUNDS

-----  $\text{FeOCl}(\text{organic compound})_{1/n}$

### 3 - 1. Introduction

Hagenmüller et al. found that  $\text{FeOCl}$  reacts with ammonia and some amines (34). Kanamaru et al. reported an intercalation of pyridine into  $\text{FeOCl}$ , and observed remarkable changes in electrical and magnetic properties (35,36). These changes can be attributed to a charge transfer from the nitrogen atom of the intercalated pyridine molecule to the  $\text{FeOCl}$  layer. Since  $\text{TiOCl}$ ,  $\text{VOCl}$ ,  $\text{CrOCl}$ , and  $\text{InOCl}$  are isostructural layer compounds with  $\text{FeOCl}$ , some of these compounds probably form similar intercalation compounds (37,38, 39,40).

Intercalation studies on  $\text{MOCl}$  were restricted in the system of  $\text{FeOCl}$ -pyridine and amines. Informations about the abilities of intercalations into  $\text{MOCl}$  were very limited. It is required to check what kinds of organic molecules are absorbed into the interlayer space of  $\text{MOCl}$ . Lewis basicity of organic base is a measure of the ability to donate electrons to acids. In order to examine the effect of basicity on intercalation, pyridine derivatives and amines with various  $\text{pK}_a$  values are used as intercalates.  $\text{pK}_a$  value can be used as a measure of basicity required for organic molecules to be intercalated. Section 3 - 2 of this chapter deals with the problem about the abilities of organic intercalation into  $\text{MOCl}$ .

Organic intercalation changes many properties of original layer compound. Properties of intercalated compounds are

different with the kinds of organic intercalates. Transition metal dichalcogenides( $\text{MX}_2$ ) intercalate organic bases. Their superconducting transition temperatures ( $T_c$ ) change with the organic intercalations (10). Bray and Sauer measured lone pair electron densities on nitrogen atoms of organic bases using nuclear quadrupole resonance (41). The electron densities were correlated with  $T_c$  of the intercalated  $\text{MX}_2$ .  $\text{p}K_a$  value is qualitatively related to the change of host's properties with intercalation if charge transfer interaction is important in the bonding between host and guest molecule.

In Section 3 - 3, effect of  $\text{p}K_a$  on the properties of  $\text{FeOCl}$ -organic compounds are checked using some kinds of pyridine derivatives having different basicities. Pyridine derivatives act as either  $n$ - or  $\pi$ -donor (17). The study on  $n$ -propylamine is useful to distinguish the effects of these two kinds of electrons in comparison with pyridine intercalated complexes. The intercalated  $\text{FeOCl}$  is investigated by measuring electrical resistivity, Mössbauer effect, ESR, and ultraviolet spectrum. Some correlations are found between the basicities of intercalates and properties of the products. On the basis of these data, the possibility of charge transfer is discussed on  $\text{FeOCl}(\text{organic compound})_{1/n}$ .

### 3 - 2. Organic Intercalations on MOCl (M= Ti, V, Cr, Fe, and In)

#### 3 - 2 - 1. Experimental Section

##### Preparations of MOCl.

FeOCl FeOCl was prepared in the same way as described in Chapter 2.

TiOCl  $\text{TiO}_2(0.3\text{g})$  was mixed with excess  $\text{TiCl}_3(1.8\text{g})$  in a dried nitrogen atmosphere. This mixture was sealed in a silica tube under vacuum and heated for 4 days in a temperature gradient of  $550^\circ\text{C}/650^\circ\text{C}$ . Dark brown and platy  $\text{TiOCl}$  crystals were obtained in a cooler zone, and they were washed with dimethyl formamide to remove excess  $\text{TiCl}_3$ .

VOCl  $\text{V}_2\text{O}_3(0.3\text{g})$  was mixed with  $\text{VCl}_3(0.5\text{g})$  and it was sealed in a silica tube under vacuum. VOCl crystalized after heating for 2 days at  $600^\circ\text{C}$  as reddish violet flakes. The product was washed with water to remove excess  $\text{VCl}_3$ .

CrOCl  $\text{Cr}_2\text{O}_3(0.1\text{g})$  was mixed well with  $\text{CrCl}_3(0.4\text{g})$ . A pellet of the mixture was made under a pressure of 150 bar and it was sealed in a silica tube under vacuum and heated at  $950^\circ\text{C}$  for one week. To prevent explosions, silica tube was heated in a stainless tube whose open end was outside of the furnace. Green flakes of  $\text{CrOCl}$  crystals were picked up and washed with dilute  $\text{CrCl}_2$  solution to remove excess  $\text{CrCl}_3$ .

InOCl      $\text{In}(\text{OH})_3$  was sealed in a Pyrex glass tube with twice amount of  $\text{InCl}_3$  and it was heated at  $400^\circ\text{C}$  for 3 days.

$\text{InCl}_3$  was made by dehydration of  $\text{InCl}_3 \cdot x\text{H}_2\text{O}$  at  $150^\circ\text{C}$  under vacuum. White powders of InOCl were obtained after washing the product with water.

Intercalation.

Those MOCl crystals were sealed with an excess amount of organic compounds in a glass tube. The temperatures of reaction were between room temperature and  $100^\circ\text{C}$ . Changes of the interlayer spacings with intercalations were observed by means of x-ray diffractometry.



### 3 - 2 - 2. Results and Discussion

The effect of Lewis basicities are studied on the system of FeOCl and pyridine derivatives. 2-Chloropyridine(CP), 3-bromopyridine(BP), pyridine(Py), 2,6-dimethylpyridine(DMP), 4-aminopyridine(AP), and 2,4,6-trimethylpyridine(TMP) are used. They will be abbreviated as denoted in the respective parentheses. Their  $pK_a$  values are 0.7, 2.8, 5.2, 6.8, 9.2, and 9.6 respectively. All of them are intercalated into FeOCl except for CP as shown in Table 1. CP molecule is bulky, but much large molecules such as TMP can be absorbed into the van der Waals gap of FeOCl. The basicity of CP is probably not large enough to be intercalated. FeOCl takes up amines whose  $pK_a$  values are more than 10. Lewis basicity can be related to ionization potential. The ionization potential is lower as the Lewis basicity is stronger. In order to donate electrons easily to an acceptor, the bases must have electrons in higher energy levels than the lowest unoccupied level of the acceptor.  $pK_a$  values of bases working as donors should be large enough to donate electrons.



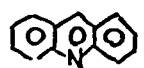
Molecular size of the base is also one of the important factors for intercalation. Quinoline, isoquinoline, and acridine are shown as , , and  using structural formula. They have almost the same basicity;  $pK_a$  values are respectively 4.8, 5.5, and 5.6. Quinoline

Table 1. Organic intercalation into MOCl.

Organic Compound	pK <sub>a</sub>	TiOCl	VOCl	CrOCl	FeOCl	InOCl
		a=3.79Å b=8.03 c=3.38	a=3.78Å b=7.97 c=3.30	a=3.84Å b=7.98 c=3.20	a=3.78Å b=7.92 c=3.30	a=4.07Å b=8.08 c=3.52
2-Chloropyridine	0.7		X	X	X	X
3-Bromopyridine	2.8		X		0	
Pyridine	5.2	0	0	X	0	X
2,6-Dimethylpyridine	6.8		0		0	
4-Aminopyridine	9.2		0	X	0	X
2,4,6-Trimethylpyridine	9.6		0	X	0	X
Propylamine	10.5	0	0	0	0	0
Ethylenediamine	{ 7.0 10.0			0	0	
Octamethylenediamine	{ 10.1 11.0			0		0
Quinoline	4.8				0	
Iso-Quinoline	5.5				X	
Acridine	5.6				0	

0 and X stand for respectively whether each organic compound is intercalated into MOCl or not.

and acridine are absorbed into FeOCl, but isoquinoline was not intercalated. Suppose the nitrogen atom donate electrons to FeOCl layer, the intercalation of isoquinoline requires a larger expansion of the interlayer distance than those of quinoline and acridine.

The abilities to intercalate Py and n-propylamine(PA) are respectively investigated on various MOCl. Both Py and PA can donate electrons to acceptor. PA has a possibility to make hydrogen bond with host layer, although its basicity is larger than that of Py. TiOCl, VOCl, and FeOCl absorb both Py and PA. CrOCl and InOCl intercalate only PA. The intercalated TiOCl, VOCl, and FeOCl showed good electrical conductivities as will be described in the case of FeOCl in the next section. Electrical conductivities of CrOCl and InOCl were not improved by the intercalations of PA. Hydrogen bonds probably play important roles for PA's intercalations into CrOCl and InOCl.

These results lead a conclusion that organic compounds are required to fit the following conditions to be intercalated into MOCl.

- (1) Their basicities are large enough to donate their electrons to the host layer. The limit of basicity is different with the kind of metal ion in MOCl. For example,  $pK_a$  was more than 2.8 to be intercalated into FeOCl.

- (2) Among the organic compounds with almost the same basicities, large molecule is not intercalated into  $\text{MOC}_l$ . Isoquinoline was not intercalated into  $\text{FeOC}_l$ . Too much expansion of the interlayer distance destabilizes the structure of host layers.

3 - 3. Intercalation Compounds  $\text{FeOCl}(\text{pyridine derivative})_{1/n}$   
and  $\text{FeOCl}(\text{n-propylamine})_{1/4}$

3 - 3 - 1. Experimental Section

Materials.

MOCl intercalated various kinds of organic bases as shown in Section 3-2. Among those MOCl compounds, FeOCl absorbed most of the intercalates examined in Table 1. In order to investigate the effects of intercalations on the properties of host layer compounds, properties of  $\text{FeOCl}(\text{organic compound})_{1/n}$  are studied in this section as a typical example.

Samples prepared in Section 3-2 are examined. Chemical analyses of C, H, and N showed that each intercalated compound has a stoichiometric composition. If the complex is represented by  $\text{FeOCl}(\text{organic compound})_{1/n}$ , n-values are four for Py, DMP, AP, and PA, and six for TMP, respectively.

Measurements.

The electrical resistivities of FeOCl and its complexes were measured in the temperature range 373K - 200K using carbon electrodes. The Mössbauer spectra were measured at room temperature and at liquid nitrogen temperature. Samples were dispersed with silicon grease, the thickness being ca.  $30 \text{ mg/cm}^2$ . Calibration was based on the Mössbauer spectrum of Fe metal. Electron spin resonance was observed on FeOCl and its complexes at 77K and at room temperature. Ultraviolet spectra of FeOCl and the intercalated complexes were obtained by the diffuse

reflectance method. Samples were dispersed in MgO.

Transmission method was used for the intercalates themselves, which were diluted with cyclohexane.

### 3 - 3 - 2. Results

The b-values corresponding to the interlayer distances are summarized in Table 2. Each b-value for the complexes is much larger than  $7.92\text{\AA}$  for FeOCl. The expansion is explained by the insertion of organic intercalates into the van der Waals gap of FeOCl. To examine the molecular orientations of the intercalated pyridine derivatives in the interlayer space of FeOCl, one-dimensional electron density projections were made on b-axis using seven (0k0) x-ray reflections. The results are shown in Fig.16 with schematic representations of molecular orientations.

FeOCl is a semiconductor with resistivity of  $10^6 \Omega\cdot\text{cm}$  at room temperature. The intercalated complexes are still semiconductive, but exhibit improved electrical conductivities along their c-axis. Their electrical resistivities are  $10 - 10^3 \Omega\cdot\text{cm}$  at room temperature. The values are smaller than that of FeOCl by a factor of  $10^{3-5}$ . The electrical activation energy also changes from 0.6eV to 0.2 - 0.3eV for the complexes.

Mössbauer spectra were obtained as shown in Fig. 17. The intensity ratios of the higher energy absorptions to the lower ones are close to 5/3. It is the value that is expected when the principal axis of the electric field gradient is perpendicular to the incident  $\gamma$ -beam and  $V_{zz}$  is negative.

Table 2. Parameters for FeOCl and FeOCl(organic compound)<sub>1/n</sub>

	$\text{pk}_a$	$b(\text{\AA})$	$\rho(\text{\AA cm})$	$E_a(\text{eV})$	I.S. (mm/s)	Q.S. (mm/s)	$\Delta H_{1/2}(\text{G})$
FeOCl		7.92	$10^6$	0.6	0.40	0.93	
FeOCl(Py) <sub>1/4</sub>	5.2	13.27	10	0.2	0.45	0.67	200
FeOCl(DMP) <sub>1/4</sub>	6.8	14.98	$10^2$	0.3	0.40	0.92	600
FeOCl(AP) <sub>1/4</sub>	9.2	13.57	$10^3$	0.2	0.42	0.84	1000
FeOCl(TMP) <sub>1/6</sub>	9.6	11.79	$10^3$	0.2	0.44	0.81	
FeOCl(PA) <sub>1/4</sub>	10.5	11.89	$10^2$	0.2	0.44	0.68	900

Py, DMP, AP, TMP, and PA respectively represent pyridine, 2,6-dimethylpyridine, 4-aminopyridine, 2,4,6-trimethylpyridine, and n-propylamine.



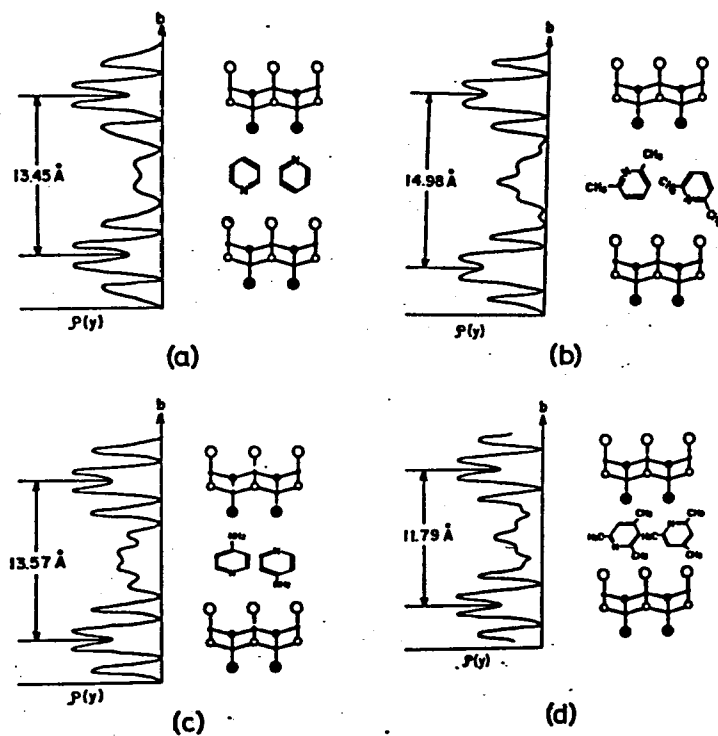


Fig. 16. One dimensional electron density maps projected on the  $b$ -axes of the complexes and schematic representations of the orientations of intercalates in the interlayer region of  $\text{FeOCl}$ .

- (a)  $\text{FeOCl(Py)}_{1/4}$ , (b)  $\text{FeOCl(DMP)}_{1/4}$ ,  
 (c)  $\text{FeOCl(AP)}_{1/4}$ , (d)  $\text{FeOCl(TMP)}_{1/6}$ .

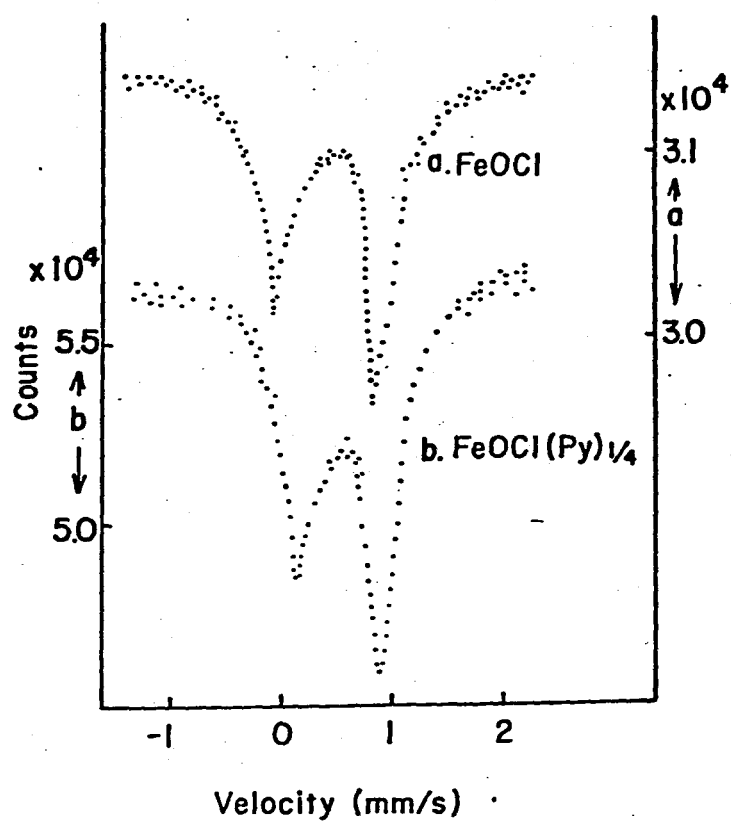


Fig. 17. Mössbauer spectra of FeOCl and FeOCl(Py) $_{1/4}$ .

The pertinent parameters at room temperature obtained with a least-squares fit computer program are summarized in Table 2. Isomer shifts of the intercalated pyridine derivative complexes are 0.40 - 0.44 mm/s. The values seem to increase with  $pK_a$  of organic intercalates, and larger than 0.40 mm/s for FeOCl. Isomer shifts of Py- and PA-FeOCl complexes are also larger than that of FeOCl. Quadrupole splittings are 0.67 - 0.92 mm/s for the intercalated complexes, being smaller than 0.93 mm/s for pure FeOCl. Q.S. tends to decrease with increase in I.S..

The ESR spectra of  $\text{FeOCl}(\text{pyridine derivative})_{1/n}$  were recorded at room temperature and at 77K. Except for TMP, broad singlet spectra were observed at  $g=2.003$ , their line shapes being almost Lorentzian as shown in Fig. 18. Neither FeOCl nor pyridine derivatives show any signals by themselves. The linewidth  $\Delta H_{1/2}$  shows no change with temperature but changes with the kind of intercalate (Table 2). No signal was detected for TMP complex. In order to avoid the skin effect, some samples were dispersed in  $\gamma$ -alumina. Neither linewidths nor  $g$ -values were affected by dilution. Anisotropic effects were checked on highly preferred oriented samples. Signals did not change with directions of the samples to magnetic field.

Iron oxychloride shows no absorption in its ultraviolet spectrum (Fig. 19). Pyridine has an intense  $\pi \rightarrow \pi^*$  absorption at 250 m $\mu$ , and a weak  $n \rightarrow \pi^*$  one at 285 m $\mu$  as shown in the curve b in Fig. 20 (42).  $\text{FeOCl}(\text{Py})_{1/4}$  complex has

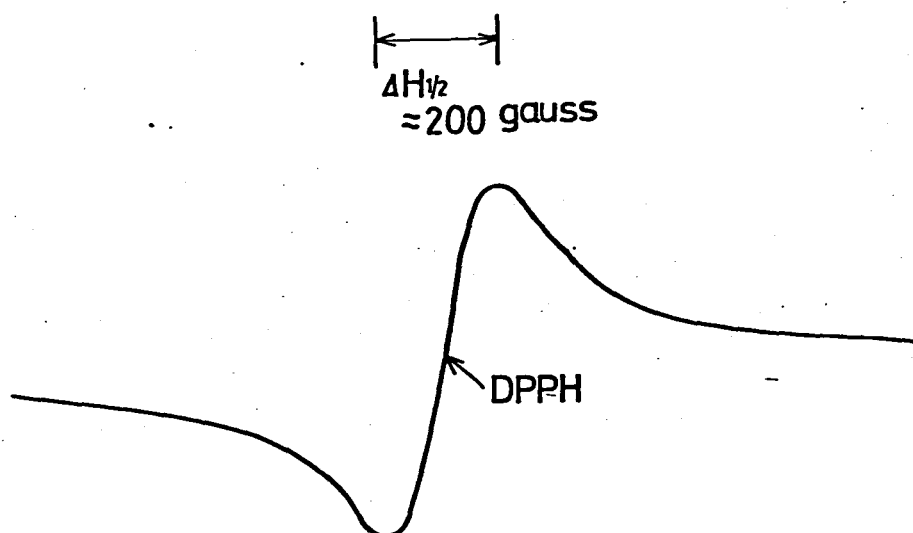


Fig. 18. ESR signal obtained for  $\text{FeOCl(Py)}_{1/4}$ .

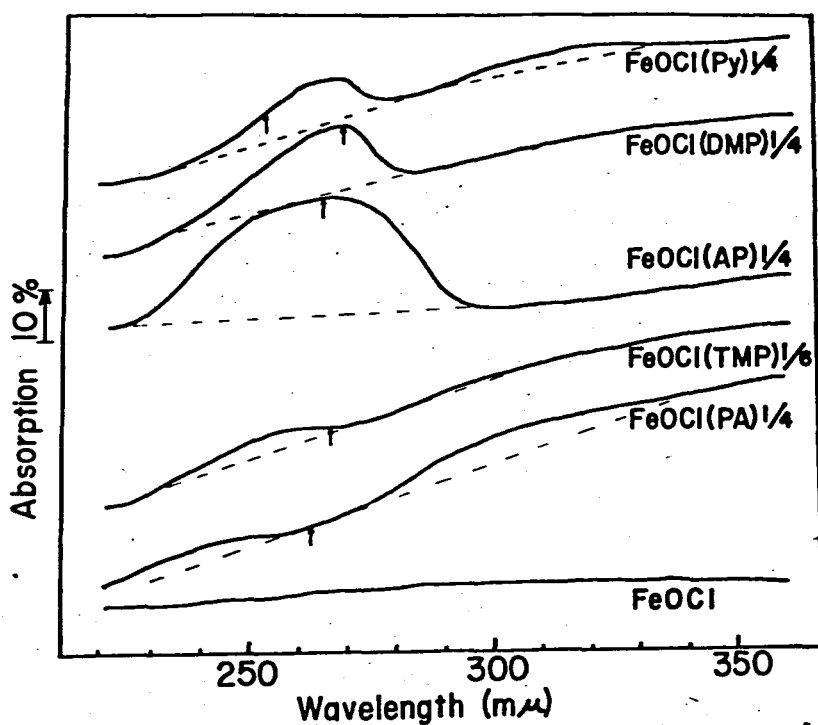


Fig. 19. Ultraviolet spectra of  $\text{FeOCl}$  and  $\text{FeOCl}(\text{organic compound})_{1/n}$  (solid line). Base lines are represented by dotted lines. Arrows show the positions of absorption maxima of organic compounds by themselves.

a broad and asymmetric absorption at about 270  $\mu$ , and  $\text{FeOCl}(\text{pyridine derivative})_{1/n}$  have absorptions around 265  $\mu$ . The latter absorptions are in almost the same region as those of pyridine derivatives. n-Propylamine without  $\pi$ -electrons has an absorption at 261  $\mu$  with a shoulder at around 252  $\mu$ , but complex  $\text{FeOCl}(\text{PA})_{1/4}$  has a weak absorption at 248  $\mu$  (see also Fig. 20). Furthermore, very broad absorptions around 310  $\mu$  were observed for both  $\text{FeOCl}(\text{Py})_{1/4}$  and  $\text{FeOCl}(\text{PA})_{1/4}$ . Neither  $\text{FeOCl}$  nor the intercalates show any absorptions in this region; DMP, TMP, and AP complexes have no prominent absorptions.

### 3 - 3 - 3. Discussions

Layered inorganic compound FeOCl intercalates some organic molecules. Each intercalated compound has an expanded spacing between  $11.79\text{\AA}$  and  $14.98\text{\AA}$  (Table 2). The expanded spacings are explained by the insertion of organic intercalates into the van der Waals gap of FeOCl. Kanamaru et al. showed that planes of pyridine rings are perpendicular to the host layers so that nitrogen atoms face the layers in the pyridine complex (36). In this case the interlayer distance expanded about  $5.5\text{\AA}$  with the intercalation. However FeOCl(PA) $_{1/4}$  seems to be in a different situation from pyridine complex since no more than approximately  $4.0\text{\AA}$  is available between the layers. This value almost corresponds to a twice of the van der Waals radius of alkyl group. Thus the alkyl chain is nearly parallel to the host layer and one of the  $sp^3$  hybridized orbitals of terminal nitrogen atom containing lone pair electrons faces to FeOCl layer. For FeOCl(DMP) $_{1/4}$ , FeOCl(AP) $_{1/4}$ , and FeOCl(TMP) $_{1/6}$ , molecular orientations of pyridine derivatives in the interlayer space of FeOCl have been estimated using the results of one-dimensional electron density projections based on x-ray diffractions as shown in Fig.16. The pyridine ring of DMP is perpendicular to the host layer, but rotates a little around the center of the ring due to the steric effect of methyl groups. For FeOCl(AP) $_{1/4}$ , the pyridine ring tilts slightly from a plane perpendicular to the layer. The inclination arises from a steric effect and the hydrogen bond between the amino group and the host layer. The pyridine ring of TMP is more tilted

than that of DMP because of the larger steric effect of methyl groups of the former. However, in all cases, organic molecules are in the van der Waals gap so that their nitrogen atoms are as close to FeOCl layer as possible.

Parameters for FeOCl and FeOCl(organic compound)<sub>1/n</sub> are summarized in Table 2 with  $pK_a$  values of organic intercalates, which are values for pure organic compounds and not for the intercalated ones (43). Formation of the complexes caused much reduction in electrical resistivity in the direction parallel to the host layer. The improved electrical conductivity can be explained by increased number of charge carriers. Mössbauer parameters change with intercalation. Isomer shifts of the complexes are slightly larger than that of FeOCl, but they are still those for ferric ions. The observed increase in I.S. values suggests the increased d-electron density around Fe atom in the intercalated FeOCl layer. However Fe<sup>2+</sup> is not detected above liquid nitrogen temperature. A correlation between  $pK_a$  and I.S. is observed for pyridine derivative complexes. But FeOCl(Py)<sub>1/4</sub> has the largest I.S., pyridine having the smallest  $pK_a$ . This suggests the importance of the effect of interaction between the side groups and Cl ions on the surface of FeOCl layer as well as that of  $pK_a$ . With increase of interaction between host and guest, charge carriers in the complexes tend to localize, electrical conductivity decreasing with increase in  $pK_a$ . The reduction



of electrical resistivity and the increase of the isomer shift are explained by assuming the charge transfer from the nitrogen atoms of the intercalated organics to the FeOCl layer. The assumption seems to be supported by the molecular arrangements of intercalated organics in the interlayer region of FeOCl. ESR and UV spectroscopy were used in order to obtain direct evidences of the charge transfer.

Charge transfer interactions which involve the formation of unpaired electrons were observed on ESR spectroscopy (44,45). Very broad signals are detected on the intercalated FeOCl except for TMP complex. These signals are Lorentzian. They show no hyperfine and fine structures and anisotropic effects to magnetic field.  $g$  values are 2.003. Conduction electrons in metals and semiconductors sometimes show resonance of Lorentzian shape at around  $g=2.003$ , and the linewidth becomes broader with increase of electrons (46). ESR signal of charge transfer complex in solid often loses its fine structure because of delocalization of the transferred electrons. In the case of  $\text{FeOCl}(\text{organic compound})_{1/n}$ , the very broad ESR signal may be attributed to the conduction electrons formed in the host layer due to intercalation.

In Fig. 20, curves a and d show ultraviolet spectra of  $\text{FeOCl}(\text{Py})_{1/4}$  and  $\text{FeOCl}(\text{PA})_{1/4}$ , respectively. They have very broad absorptions around 310 m $\mu$  observed in neither FeOCl nor the intercalates. These absorptions may be assigned to

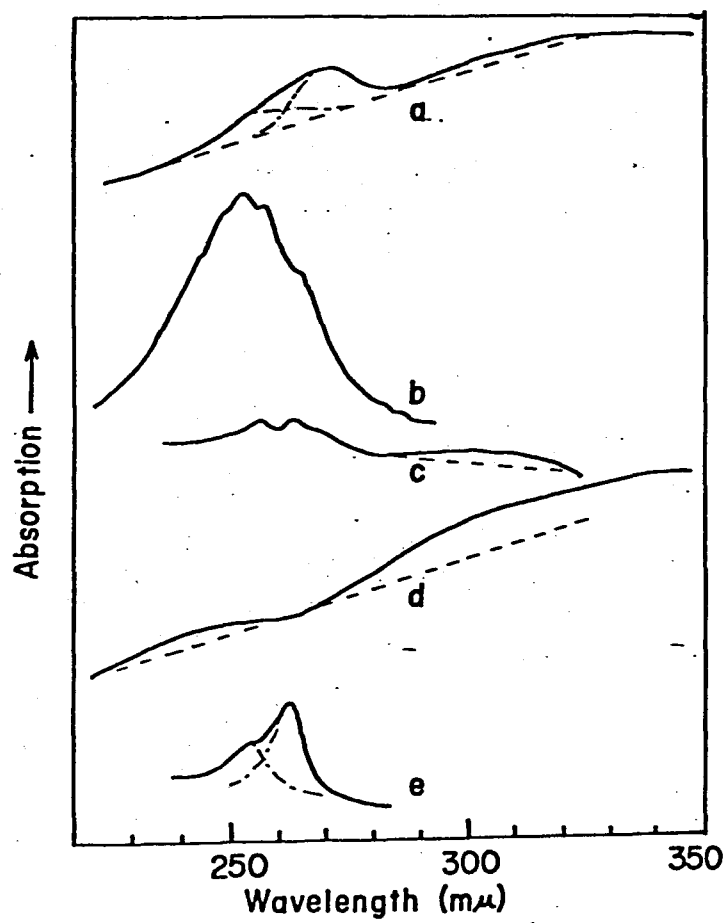


Fig. 20. Ultraviolet spectra of  $\text{FeOCl}(\text{organic compound})_{1/n}$ .  
 a.  $\text{FeOCl}(\text{Py})_{1/4}$ , b.  $\text{Py}$ , c.  $[\text{IrOH}(\text{Py})_2(\text{NH}_3)_3]^{2+}$ ,  
 d.  $\text{FeOCl}(\text{PA})_{1/4}$ , e.  $\text{PA}$ .

charge transfer bands as compared with that of  $[\text{IrOH}(\text{Py})_2(\text{NH}_3)_3]^{2+}$  in which a similarly broad charge transfer band is observed at around 300 m $\mu$  (Fig.20 (c)) (47). For DMP-, AP-, and TMP-complexes, however, no clear charge transfer absorptions are found in ultraviolet and visible regions. On the other hand, absorptions of the intercalates are perturbed by the intercalation into FeOCl. The pyridine  $\pi \rightarrow \pi^*$  absorption in  $\text{FeOCl}(\text{Py})_{1/4}$  shifts to longer wavelength by 20 m $\mu$ , turning asymmetric. Red shift of pyridine absorption is also observed on Ir-Py complexes (47). Absorptions of the pyridine derivatives do not clearly shift by intercalation, the peaks being broad and asymmetric in the respective FeOCl complexes. The asymmetric absorption can be divided into two or more components (Fig.20 (a)). Further analysis is difficult, since pyridine and pyridine derivatives have both lone pair and  $\pi$ -electrons. These two kinds of electrons can contribute to charge transfer. In order to observe the absorption of lone pair electron which is in non-bonding orbital, aliphatic amine is more suitable than pyridine derivatives. n-Propylamine shows an absorption from non-bonding orbital to  $\sigma^*$  one at 261 m $\mu$ . A broad blue shifted absorption is observed at around 248 m $\mu$  on the spectrum of  $\text{FeOCl}(\text{PA})_{1/4}$ . Since chlorine is the outermost ion in each FeOCl layer and the nitrogen atoms of the intercalates are very close to FeOCl layer, it is reasonable to assume a certain interaction between the non-bonding orbital of the intercalated donor and the  $\sigma$  orbital

of chlorine. The amount of blue shift of  $n \rightarrow \sigma^*$  absorption is 13 m $\mu$  on PA. The present value for the Cl...N pair is in the range of blue shifts of other n-donor and iodine pairs. Thiourea and thioacetoamide show blue shifts of 10 m $\mu$  and 21 m $\mu$ , respectively (48). This suggests that the bonding between FeOCl and PA is similar to that of other n-donor and I<sub>2</sub> molecular complexes. A similar blue-shift of lone pair electron absorption might also contribute to the asymmetric absorption observed on FeOCl(pyridine derivative)<sub>1/n</sub>.

FeOCl(PA)<sub>1/4</sub> is similar to FeOCl(pyridine derivative)<sub>1/n</sub> as regards electrical resistivity, Mössbauer effect and ESR. This suggests that FeOCl(pyridine derivative)<sub>1/n</sub> having lone pair electrons has almost the same bonding character between host and guest as FeOCl(PA)<sub>1/4</sub>.

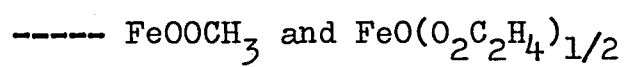
The charge transfer interaction has been confirmed in the intercalated FeOCl complexes. In Mulliken's charge transfer formulation of donor-acceptor systems, pyridine can work as either a  $\pi$ -donor or an n-donor (17). Correlations are found between  $pK_a$  and properties of the obtained complexes. It is assumed that lone pair electrons of the nitrogen atom are involved in the donor-acceptor interactions, and  $pK_a$  values of the respective compounds can be used as a measure of n-ionization potential. A similar speculation was made by Chaudhuri and Basu for the system of iodine and many aza-aromatics (49). They found a proportionality between the logarithm of equilibrium constants for charge

65

transfer type interaction and  $pK_a$  values.

In conclusion, pyridine, pyridine derivatives and propylamine molecules having nitrogen atoms are intercalated into the van der Waals gap of FeOCl. The properties of the products are explained by means of a charge transfer model. It is assumed that lone pair electrons on the nitrogen atoms of the organic molecules transfer to FeOCl layer in the intercalated complexes.

## CHAPTER 4:

PREPARATIONS AND PROPERTIES OF GRAFT TYPE  
INTERCALATION COMPOUNDS

#### 4 - 1. Introduction

Iron oxychloride has the structure derived from  $\gamma$ -FeOOH by a substitution of the hydroxyl groups with chloride ions (33). The layer of FeOCl pack together so that the Cl on the outsides of adjacent layers are close packed. The inter-layer bonding is van der Waals interaction. Because of the weak interaction between the layers, this compound easily intercalates some kinds of organic bases such as amine and pyridine as described in Chapter 3. Hagenmüller et al. showed that ammonium reacts with FeOCl forming  $\text{FeONH}_2$  (34). This fact suggests that it is possible to substitute chloride ions in FeOCl layer with other monovalent anions.

Alcohol is amphoteric just as water and it changes to alkoxyl group in an appropriate condition. Alkoxyl group  $\text{RO}^-$  forms a homologous series with  $\text{OH}^-$ . The similarities between  $\text{RO}^-$  and  $\text{OH}^-$  and those between FeOCl and  $\gamma$ -FeOOH suggest that chloride ions in FeOCl layer are substituted with  $\text{RO}^-$  groups.

Alcohol was not directly intercalated into FeOCl. The intercalation of pyridine derivatives in advance is applied to expand the interlayer distance of FeOCl. Although alcohol is not a strong base, it is intercalated into the expanded interlayer region. It is tried to graft methanol molecules to FeOCl layer in Section 4-2.

A further interest is to make another type of organic derivative of  $\text{FeOCl}$ . Intercalated diols working as divalent anions may bridge two adjacent  $\text{FeO}$  double layers. Fuls et al. investigated the reactions of glycerol with goethite, lepidchrocite, and hematite, respectively (50). They proposed two kinds of structural models for the product. One was an interlayer bridging model where both ends of a glycerol molecule were linked respectively to the upper and the lower layers with its OH groups. The other was an intralayer bridging model. Glycerol molecules were bonded to the host layer within the same layer. It was not determined which model was correct in the manuscript. Section 4-3 deals with a preparation of an ethylene glycol grafted  $\text{FeOCl}$ .



#### 4 - 2. Graft Type Intercalation Compound --- $\text{FeOOCH}_3$

##### 4 - 2 - 1. Experimental Section

$\text{FeOCl}(\text{AP})_{1/4}$  was soaked in methanol in a sealed Pyrex glass tube. The duration of the reaction which produced brown crystals of  $\text{FeOOCH}_3$  was about 10 days at  $80^\circ\text{C}$  and 6 days at  $110^\circ\text{C}$ .

X-ray analysis was conducted with a Rigaku-Denki diffractometer using  $\text{Cu K}\alpha$  and  $\text{Co K}\alpha$  radiation. C, H, and N analysis of this compound was made using standard techniques. Infrared absorption spectra were obtained using DS-402G spectrometer made by Japan Spectroscopic Co., Ltd. by the usual KBr pellet technique and Nujol method. Mössbauer spectra using radiation from  $^{57}\text{Co}$  in Pd metal were measured at room temperature with a 200 channel multichannel analyzer. Calibration was based on the Mössbauer spectrum of Fe metal. For differential thermal analysis a Rigaku-Denki apparatus fitted with a platinum-platinum-rhodium thermocouple was used and  $\text{Al}_2\text{O}_3$  was used as reference. The rate of temperature increase was  $10^\circ\text{C}/\text{min}$ .

#### 4 - 2 - 2. Results and Discussions

During the reaction of the sorption complex  $\text{FeOCl}(\text{AP})_{1/4}$  with methanol, methanol molecules were easily intercalated in the expanded interlayer spaces of  $\text{FeOCl}$ , and a new phase appeared. This phase gave the basal spacing of  $9.97\text{\AA}$  as depicted in Table 3. After the reaction, Cl ion and AP were qualitatively detected in the solution.

In order to determine the chemical composition of the final product, a chemical analysis of C, H, and N was conducted. The results are given in Table 4. For carbon and hydrogen the experimental values were smaller than the theoretical ones. Small amount of nitrogen was observed. The chemical formula of the product is evaluated to be  $\text{FeOOCH}_3$  from the C, H, and N values. The above mentioned reaction is described as follows.



where HCl and AP go into solution leaving solid  $\text{FeOOCH}_3$ . On the other hand, any direct reaction between  $\text{FeOCl}$  and methanol was not observed in a temperature range from room temperature to  $110^\circ\text{C}$ . These results represent that the expansion of interlayer distance of  $\text{FeOCl}$  makes it easy for methanol molecules to penetrate into interlayer spaces resulting in desorption of AP molecules and chloride ions from the interlayer.

Table 3. X-ray powder diffraction  
data for  $\text{FeOCH}_3$

hkl	I	$d_{\text{obsd.}}$	$d_{\text{calcd.}}$
010	vs	9.91	9.97
020	m	4.99	4.98
001-	w	3.99	3.99
110	mm	3.58	3.58
030	mm	3.33	3.32
120	w	3.03	3.04
040	w	2.491	2.492
002	vw	2.003	1.995
050	mm	1.992	1.994
200	w	1.921	1.915
060	mm	1.662	1.662
070	vw	1.426	1.425

a. Debye-Scherrer data based on Co  $K\alpha$  radiation.

b.  $a=3.83(1)\text{\AA}$ ,  $b=9.97(1)\text{\AA}$ ,  $c=3.99(1)\text{\AA}$ .

Table 4. Chemical analysis data for  $\text{FeOCH}_3$  (Weight percent)

Element	C	H	N
Obsd value	9.29	2.43	0.33
Calcd value	11.7	2.94	0.00

Infrared spectra and Mössbauer effect study of  $\text{FeOOCH}_3$  also showed this displacement. The solid line in Fig. 21 indicates the infrared spectrum of  $\text{FeOOCH}_3$  obtained using KBr pellet technique. This spectrum gives an absorption band at  $1050 \text{ cm}^{-1}$  assigned to the stretching vibration of a C-O bond, but none for a O-H stretching vibration. This result indicates that the methanol molecule absorbed in the interlayer region changed to methoxide ion,  $\text{CH}_3\text{O}^-$ , which substituted the chloride ion, the outermost ion of the  $\text{FeOCl}$  layer. Moreover, the absorption band of the C-O stretching vibration split into two bands. Since these bands have almost the same intensities, this compound is considered to have two kinds of C-O bond. An orientation effect of the  $\text{FeOOCH}_3$  crystal was investigated to find the cause of this splitting. Large and very thin  $\text{FeOOCH}_3$  crystals were held between NaCl disks dipped with Nujol mull and exposed vertically to infrared rays. The dotted line in Fig. 21 shows the result. The absorption band of higher wavenumber disappeared and only the lower one remained. This fact indicates that the former is the absorption of C-O bond which is perpendicular to the inorganic layer and the latter is slightly inclined. Furthermore, the intensity of the absorption band at  $1150 \text{ cm}^{-1}$  increased and was assigned to a rocking mode of methyl groups (51). The increase of this absorption intensity is quite reasonable from a viewpoint of bond orientation.

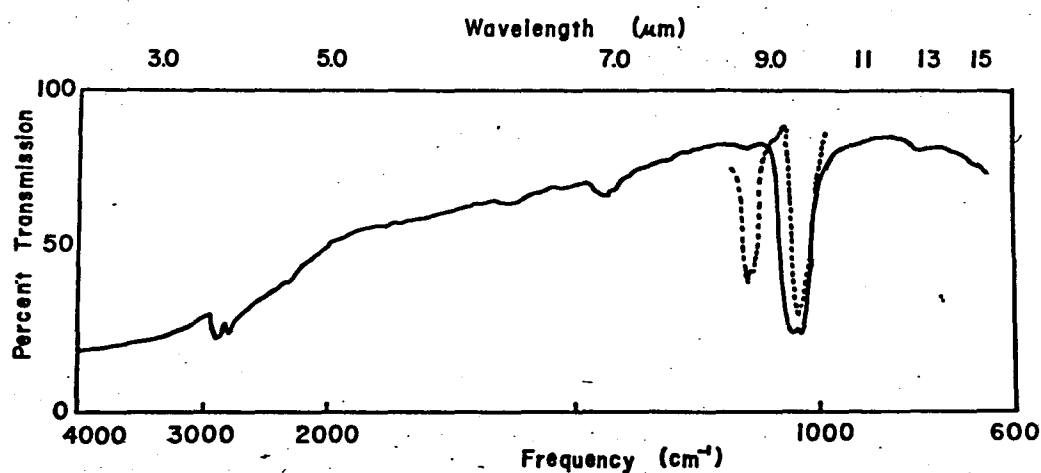


Fig. 21. Infrared spectrum of  $\text{FeOOCCH}_3$  using the KBr pellet technique (solid line) and orientation infrared spectrum obtained by Nujol method (dotted line).

The Mössbauer spectra of  $\text{FeOCl}$  and  $\text{FeOOCH}_3$  are illustrated in Fig. 22 and the pertinent parameters are summarized in Table 5. The measured value of quadrupole splitting for  $\text{FeOOCH}_3$  is much smaller than that for  $\text{FeOCl}$ . This result is explained as follows. The chlorine atoms of distorted  $\text{FeCl}_2\text{O}_4$  octahedra in  $\text{FeOCl}$  layer have been replaced by oxygen atoms of methoxide ions. Consequently the crystal field symmetry around the Fe atom has been raised. On the other hand, isomer shift of  $\text{FeOOCH}_3$  showed almost the equal value to that of  $\text{FeOCl}$ . Thus the valence state of Fe atom is still  $3+$ , when the methoxide ions are coordinated to Fe atoms.

Figure 23 presents the result of differential thermal analysis and thermogravimetry of  $\text{FeOOCH}_3$ . As seen in the figure, no change was observed below  $290^\circ\text{C}$ , indicating that  $\text{FeOOCH}_3$  is not a sorption type complex, but a new layered compound with a strong bonding between the intercalated  $\text{CH}_3\text{O}^-$  and the inorganic layer. A sharp exothermic peak and a 20% weight loss were observed in the temperature region from  $290$  to  $300^\circ\text{C}$ . The sample cooled from  $350^\circ\text{C}$  exhibited strong magnetism and was identified to be  $\gamma\text{-Fe}_2\text{O}_3$  by x-ray diffractometry. If  $\text{FeOOCH}_3$  thermally decomposes at  $290^\circ\text{C}$  and gives rise to  $\gamma\text{-Fe}_2\text{O}_3$ , this observed weight loss agrees with the theoretical one.

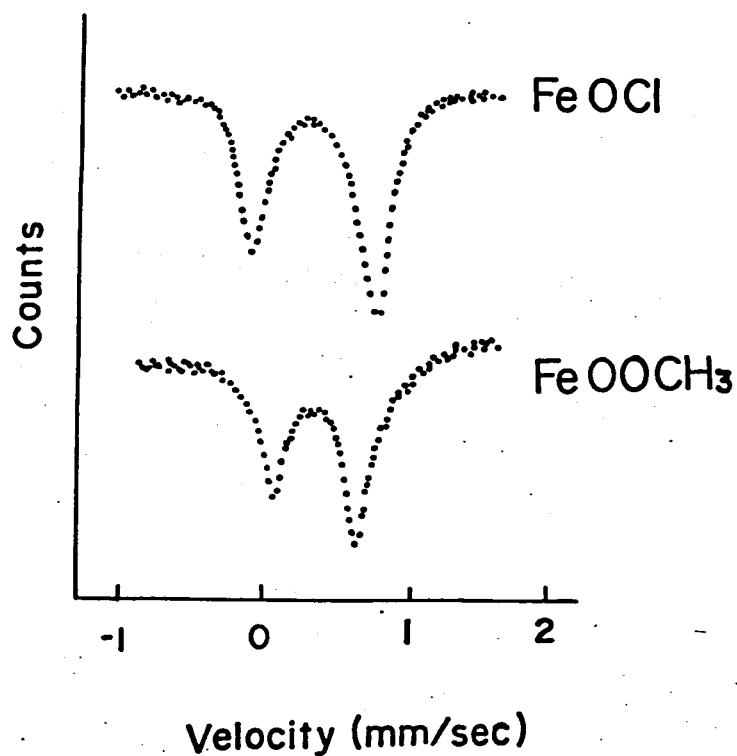


Fig. 22. Mössbauer spectra of FeOCl and FeOOCH<sub>3</sub> at room temperature. Velocity scale is relative to Fe metal.



Table 5. Mössbauer parameters (mm/s) of FeOCl and FeOOCH<sub>3</sub>.

	Quadrupole	
	Isomer shift	splitting
FeOCl	0.40	0.92
FeOOCH <sub>3</sub>	0.37	0.60

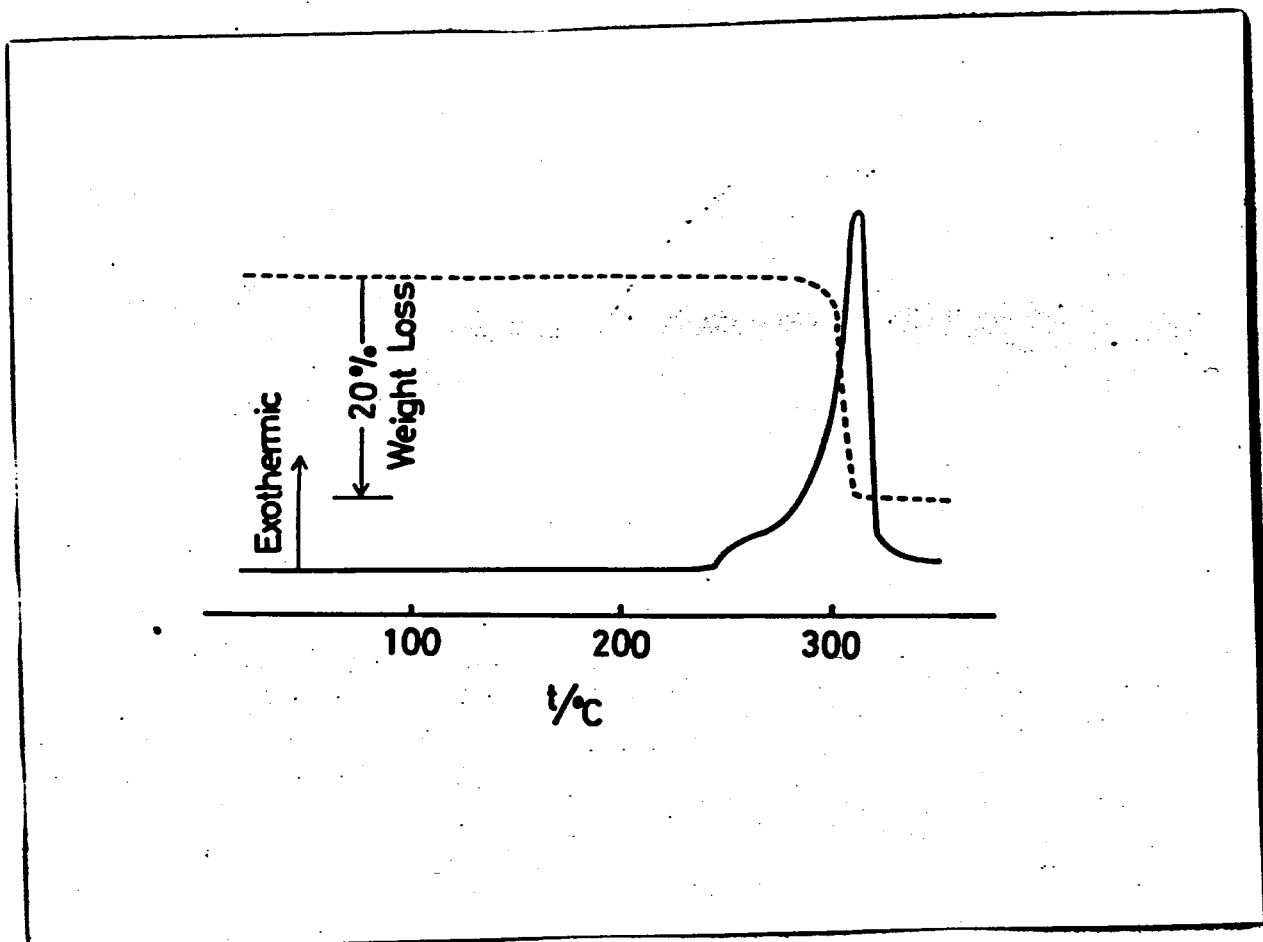


Fig. 23. Differential thermal analysis and thermogravimetry of  $\text{FeOOCH}_3$ .

One-dimensional electron-density projection on the b-axis was synthesized using seven (0k0) X-ray reflections. The sign of each reflection was determined by considering the contribution of Fe and O in the skeleton of the inorganic layer. There are five peaks in the interlayer region as shown in Fig.24. On the basis of this projection together with the above-mentioned Mössbauer effect, IR and oriented IR absorptions and so on, the crystal structure of  $\text{FeOOCH}_3$  is deduced as indicated in Fig.24. It is apparent that the oxygens of methoxide groups are directly bonded to the ferric ions, and that there are two kinds of methoxide groups. A small central peak in the electron-density projection may arise from a small amount of AP molecules remaining in the final product.

The crystal structure of  $\text{FeOOCH}_3$  is closely related to that of  $\gamma\text{-FeOOH}$ . Hydrogen of the latter is substituted with  $\text{CH}_3^+$  in the former.  $\gamma\text{-FeOOH}$  topotaxially converts to  $\gamma\text{-Fe}_2\text{O}_3$  with the cubic closest packing of oxygens, which is a metastable phase of iron oxides, by dehydration.  $\text{FeOOCH}_3$  also converts to  $\gamma\text{-Fe}_2\text{O}_3$  in the temperature region between 290 and 300 °C in air. Thermomagnetic measurements showed that  $\text{FeOOCH}_3$  converted to a ferromagnetic compound at 290 °C and then to a weak ferromagnetic  $\alpha\text{-Fe}_2\text{O}_3$  above 450 °C in vacuo. If the magnetic substance was magnetite,  $\text{Fe}_3\text{O}_4$ , the substance did not convert to  $\alpha\text{-Fe}_2\text{O}_3$  at 450 °C in vacuum.

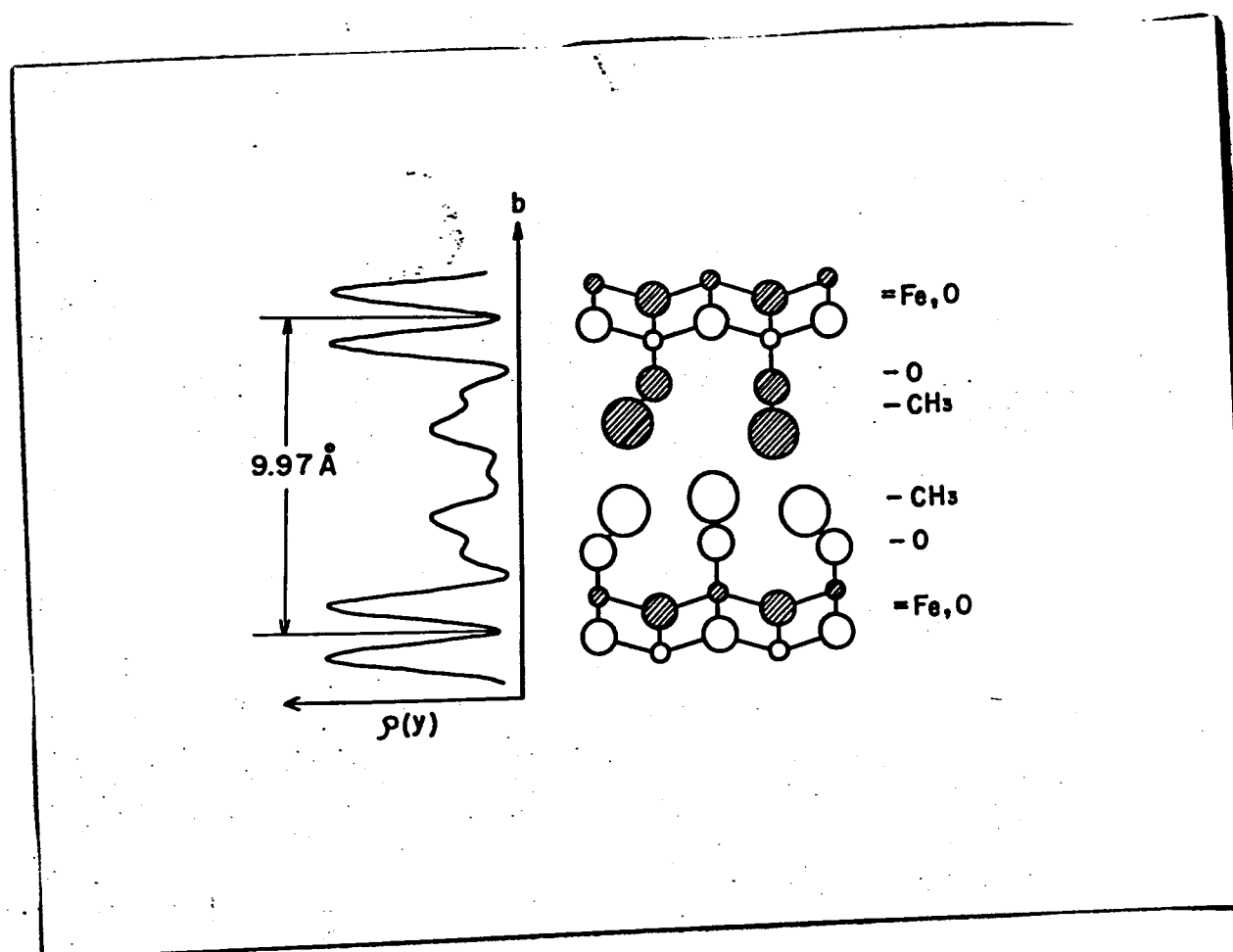


Fig. 24. One-dimensional electron-density map, obtained using diffractometry, projected on the  $b$ -axis and schematic representation of the structure of  $\text{FeOOCH}_3$ . A small central peak and a larger peak intensity for carbon than for oxygen in the electron-density projection may arise from a small amount of AP molecules remained in the last product.

This fact indicates that  $\text{FeOOCH}_3$  did not convert to magnetite at  $290^\circ\text{C}$ , but changed directly to  $\gamma\text{-Fe}_2\text{O}_3$ . The easy conversion from  $\text{FeOOCH}_3$  to  $\gamma\text{-Fe}_2\text{O}_3$  is considered to be due to the similar atomic arrangements of oxygen and iron ions between  $\text{FeOOCH}_3$  and  $\gamma\text{-FeOOH}$ . The dense packing of the methyl group,  $\text{CH}_3^-$ , in the interlayer region caused slight expansions of a and c axes from 3.78 and  $3.30\text{\AA}$  of  $\text{FeOCl}$  to 3.83 and  $3.99\text{\AA}$  of  $\text{FeOOCH}_3$ .

In conclusion, methanol is grafted to FeO layer of  $\text{FeOCl}$  substituting Cl with  $\text{CH}_3\text{O}$  with an aid of AP. The obtained product  $\text{FeOOCH}_3$  has a crystal structure derived from  $\text{FeOCl}$  and  $\gamma\text{-FeOOH}$ .

62

4 - 3. Graft Type Intercalation Compound ---  $\text{FeO}(\text{O}_2\text{C}_2\text{H}_4)_{1/2}$

4 - 3 - 1. Experimental Section

Well ground  $\text{FeOCl}(\text{AP})_{1/4}$  was soaked in ethylene glycol with a small amount of AP in a sealed glass tube. The addition of AP was important in order to complete the reaction of  $\text{FeOCl}(\text{AP})_{1/4}$  with ethylene glycol (hereafter denoted as EG). The duration of the reaction was about a week at  $110^\circ\text{C}$ . The reaction product was a brown crystal. It was washed with acetone until silver chloride test was negative. Analytical methods were almost the same as those used for  $\text{FeOOCH}_3$ .

#### 4 - 3 - 2. Results and Discussions

$\text{FeOCl}(\text{AP})_{1/4}$  is a sorption type compound with the basal spacing of  $13.57\text{\AA}$ . The structure and properties of this compound have already been given in Chapter 3. The reaction product of  $\text{FeOCl}(\text{AP})_{1/4}$  with EG was examined by x-ray diffractometry. The interlayer distance was  $14.5\text{\AA}$  for the obtained complex before washing with acetone. The basal spacing was reduced to  $10.89\text{\AA}$  when the product was washed to remove free EG. The linewidths of the basal reflections were broadened because of a small amount of EG molecules still remained in the interlayer region. The sharpness of the lines was recovered by heating the product at  $100^\circ\text{C}$  for 3 hrs, but the spacing did not change. The interlayer distance did not reexpand to  $14.5\text{\AA}$  even if the contracted complex was dipped again in EG. Measurements mentioned below were done for the finally contracted sample.

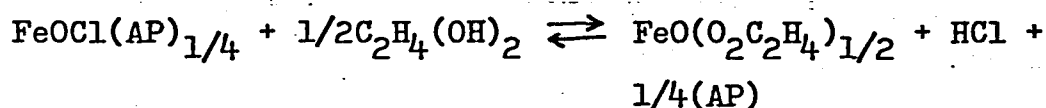
C, H, and N were analyzed by the usual method for organic analysis. Fe content was determined by atomic absorption. The results of the chemical analyses are given in Table 6. Only a trace amount of nitrogen was detected. Chlorine was absent in the product because Beilstein's test was negative. These results suggest that  $\text{FeOCl}(\text{AP})_{1/4}$  complex has lost its chloride ions and the intercalated AP molecules during the reaction with EG. Under a supposition that EG molecules

Table 6. Chemical analysis data (Weight percent) for  
 $\text{FeO}(\text{O}_2\text{C}_2\text{H}_4)_{1/2}$ .

Element	Fe	C	H	N	O
Obsd value	54.2	11.61	2.21	---	32.0
Calcd value	54.82	11.78	1.98	0.00	31.43



do not decompose during the reaction, the carbon content gives a glycol/Fe ratio of 0.50. Thus the chemical formula of the product is evaluated to be  $\text{FeO}(\text{O}_2\text{C}_2\text{H}_4)_{1/2}$ . Observed values of chemical analysis are fairly in good agreement with a calculated one for  $\text{FeO}(\text{O}_2\text{C}_2\text{H}_4)_{1/2}$ . HCl produced after the reaction;



was qualitatively detected in the reaction system.

Figure 25 shows a data of differential thermal analysis. A large exothermic peak and 23% weight loss are observed at about 300°C, but there is no drastic change below this temperature for both TG and DTA. This fact points that the intercalated organic compound is strongly bonded to the inorganic layer. Sample calcined at about 350°C showed strong magnetism. This magnetism would be due to the produced  $\gamma\text{-Fe}_2\text{O}_3$  which was detected by x-ray diffractometry of the heated sample. The observed weight loss at 300°C agrees well with the calculated ignition loss of 22% under a supposition that  $\text{FeO}(\text{O}_2\text{C}_2\text{H}_4)_{1/2}$  changes to  $\text{Fe}_2\text{O}_3$ .

The Mössbauer spectrum of  $\text{FeO}(\text{O}_2\text{C}_2\text{H}_4)_{1/2}$  consisted of a quadrupole doublet at room temperature. The pertinent parameters are summarized in Table 7, with those of  $\text{FeOCl}$ . Isomer shift values are almost the same for both compounds.

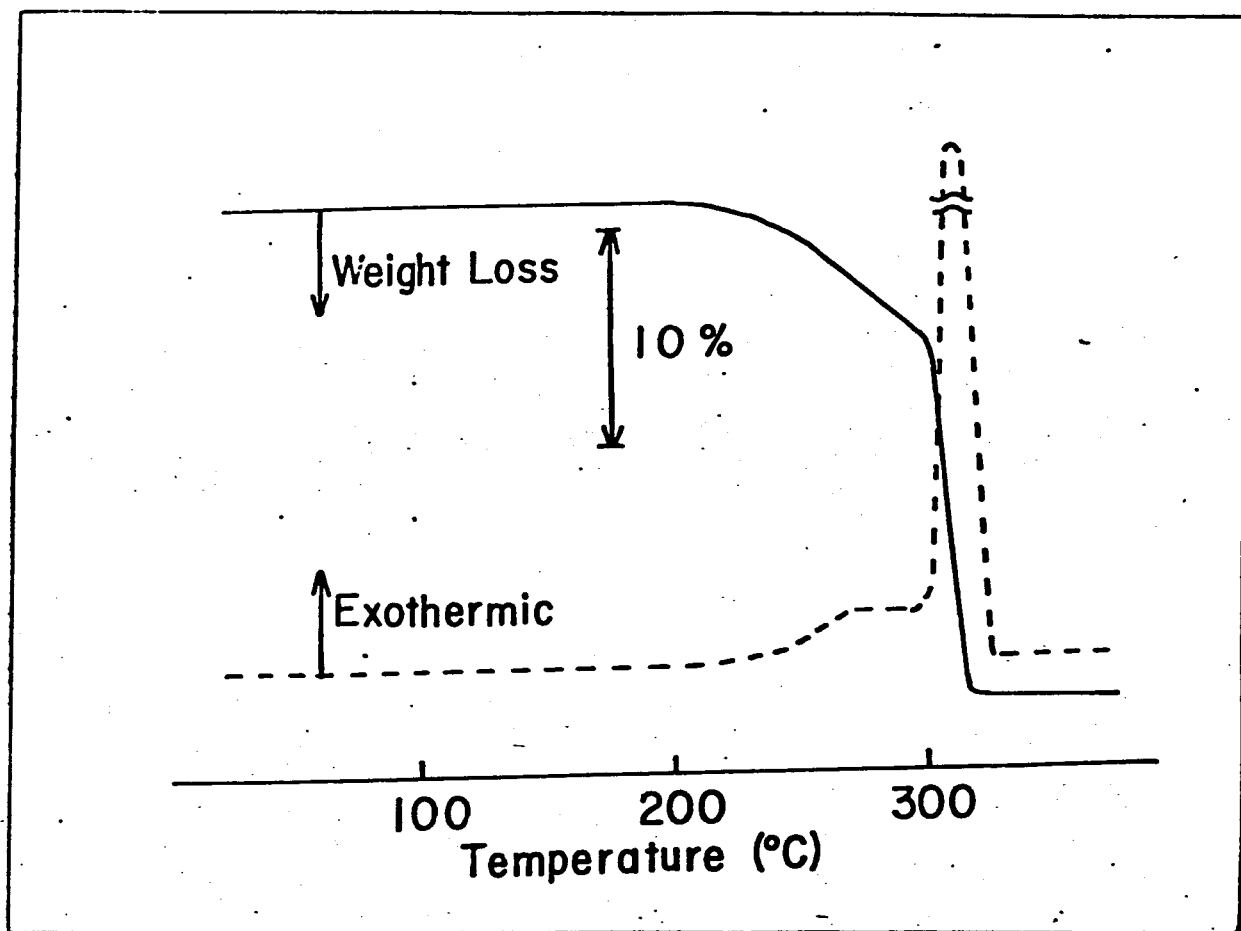


Fig. 25. Differential thermal analysis (dotted line) and thermogravimetry (solid line) of  $\text{FeO}(\text{O}_2\text{C}_2\text{H}_4)_{1/2}$ .

Table 7. Mossbauer parameters (mm/s) of  $\text{FeO}(\text{O}_2\text{C}_2\text{H}_4)_{1/2}$  and  $\text{FeOCl}$ .

	Isomer shift	Quadrupole splitting
$\text{FeOCl}$	0.40	0.92
$\text{FeO}(\text{O}_2\text{C}_2\text{H}_4)_{1/2}$	0.38	0.59

28

All Fe ions in the product are ferric. Quadrupole splitting (Q.S.) of  $\text{FeO}(\text{O}_2\text{C}_2\text{H}_4)_{1/2}$  is 0.59 mm/s and is much smaller than 0.92 mm/s for FeOCl. This reduction of Q.S. value corresponds to an improvement of crystal field symmetry around the Fe atom. This higher symmetry would be produced by the replacement of chloride ions of FeOCl with oxygen ions of EG as in the case of  $\text{FeOCH}_3$ . Fuls et al. obtained an iron alkoxide by the reactions of iron oxides with glycerol at 245 °C (50). But their product contained ferrous and ferric ions together. In the present study, the reaction of  $\text{FeOCl}(\text{AP})_{1/4}$  with EG was carried out at 110 °C. Mössbauer result showed that ferric ions in the starting material were not reduced during the reaction.

The infrared spectrum of this compound had characteristic absorptions for ethylene glycol in the region below  $1500\text{ cm}^{-1}$ , but none for O-H above  $3000\text{ cm}^{-1}$  as shown in Fig.26.

These features of the spectrum show that this compound certainly contains EG, but that the EG molecules are not free in the host lattice. There are split absorptions of C-O stretching vibrations at about  $1050\text{ cm}^{-1}$ . Miyake also observed the splitting of C-O bands between 1000 and  $1100\text{ cm}^{-1}$  into several components in nickel and cobalt complexes of ethylene or diethylene glycols (52).

There have been reports of splitting C-O vibration absorptions on alkoxides, but the origin is not well known (50,53).

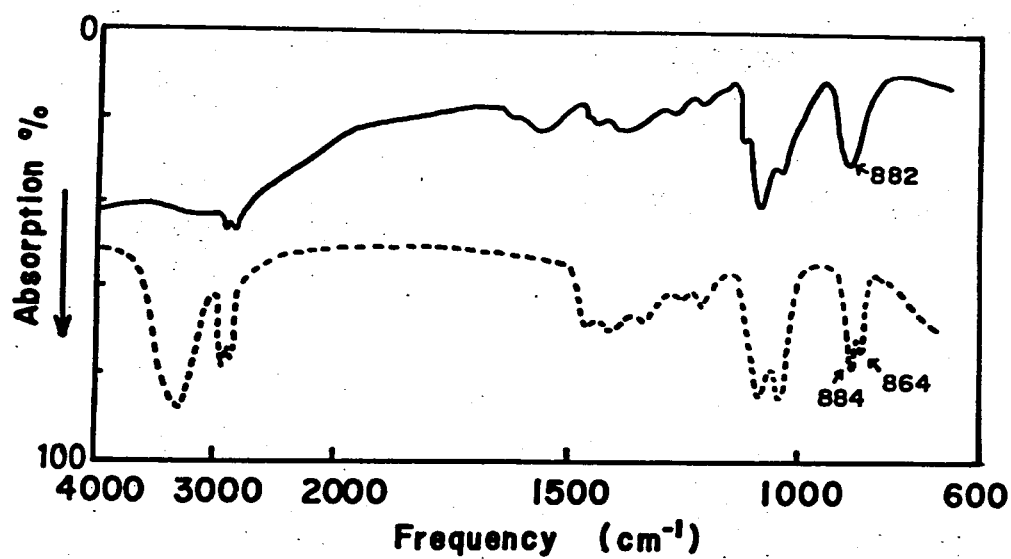


Fig. 26. Infrared spectra of  $\text{FeO}(\text{O}_2\text{C}_2\text{H}_4)_{1/2}$  (solid line) and free ethylene glycol (dotted line).

The spectrum of  $\text{FeO}(\text{O}_2\text{C}_2\text{H}_4)_{1/2}$  has an extra absorption at about  $1600\text{ cm}^{-1}$ , which is not observed for EG. The origin of this absorption is not known, but spectra of  $\gamma\text{-FeOOH}$  and  $\text{FeOCl}$  have this absorption in the same region (54). It would be related to the vibration of the host FeO double layer.

From these several facts, it is concluded that a new organic derivative  $\text{FeO}(\text{O}_2\text{C}_2\text{H}_4)_{1/2}$  having a crystal structure derived from that of  $\text{FeOCl}$  is obtained. Ferric ions are octahedrally coordinated by oxygens. EG is directly bonded to the FeO double layers by its own oxygen atoms. Two model-structures shown in Fig.27 are proposed for the product as EG molecules would not break to pieces. One is an interlayer bridging model illustrated in Fig.27(a), and the other is an intralayer bonding indicated in Fig.27(b). Bond lengths are evaluated to be about  $1.2\text{\AA}$  for C-O bond,  $1.3\text{\AA}$  for C-C bond, and  $1.5\text{\AA}$  for Fe-O bond when they are projected to the direction vertical to the layer. Suppose the EG molecules bridge two adjacent FeO layers as shown in Fig. 27(a). The interlayer distance is estimated to be below  $8.2\text{\AA}$  even if the molecules have the trans-configurations in order to have the longest molecular lengths possible. On the contrary it is about  $11.0\text{\AA}$  if EG molecules coordinate to Fe ions within the same layer as shown in Fig. 27(b). Methyl groups belonging to an upper and a lower layers.

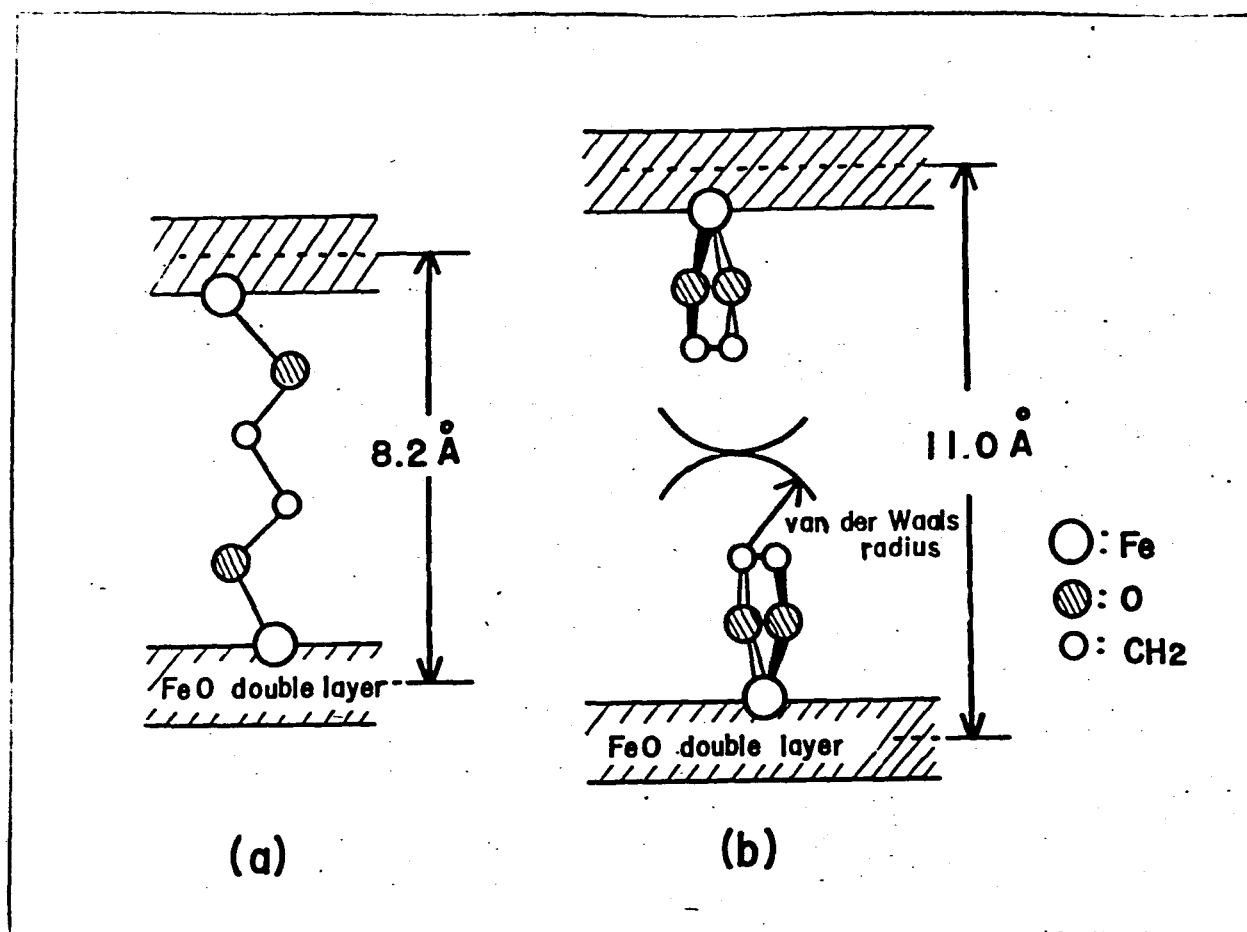


Fig. 27. Model structures for  $\text{FeO}(\text{O}_2\text{C}_2\text{H}_4)_{1/2}$ .  
 (a) and (b) represent the interlayer bridging and the intralayer bonding respectively.

contact each other in a distance of twice of van der Waals radius. The observed interlayer distance was  $10.89\text{\AA}$  after excess EG was removed by washing with acetone. Thus the intralayer bonding model given in Fig. 27(b) is more probable in this case. The basal spacing of the product contracted from  $14.5\text{\AA}$  to  $10.89\text{\AA}$  when the sample was washed with acetone. The difference of  $3.6\text{\AA}$  almost corresponds to a twice of the van der Waals radius of methyl group. When  $\text{FeO}(\text{O}_2\text{C}_2\text{H}_4)_{1/2}$  is before washing with acetone, it probably contains a monolayer of an excess amount of EG molecules lying parallel to the host layer.

The intralayer bonding structure is also supported by infrared data. An absorption at  $864\text{ cm}^{-1}$  appears only for free EG as seen in Fig. 26. The assignment of this absorption has been confused for a long time. Kanbayashi and Nukada described the dependence of the vibrational band of EG on kinds of solvents and temperature. They concluded that only the gauche-configuration is present in all states of the compound (55). They assigned this absorption to the A-type rocking mode of the  $\text{CH}_2$ -group. On the other hand, Sawodny et al. allotted this absorption to the C-C valence vibration shown in Fig. 28 from the comparison of IR and Raman spectra of  $\text{DO}(\text{CH}_2)_2\text{OD}$  and  $\text{HO}(\text{CH}_2)_2\text{OH}$  (56). In the intralayer bonding model, EG molecules have the gauche-



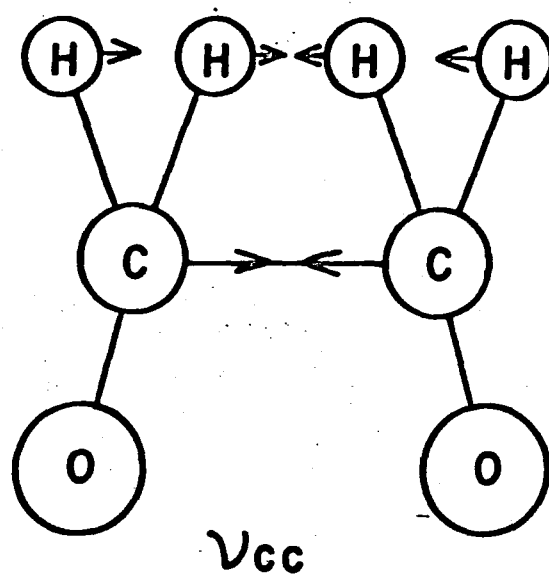


Fig. 28. C-C valence vibration of ethylene glycol described by Sawodny et al.(56).

configuration and are fixed to FeO double layer by their own oxygen ions. Thus neither A-type rocking nor C-C valence vibration would occur in the obtained complex. Then the spectrum of the complex lacks the absorption at about  $864\text{ cm}^{-1}$ .

To gain a better insight into this structure, a one-dimensional electron density projection on the b-axis was synthesized using seven (0k0) x-ray reflections of  $\text{FeO}(\text{O}_2\text{C}_2\text{H}_4)_{1/2}$ . The result is illustrated in Fig. 29. The sign of each reflection was determined by considering the contribution of Fe and O in the skeleton of inorganic layer. There are five peaks in the interlayer region except for those of FeO layer. The partial crystal structure of  $\text{FeO}(\text{O}_2\text{C}_2\text{H}_4)_{1/2}$  is deduced as shown in Fig. 29. The ionized glycol molecules,  $(\text{O}_2\text{C}_2\text{H}_4)^{2-}$ , coordinate to ferric ions by their own two oxygen atoms in the product. The ferric ions are octahedrally surrounded by six oxygens. This improved symmetry around ferric ion results in a smaller Q.S. value than that for  $\text{FeOCl}$  in which ferric ions are surrounded by four oxygens and two chlorines. Two kinds of ferric ions should be observed in the Mössbauer spectrum because the ionized glycol molecules coordinate only to every second ferric ions. One is chelated by two oxygen atoms in the same  $(\text{O}_2\text{C}_2\text{H}_4)^{2-}$  ion, and the other is coordinated with two oxygens in different  $(\text{O}_2\text{C}_2\text{H}_4)^{2-}$  ions. However the spectrum could not be clearly divided into two sets of doublets, probably because the

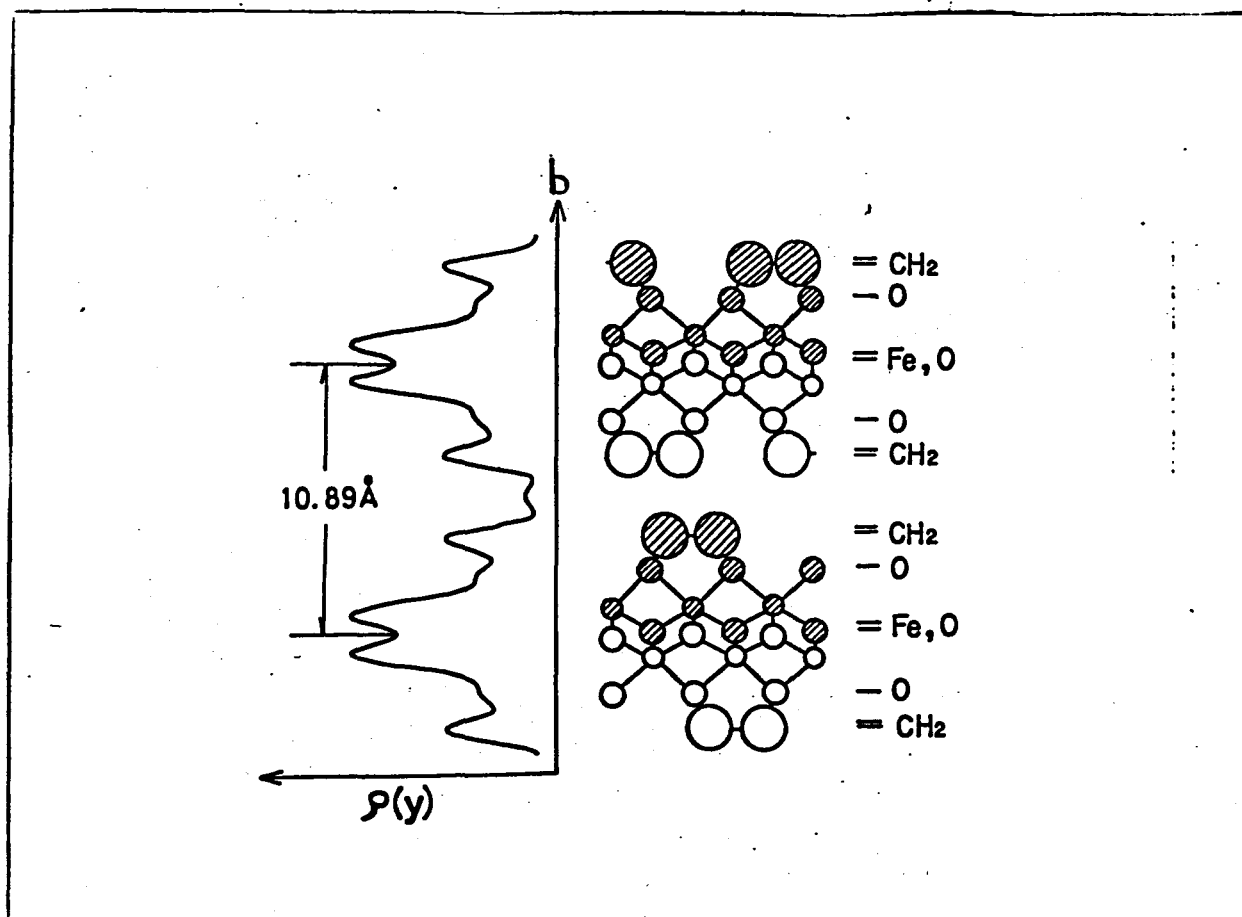


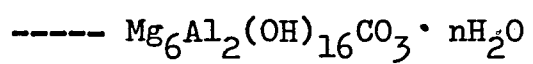
Fig. 29. One-dimensional electron density map projected on b-axis obtained by x-ray diffractometry and schematic representation of partial structure of  $\text{FeO}(\text{O}_2\text{C}_2\text{H}_4)_{1/2}$ . Open and shaded circles are  $x=0$  and  $1/2$ , respectively. A small central peak in the map may arise from the remained EG and AP in the final product.

ethylene group does not have much effect on ferric ion.

In final, a new type organic derivative of  $\text{FeOCl}$  has been prepared. Ethylene glycol molecules are grafted to  $\text{FeO}$  double layer within the same plane, and they are chelated to ferric ions.

## CHAPTER 5.

PREPARATIONS AND PROPERTIES OF ANION EXCHANGE  
TYPE INTERCALATION COMPOUNDS



## 5 - 1. Introduction

Electrically neutral substances such as amine and pyridine have already been intercalated into interlayer van der Waals gap of lamellar compounds  $\text{FeOCl}$  and transition metal dichalcogenides (1). They form charge transfer type complexes such as  $\text{FeOCl}(\text{Py})_{1/4}$ . Montmorillonite also intercalate some kinds of neutral molecules such as alcohol substituting its interlayer water (3,4). It has exchangeable cations in its interlayer space with variable amount of water. Both the interlayer cations and the adsorbed water are respectively replaced with organic cations and molecules in montmorillonite. Are there any examples of intercalations of exchangeable anions?  $\text{FeOOCCH}_3$  is a compound where  $\text{CH}_3\text{O}^-$  ion is intercalated between  $\text{FeOCl}$  layers. In this case, the anion is firmly grafted to the host layer. It is not exchangeable.

Montmorillonite has negative charge in the host aluminosilicate layer because aluminum in the octahedral site is partly substituted with magnesium. Exchangeable cations are in the interlayer region to balance the remained charge. The opposite situation to montmorillonite will give us an example of exchangeable anion intercalation. If a part of  $\text{Mg}^{2+}$  in the layer compound  $\text{Mg}(\text{OH})_2$  is replaced by  $\text{Al}^{3+}$ , the layer of  $\text{Mg}(\text{OH})_2$  becomes positively charged. The charged layers are interleaved with anions to balance the charge.

Hydrotalcite  $\text{Mg}_6\text{Al}_2(\text{OH})_{16}\text{CO}_3 \cdot n\text{H}_2\text{O}$  is a natural mineral of this kind (20). Its structure is schematically shown in Fig. 30. General formula is given as  $[\text{M}_{1-x}^{2+} \text{M}_x^{3+}(\text{OH})_2]^{+x} (\text{x/n})\text{R}^{-n} \cdot y\text{H}_2\text{O}$  for this type of compounds. There are many natural minerals and synthetic products with  $\text{M}^{2+} = \text{Mg}, \text{Fe}, \text{Ni}, \dots$ ,  $\text{M}^{3+} = \text{Al}, \text{Fe}, \text{Cr}, \dots$ ,  $\text{R}^{-n} = \text{CO}_3, \text{SO}_4, \text{NO}_3, \dots$ . The ratio  $\text{M}^{2+}/\text{M}^{3+}$  is generally near 3.0 but it varies over a range of values. The range of this ratio is not yet precisely known (23). Properties of the materials probably change with the remained charge in the host layer. Exchangeability of the interlayer anion also must be studied. The hydroxide layers can be stacked with three layers/unit cell and rhombohedral symmetry or with two layers/unit cell and hexagonal symmetry. Less symmetrical stacking sequences also can occur, particularly in synthetic products prepared at normal temperature.

Important questions not fully solved relate to the extent of the variation of the cation ratio,  $\text{M}^{2+}/\text{M}^{3+}$ , order-disorder of the cations in the octahedral sheet, the organization of the interlayer anions and water molecules, the exchangeability of the anions, and the variability of the interlayer spacings.

This chapter is concerned with the range of  $\text{Mg}/\text{Al}$  and  $\text{Ni}/\text{Al}$  ratios compatible with this type of structure, and the variation of basal spacing with layer charge and with different interlayer anions. Anion exchange is also examined on natural hydrotalcite. The behavior of the structures with

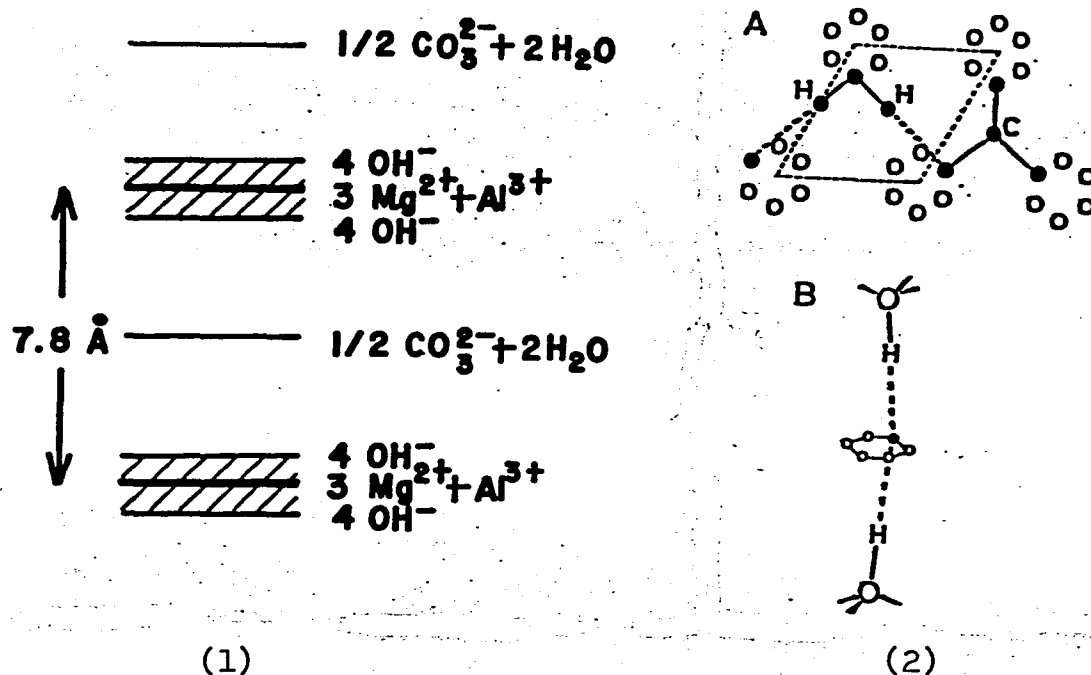


Fig. 30. (1): Layer sequences in hydrotalcite. The bricite-like layers are shaded.

(2): The interlayer of  $\text{CO}_3^{2-}$  ions and  $\text{H}_2\text{O}$  molecules in hydrotalcite. A: Plane view, showing arrangement of oxygen sites, assuming these to occur in group of 6. Open circles represent empty sites. Typical situations of a  $\text{CO}_3^{2-}$  group and of a  $\text{H}_2\text{O}$  molecule are shown. Broken lines denote the unit cell ( $a=3.1\text{\AA}$ ).

B: Special relationship between any of the oxygen sites in the interlayer and the  $\text{OH}^-$  groups above and below it, showing the possibility of hydrogen bonding to an occupied site.



respect to humidity and temperature is studied on the products prepared by the exchange of anions.

102

5 - 2. Crystal-chemical Properties of Mg,Al and Ni,Al  
Hydroxy-perchlorate and Hydroxy-carbonate

5 - 2 - 1. Experimental Section

Preparation.

Preliminary experiments using mixed solution of Mg (or Ni) and Al chlorides and slow addition of NaOH followed closely the previous experiments of Gastuche et al. (23). Perchlorate solutions are used because of the uncertainty regarding the role of  $\text{Cl}^-$  ions which might occupy positions in the octahedral layers as well as in the interlayer. The perchlorate ion is detected readily by infrared analysis and can be present only in interlayer positions.

Mixed solution of Mg (or Ni) and Al perchlorates, 0.1M in total cation content, was reacted at about pH 10 with NaOH solutions added drop-wise and with vigorous stirring. To reduce (or eliminate) the adventitious role of dissolved  $\text{CO}_2$ , solutions were prepared with boiled distilled water cooled in stoppered flasks. Reaction was carried out for periods of 5 - 7 days in closed plastic vessels, except when opened to add NaOH and to check pH. Products were washed with boiled distilled water after centrifugation, dried overnight at 55 °C in normal atmosphere, and stored in stoppered tubes. The precautions taken reduced but did not eliminate  $\text{CO}_3$  anions from the products. The results, however, proved

103

interesting in other respects. The use of plastic vessel was important. Products prepared initially in glass vessel were contaminated with amorphous silica, revealed by micro-probe test; better crystalline products were obtained when silica was eliminated.

The initial products, which contained both  $\text{ClO}_4^-$  and  $\text{CO}_3^{2-}$  anions, were treated with 0.1M sodium carbonate solution, or with 1/100 perchloric acid solution with a view to obtain single anion products.

Anion exchanged forms of hydrotalcite were prepared from powders ground to pass 120 mesh sieve by treatment with 1/100 HCl, 1/100  $\text{HClO}_4$ , and 1/100 and 1/1000  $\text{H}_2\text{SO}_4$ . Samples were examined after exposures to various relative humidities ranging from 100% to near 0% at room temperature, and after 3 hrs heat-treatments at temperature up to 400 °C in normal atmospheres.

#### Product examination.

The principal methods of examination have been x-ray powder diffraction using both random and oriented powder mounts, transmission infrared spectroscopy using the KBr pellet technique, and atomic absorption analysis of solution and products to determine Mg/Al and Ni/Al ratios. Stability of various anion phases with respect to temperature and humidity was studied by following the changes of the basal spacings after various treatments.

## 5 - 2 - 2. Results and Discussions

The proportions of Al in the initial solutions and in the crystalline double hydroxides are conveniently represented by the mole fractions  $R(\text{sol})$  and  $R(\text{cryst})$ ,  $R = \text{Al}/(\text{Al} + \text{M})$  with  $\text{M} = \text{Mg}$  or  $\text{Ni}$ . It is important to distinguish between these ratios and particularly to use  $R(\text{cryst})$  when considering the compositions of the solids. Failures to make this distinction has already led to some confusion (23).

The double hydroxides are formed from solutions in the range of  $R(\text{sol})$  20% - 35% (approximate values) and outside this range mixtures are formed with  $\text{Mg}, \text{Ni}$  or  $\text{Al}$  hydroxides. Data for the  $\text{Ni}, \text{Al}$  system are shown in Fig. 31. The intensities  $I_r$  of x-ray reflections of (001) from  $\text{Ni}(\text{OH})_2$  with brucite structure and of (001) from  $\text{Al}(\text{OH})_3$  mainly with the bayerite structure tend to zero near  $R(\text{sol}) = 23\%$  and  $37\%$ . Similar results have been obtained for  $\text{Mg}, \text{Al}$  system and in most respects they confirm the earlier data of Gastuche et al. (23). The double hydroxides are recognized easily in the x-ray diffraction patterns by their distinctive basal spacings. Only the products are formed in the composition range stippled in Fig. 31.

Figure 32 shows the relations between  $R(\text{cryst})$  and  $R(\text{sol})$  for the  $\text{Mg}, \text{Al}$  and  $\text{Ni}, \text{Al}$  systems and the corresponding data

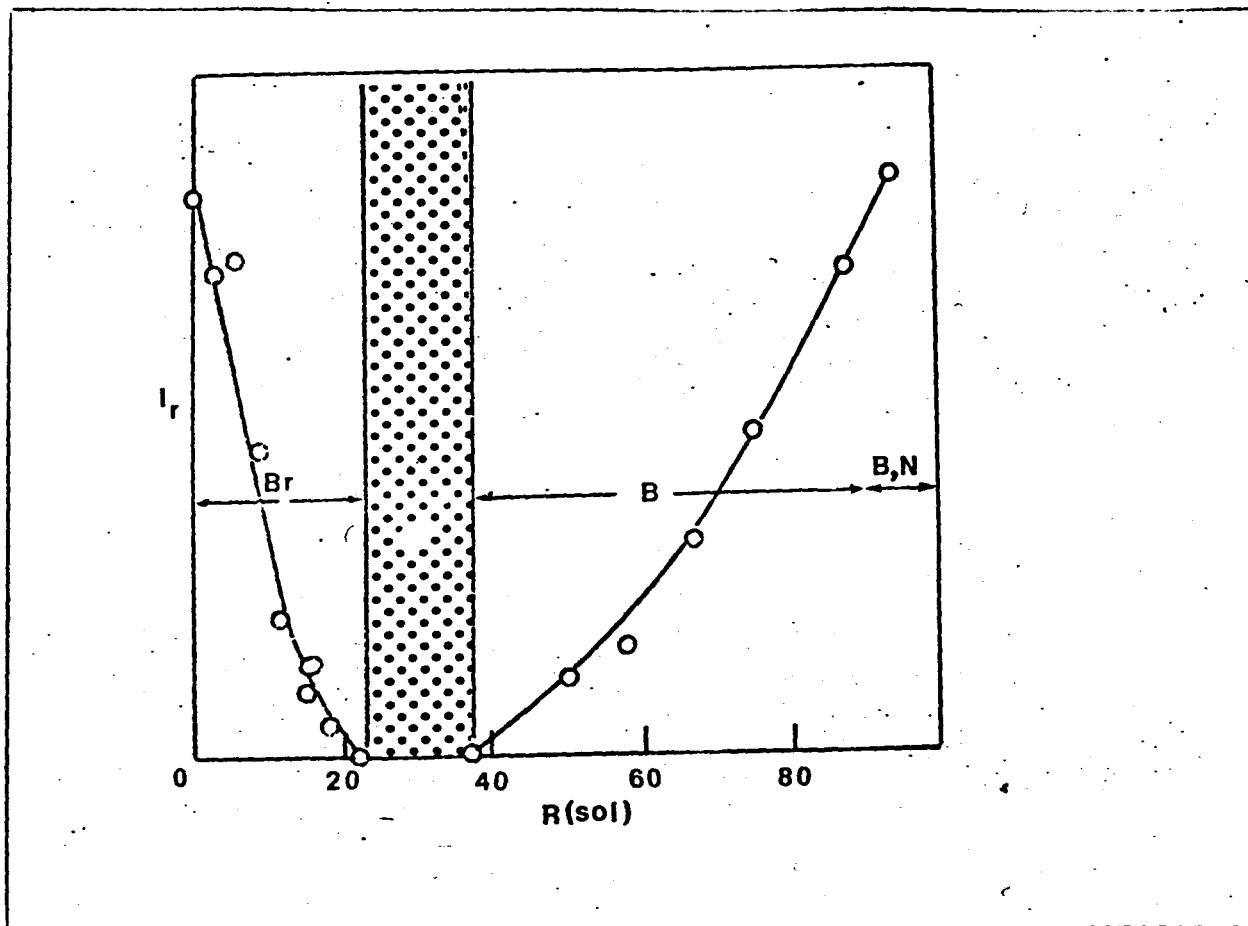


Fig. 31. Reflected x-ray intensity,  $I_r$ , plotted against  $R(\text{sol}) = \left[ \frac{\text{Al}}{\text{Al} + \text{Ni}} \right] \times 100$ . Hydroxide phases:  $\text{Br} = \text{Ni}(\text{OH})_2$  with brucite structure,  $\text{B} = \text{Al}(\text{OH})_3$  with bayerite structure,  $\text{B,N}$  = mixture of bayerite and nordstrandite. Stipled area = zone where only mixed Ni,Al hydroxy phases are formed.

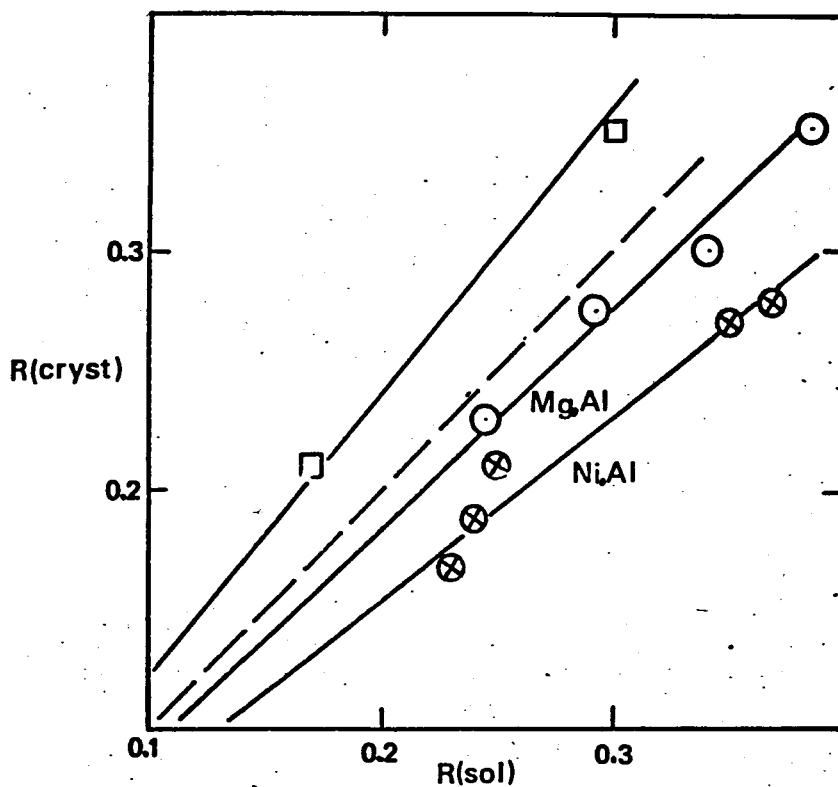


Fig. 32.  $R(\text{cryst})$  vs.  $R(\text{sol})$ .  $R = \text{Al}/(\text{Al} + \text{M})$  and  $\text{M} = \text{Mg}$  or  $\text{Ni}$ . Squares indicate data of Gastuche et al. (23) for  $\text{Mg,Al}$  system. Dashed line corresponds to  $R(\text{cryst}) = R(\text{sol})$ . All data are for carbonate-saturated systems. Straight lines are drawn to pass through the origin of coordinates.

of Gastuche et al. for the Mg,Al system (23). The dashed line drawn at  $45^\circ$  to the axes corresponds to  $R(\text{cryst}) = R(\text{sol})$ .

The present data indicates less Al in the products than in the solutions, whereas Gastuche et al. found more Al in the products. There is no obvious explanation for this difference unless it arises from the particular experimental conditions; Gastuche et al. used chloride solutions and long periods of washing by dialysis, and, in this particular experiment, perchlorate solutions, much shorter washing periods and a partial elimination of  $\text{CO}_3$  ion from the systems were used.

The composition range of Mg,Al hydroxides after carbonation extends from  $R(\text{cryst})=23\%$  to  $35\%$  in the present experiments and  $21.5\%$  to  $35.0\%$  in those of Gastuche et al.. In terms of the Mg:Al ratio, these data correspond to a range from  $3.5:1$  to  $1.86:1$ . For the Ni,Al system after carbonation, The  $R(\text{cryst})$  range is from  $17\%$  to  $28\%$  or Ni:Al ratios from  $4.9:1$  to  $2.6:1$ .

There is general agreement that the highest proportion of  $\text{M}^{3+}$  ion is near  $33\%$  which corresponds to a ratio  $\text{M}^{2+}:\text{M}^{3+}$  of  $2:1$ . There is less certainty regarding the lowest proportion, but it is probably near  $20\%$  or a ratio  $\text{M}^{2+}:\text{M}^{3+}$  near  $4:1$ .

Figure 33(a) shows the distribution of Mg ions in an octahedrally coordinated layer of the brucite structure.

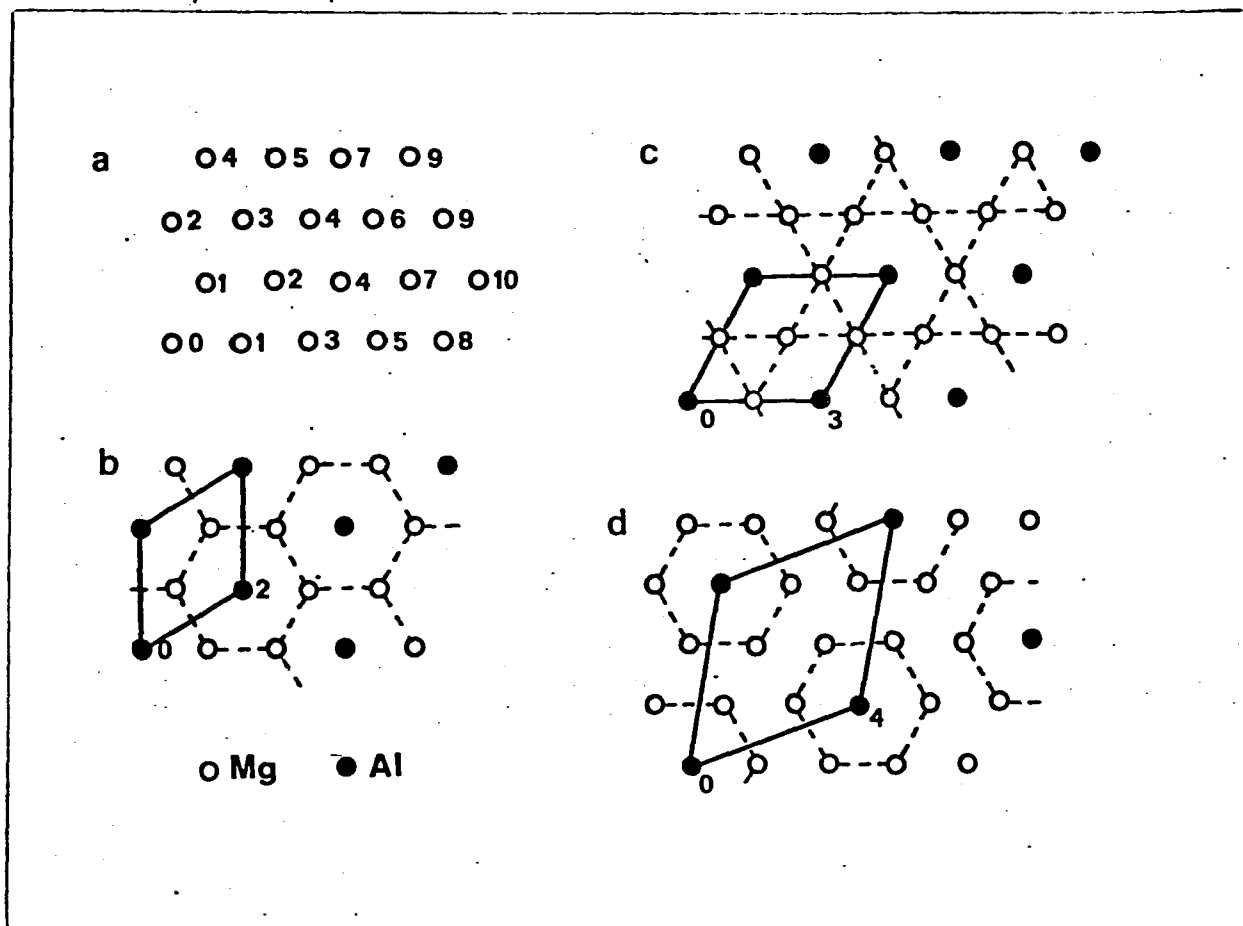


Fig. 33. Possible distributions of  $Mg^{2+}$  ions, open circles, and  $Al^{3+}$  ions, solid circles, in octahedral layer structure. (a) arrangement in brucite, (b)  $Mg:Al=2:1$ , (c)  $Mg:Al=3:1$ , (d)  $Mg:Al=6:1$



Substitution of  $\text{Al}^{3+}$  for  $\text{Mg}^{2+}$  creates a center of resultant positive charge. Substitutions are likely to be as far as possible from each other because of mutual repulsions. ... The cation positions in Fig.33(a) are numbered 1,2,3,...at progressively greater distances from the cation 0 at the origin position. Let the first substitutions of Al for Mg take place at the origin. Substitution at position 1 is unlikely because this would place two Al ions in adjacent octahedra. The next nearest substitution is in position 2 and if this mutual arrangement of Mg and Al ions is continued, the distribution shown in Fig.33(b) is obtained. Each Al ion is now surrounded by six Mg ions, the ratio Mg:Al is 2:1, and the hexagonal a-parameter is  $\sqrt{3}a'$ , where  $a'$  refers to the sub-cell which makes no differentiation between the two cations. A simple explanation can be given for the maximum proportion of  $\text{M}^{3+}$  ions. Although evidence has been obtained for a supercell with  $a=\sqrt{3}a'$ , it is not invariably obtained (58,59). Then the question about short range vs. long range order arises. Fig. 33 (b) shows that although each Al is ringed by six Mg, the Al ions are not fully screened from each other.

The next-nearest distribution of Al ions is shown in Fig.33(c), which is developed from the initial positions 0 and 3. The ratio Mg:Al is now 3:1, the supercell  $a=2a'$ ,

and a Mg ion is located between every pair of Al ions, so that they are now fully screened from each other. This 3:1 ratio corresponds to that found in many mixed hydroxide minerals. Again, direct evidence is not always obtained for the supercell and a question of local order versus long-range order arises.

The process by which Fig.33(b) and (c) have been developed can be continued. The next-nearest distribution of Al ions, shown in Fig.33(d), starts from positions 0 and 4 in Fig.33(a). The Mg:Al ratio is now 6:1 and the supercell  $a=\sqrt{7}a'$ . This proportion of Al ions is smaller than the minimum found experimentally. Each cell contains six adjacent Mg-occupied octahedra. Evidently at this stage there is a considerable chance of developing nuclei of brucite. Beyond this stage represented in Fig.33(d), other arrangements can be developed with Al ions placed increasingly further from each other and with still greater chance of development of brucite nuclei.

The above mentioned superlattices were not observed using x-ray diffraction in the present study. The initial products contained  $\text{ClO}_4^-$  as well as  $\text{CO}_3^{2-}$  as their interlayer anions. Characterization of the products was made as follows and then single anion phases were obtained exchanging the interlayer anions.

The detailed results on Mg,Al system are discussed at first. X-ray diffraction patterns with filtered Cu K $\alpha$  radiation, recorded at 1°(2 $\theta$ )/min, and infrared patterns (KBr pellet technique, 2mg of sample, 200 mg of KBr) for selected samples are shown in Fig. 34. Only these parts of the x-ray and infrared patterns are given which are relevant to the immediate discussion. The products are specified by value of R(cryst) x 100. The products change progressively from mainly perchlorate forms to mainly carbonate forms in passing from R(cryst)=23% to 37%. Since R(cryst) represents the proportion of Al ions in the products, it also measures the positive charge of the octahedral layers. Evidently the lower-charge products prefer the monovalent perchlorate ions and the higher-charge products the divalent ions.

With R(cryst)=23%, the principal diffraction peaks correspond to a basal spacing of about 9.2 $\overset{\circ}{\text{A}}$  which is characteristic of hydroxy-perchlorate forms. The infrared absorption centered near 1100 cm $^{-1}$  is attributable to the  $\nu_3$  frequency of the ClO $_4^-$  ion. As R(cryst) increases, the diffracted intensity from a spacing near 7.9 $\overset{\circ}{\text{A}}$  increases, and the infrared absorption centered near 1355 cm $^{-1}$ , attributable to the  $\nu_3$  frequency of the CO $_3$  ion, also increases. The absorption band near 1625 cm $^{-1}$ , arises from water molecules and for the most part diminishes the ClO $_4^-$  absorption diminishes. These results seems entirely

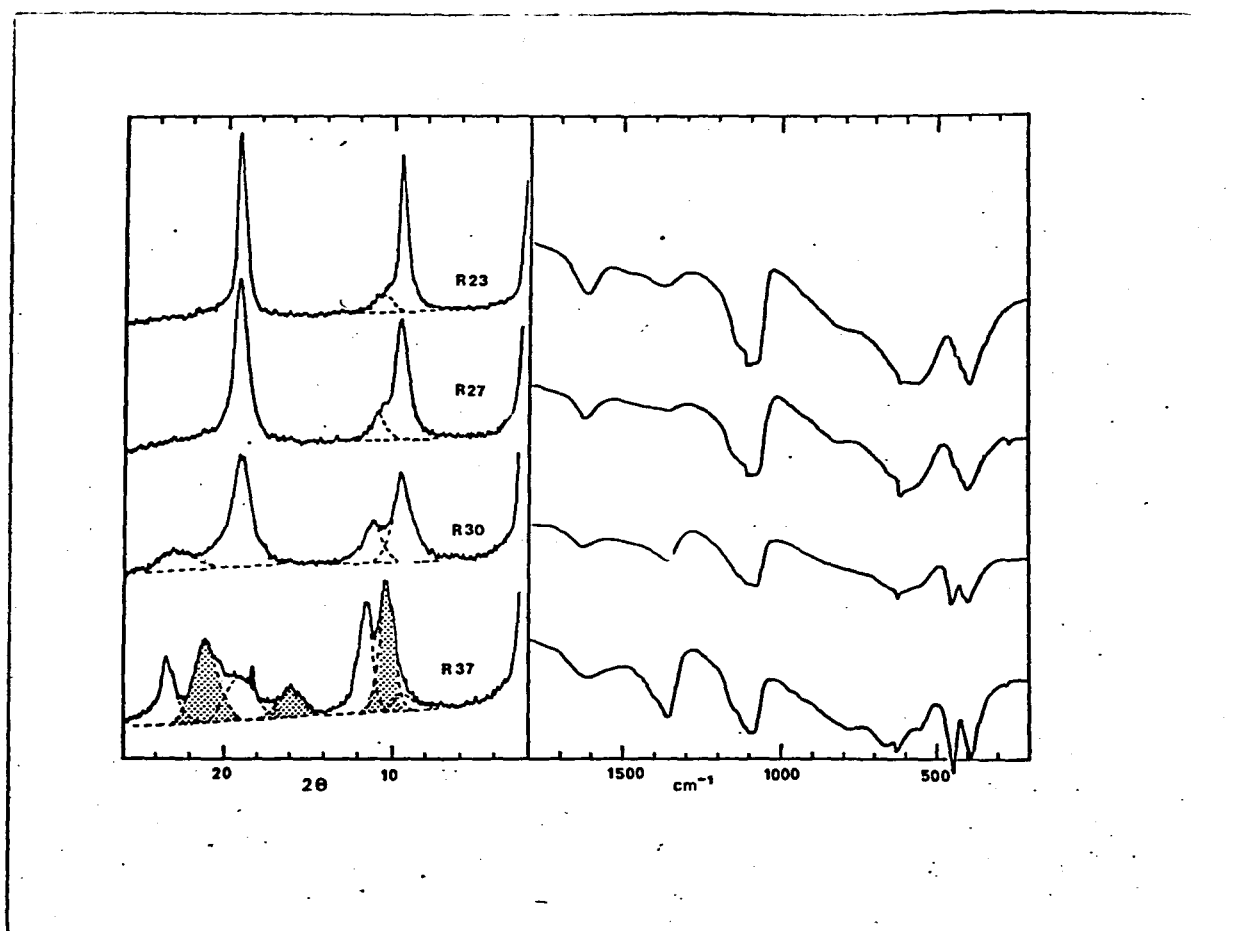


Fig. 34. X-ray diffraction (Cu K $\alpha$  radiation) and infrared absorption patterns for Mg,Al products prepared from perchlorate solutions. R values relate to crystalline products.  $R = \left[ \frac{\text{Al}}{\text{Al} + \text{Mg}} \right] \times 100$ . Stippled x-ray diffraction peaks from an inter-stratified phase. A peak shaded black is due to a trace of bayerite.

reasonable. Octahedral layers with low charge accomodate the more bulky  $\text{ClO}_4$  ions and the remaining interlayer space accomodate water molecules. Octahedral layers with high charge accept preferentially the flat triangular  $\text{CO}_3$  ions and less space is available for water molecules.

When  $R(\text{cryst})=37\%$ , the x-ray pattern shows basal reflections, stippled in Fig.34, which suggest a superlattice consisting of a regular alternation of  $9.2\text{\AA}$  and  $7.6\text{\AA}$  spacings.

The three diffraction peaks marked in Fig.34 have spacings 8.5, 5.5 and  $4.2\text{\AA}$ . If these reflections are respectively (002), (003), and (004), the corresponding  $d(001)$  values are 17.0, 16.5 and  $16.8\text{\AA}$ , with an average value  $16.8 = 9.2 + 7.6\text{\AA}$ . The (001) diffraction is not observed.

Turning again to the infrared patterns, the absorptions associated with the perchlorate and carbonate anions and water molecules change in an orderly way as  $R$  varies from 23, to 27, to 30%, but the data for  $R=37\%$  do not fit well into the sequence. The appearance of the additional phase when  $R=37\%$  probably the reason of the deviation.

The x-ray evidence indicates that in these preparations the  $\text{ClO}_4$  and  $\text{CO}_3$  anions tend to segregate rather than to mix in the same crystals or in the same layers. Gastuche et al. also obtained results suggesting mixtures of phases, which they interpreted as arising from the end compositions of the range shown by stippling in Fig.31 (23,24). By using

distinctly different anions,  $\text{ClO}_4$  and  $\text{CO}_3$ , it is shown that the mixture of phases in the present experiments corresponds to segregation of the anions.

In order to obtain single anion phase of Mg,Al hydroxide, the initial products are respectively treated with sodium carbonate and 1/100  $\text{HClO}_4$  acid. Treatment of the initial products with 0.1M sodium carbonate solution readily exchanges the  $\text{ClO}_4$  ions with  $\text{CO}_3$  ions. The resulting x-ray diffraction and infrared patterns are shown in Fig. 35. The diffraction peaks are sharp and symmetrical. Only one set of basal reflections is observed for any given value of R. The basal spacing becomes smaller as R, i.e., layer charge, increases. The infrared absorption near  $1350 \text{ cm}^{-1}$  also increases progressively with the value of R as would be expected.

To obtain Mg,Al hydroxy-perchlorates, most of the carbonate anions were removed from the initial products with a 5 hrs treatment with 1/100 perchloric acid solution. With the higher value of  $R(\text{cryst}) \simeq 30\%$ , the product initially had a basal spacing of  $11.7 - 11.8 \text{ \AA}$  probably due to water molecules as well as perchlorate ions separating the layers. At relative humidities less than about 50 %, the spacing diminishes to about  $9.2 \text{ \AA}$ , which agrees with the value found for the initial perchlorate phases (Fig.34). Bish reported similar observations for  $\text{SO}_4$  exchanged materials (51).

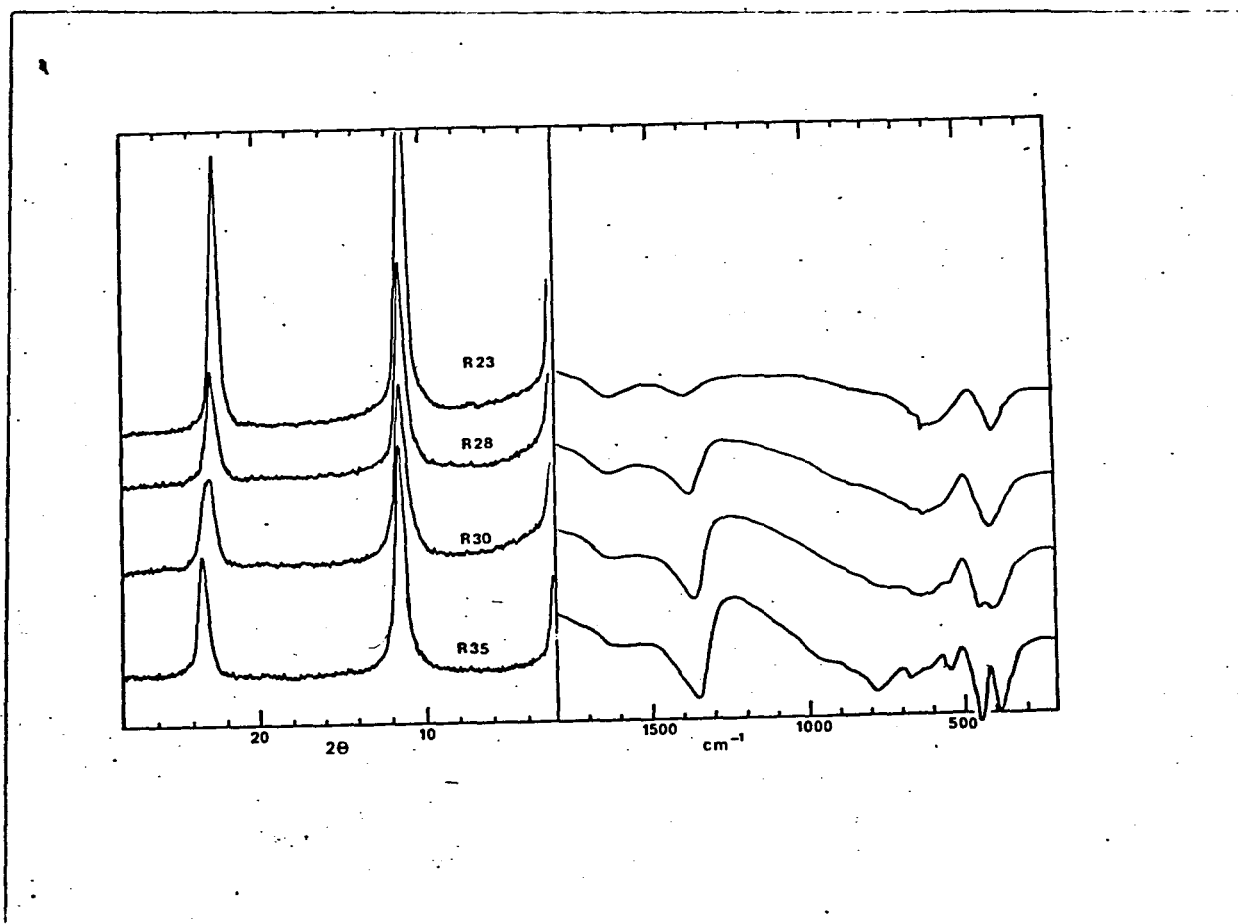


Fig. 35. X-ray diffraction (Cu  $K\alpha$  radiation) and infrared absorption patterns for Mg,Al hydroxy-carbonate phases.

Products with lower values of  $R(\text{cryst}) \approx 25\%$  gave very poor x-ray patterns after treatment with 1/100 perchloric acid solution. Only one broad basal reflection was obtained with a spacing near  $9\text{\AA}$ . It is not clear why an initial product containing mainly perchlorate ions, after treatment with perchloric acid solution deteriorated considerably. Possibly the products with low  $R(\text{cryst})$  values decompose more readily in the acid than those with high  $R(\text{cryst})$  values.

The results on Ni,Al hydroxy phases were generally similar to those for the Mg,Al phases but the diffraction patterns usually were less clearly defined. The initial products contained both perchlorate and carbonate ions. The perchlorate content decreased and the carbonate content increased as  $R(\text{cryst})$  increased. The range of  $R(\text{cryst})$  value in which only Ni,Al hydroxy products were formed, about 17 - 28 %, was somewhat different from that for the Mg,Al system, about 23 - 35 %. After carbonate treatment, the products contained only  $\text{CO}_3$  anions and the x-ray patterns showed sharper and more symmetrical peaks.

To obtain a better insight into the structure of the mixed hydroxides, lattice parameters  $a$  and  $c'$  are discussed on Mg,Al and Ni,Al hydroxy-carbonate phases. Values of  $c'$  obtained from the first and second basal reflections give



the combined thickness of the hydroxide layers and the inter-layer anions and water molecules. Diffractions based on superlattice such as  $c=2c'$  and  $3c'$  are not observed in the present results. Previous studies have shown that a spacing near  $1.5\text{\AA}$  can be indexed as (110) with hexagonal indices and the hexagonal  $a$ -parameter is  $2d(110)$  (58).

The results for the Mg,Al and Ni,Al hydroxy-carbonates are shown in Fig. 36. Also shown are results for two Mg,Al products prepared by Gastuche et al. (23), results for a natural hydrotalcite from Snarum, Norway, analyzed for Mg and Al in the present studies, and data for takovite, a mainly Ni,Al hydroxy-carbonate studied by Bish and Brindley (58). For the most part the data for the natural minerals agree well with the straight lines drawn through the observed value for the prepared products.

The decrease of the layer spacing,  $c'$ , with increase of the ratio  $R$  can be attributed to the increase in electrostatic attraction between the positive hydroxide layers and the negative interlayers. The separation of the Ni,Al and Mg,Al lines is about the same as that between the  $c$ -parameters of  $\text{Mg}(\text{OH})_2$  and  $\text{Ni}(\text{OH})_2$ . When the straight line relations are extrapolated to  $R=0$ , the resulting values of  $c'$  are  $8.52$  and  $8.37\text{\AA}$

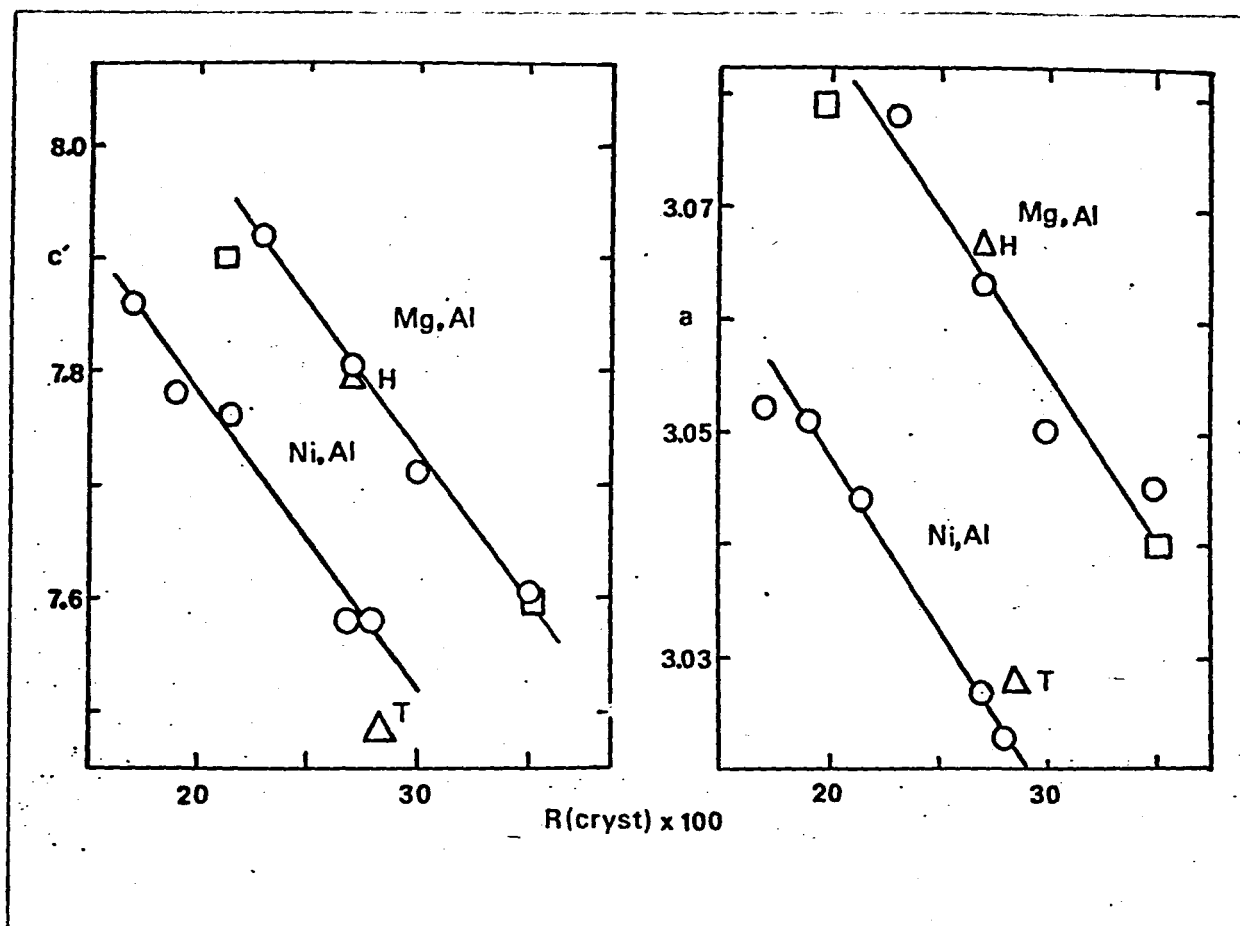


Fig. 36. Lattice parameters,  $c'$  and  $a$ , for Mg,Al hydroxycarbonate phases. Circles show present experimental data. Squares show data of Gastuche et al. (23) for the Mg,Al system. Triangles marked H, data for hydrotalcite; triangles marked T, data for takovite.

and the difference is  $0.15\text{\AA}$ . The c-parameters of  $\text{Mg}(\text{OH})_2$  and  $\text{Ni}(\text{OH})_2$ , taken from the X-ray Powder Diffraction File, are  $4.769$  and  $4.605\text{\AA}$  and the difference is  $0.164\text{\AA}$ . In other words, when the electrostatic attraction is reduced to zero, the difference in the c'-parameters is essentially the same as that between the c-parameters of the single hydroxides.

The a-parameters also decrease as R increase mainly because of the substitution of the smaller  $\text{Al}^{3+}$  ion for the larger  $\text{Mg}^{2+}$  and  $\text{Ni}^{2+}$  ions. The change of a-parameter with R,  $\Delta a/\Delta R$ , can be considered as follows: For an ideal octahedral layer the a parameter equals  $\sqrt{2}(\text{M-O})$  where M-O is the metal ion-oxygen ion distance. The mean metal ion radius,  $\bar{r}$ , is given by;

$$\bar{r} = (1-x)r(\text{M}) + xr(\text{Al}) = r(\text{M}) - x[r(\text{M}) - r(\text{Al})],$$

where M= Mg or Ni. The negative slope of a-parameter with R, or with x, is given by;

$$\Delta a/\Delta x = -\sqrt{2}[r(\text{M}) - r(\text{Al})].$$

With the Shannon-Prewitt ionic radii,  $\text{Mg}^{2+}$   $0.720\text{\AA}$ ,  $\text{Ni}^{2+}$   $0.700\text{\AA}$  and  $\text{Al}^{3+}(\text{VI})$   $0.530\text{\AA}$ , the calculated values of  $\Delta a/\Delta x$  are  $0.269$  and  $0.240$  for the Mg, Al and Ni, Al systems respectively. The experimental values from the data in Fig. 35 are respectively  $0.300$  and  $0.310$ .

The a vs. R relations, extrapolated to  $R=0$ , i.e., zero Al substitution, give extrapolated a-values of  $3.144$  and  $3.110$  for the Mg, Al and Ni, Al system respectively. The former

agrees very well with the  $a$ -parameter of  $\text{Mg}(\text{OH})_2$ ,  $3.147\text{\AA}$ ; the latter agrees less well with the value  $3.126\text{\AA}$  for  $\text{Ni}(\text{OH})_2$ . Small changes in the slope of the observed lines, however, have large effects on the extrapolated values.

Basal spacings of hydrotalcite-like compounds are affected also by the kinds of interlayer anions. The experiments on anion exchange are done on the natural hydrotalcite. Synthetic mixed hydroxide prepared at normal temperature and pressure does not crystallize so well as natural minerals. It was easily deteriorated with acid treatments. The use of acids,  $\text{HCl}$ ,  $\text{HClO}_4$  and  $\text{H}_2\text{SO}_4$  was important to obtain chloride, perchlorate and sulfate forms of hydrotalcite. Sodium salts of these anions did not exchange carbonates in hydrotalcite even if the concentrated solution of these salts were used.

Various anion forms show different basal spacings presented in Table 8. Original hydrotalcite containing  $\text{CO}_3$  had a basal spacing of  $7.8\text{\AA}$ . Decomposition began near  $220^\circ\text{C}$ . The fully chlorinated and perchlorated forms respectively show phases of the basal spacings of  $8.0\text{\AA}$  and  $9.2\text{\AA}$ . These forms are stable against humidity and temperature up to  $300^\circ\text{C}$  and  $180^\circ\text{C}$ , respectively.

Humidity and temperature sometimes affect the basal spacing. Sulfate form is an typical example. It has three different phases with various humidities. The most highly expanded phases I has a spacing of  $11.15\text{\AA}$  in atmosphere of relative humidity 50 - 100%. Under normal room conditions with humidities less than 50%, an interstratified phase II is obtained with a basal spacing of

Table 8. Basal spacings of hydrotalcite and anion exchanged hydrotalcite in relation to humidity and temperature.

Interlayer anion	Basal spacing	Conditions
$\text{CO}_3^{2-}$	7.8 Å	220 °C
$\text{Cl}^-$	8.0 Å	300 °C
$\text{ClO}_4^-$	9.2 Å	180 °C
$\text{SO}_4^{2-}$	11.15 Å (phase I)	100~50%RH at R.T.
	10 Å (phase II)	<50% RH at R.T.
	8.7~8.15 Å (phase III)	55~175 °C

near  $10\text{\AA}$ . This phase collapses to phase III, with basal spacing  $8.7\text{\AA}$  at  $55^\circ\text{C}$ . The interstratified phase can be regarded as a regular alteration of  $11.15$  and  $8.7\text{\AA}$  layers. Phase III is stable over the range  $55 - 175^\circ\text{C}$  with a spacing which changes gradually from  $8.7$  to  $8.15\text{\AA}$ .

Carbonate in natural hydrotalcite is exchanged with chloride, perchlorate and sulfate by the treatment with respective acids. As mentioned in the previous section, perchlorate ions in the synthetic product are easily exchanged with carbonates by the treatment with  $\text{Na}_2\text{CO}_3$ . Hydrotalcite mostly prefers carbonate as its interlayer anion, but its anion exchange was possible by acid treatments.

Basal spacing of hydrotalcite changes with the layer charge as shown for synthetic product. The interlayer distance of fully carbonated form increases from  $7.6\text{\AA}$  to  $7.9\text{\AA}$  with the decrease of the host layer charge. It is also affected by the kind of interlayer anion, and the amount of interlayer water especially in the case of sulfate form.

In summary hydrotalcite-like compounds having various ratios of  $\text{M}^{2+}/\text{M}^{3+} \geq 2/1$  are prepared from mixed Mg(or Ni), Al perchlorate solutions. The behavior of the interlayer anion is different with the ratio of  $\text{M}^{2+}/\text{M}^{3+}$ . The interlayer anions are exchangeable and various anion phases are obtained.

CHAPTER 6.

TOTAL DISCUSSIONS

Summarizing the results reported in the present study and the previous literatures, intercalation compounds are classified into three types according to their interactions between the host layer and the guest species as listed in Table 9. In a so-called SORPTION TYPE complex, electrically neutral materials such as water, alcohol, pyridine, amine, and so on, are absorbed into the interlayer region of host layer with weak bondings. The absorbed water in clay minerals is a typical example (3,4). It is kept in the interlayer region of the host alumino-silicate layer with the interaction between its dipole moment and the interlayer cation or with the hydrogen bond to the host layer. This water molecule can be replaced with organic compounds such as alcohol.

Transition metal dichalcogenides form another sorption type compounds. The intercalated organic molecules or metals transfer partially their electrons to the host layer (1,2). Extensive studies are made on preparations of intercalation compounds and on their physico-chemical properties using transition metal dichalcogenides as host layer materials (9). These investigations are limited to those of VB metal-chalcogen systems which are electrically metallic. Organic intercalations easily occur only on this group. Graphite also forms charge transfer type sorption compounds. It works both as an electron donor and as an acceptor forming charge transfer complexes with metals and with halogens (60,61).



Table 9. Classification of intercalation compounds

Type of compound	Bonding character between host and guest	Examples
Sorption	Molecular interaction <div> <div> Ion-dipole interaction Hydrogen bond </div> <div> Charge transfer interaction </div> </div>	<div> Water and alcohols in clay minerals Water in <math>A^+(H_2O)MX_2^-</math> Water in <math>A^+(H_2O)MoO_3^-</math> Water in hydrotalcite-like compounds </div> <div> <math>MX_2 \leftarrow</math> organic compounds <math>FeOCl \leftarrow</math> organic compounds <math>MPS_3 \leftarrow</math> organic compounds Graphite <math>\rightarrow</math> halogen, acid, and halide Graphite <math>\leftarrow</math> metal(alkali and alkaline earth) </div>
Ion-exchange <div> Cation Anion </div>	Coulomb force	<div> <math>A^+</math> in <math>A^+(H_2O)MX_2^-</math> <math>A^+</math> in <math>A^+(H_2O)MoO_3^-</math> Exchangeable cation in clay minerals </div> <div> Exchangeable anion in hydrotalcite-like compounds </div>
Graft	<div> Covalent bond Ionic bond </div>	<div> Ethylene oxide in <math>Zr(HPO_4)_2</math> Alcohols in <math>FeOCl</math> </div>

Consequently, many studies have been reported on the formations and physico-chemical properties of the charge transfer type sorption compounds using the metallic layer compounds as host materials. However organic intercalations have not yet been studied on semiconductive materials. A question is whether semiconductive layer compounds intercalate organic molecules forming charge transfer type intercalation compounds or not? One of the present results described in Chapter 3 clearly solved this problem.  $\text{FeOCl}$  intercalates some kinds of organic compounds in spite of its semiconductive property.

Interlayer cations are exchangeable in some kinds of clay minerals (3,4). These are substituted even with organic cations forming ION-EXCHANGED intercalation compounds. Host layers have negative charges because of the partial substitution of octahedral aluminum with magnesium. The interlayer cations are bonded to the host aluminosilicate layer with Coulomb force to keep the balance of total charge. Some of charge transfer type complexes also belong to this criteria when the degrees of charge transfer are large. Graphite is almost completely ionized when it intercalates alkali metals as donors (62,63). Recently cathodic reduction was applied to intercalate some kinds of cations into transition metal dichalcogenides and  $\text{MoO}_3$  (64,65). The reduced host layers intercalated mainly alkali and alkaline earth ions

with some amounts of water molecules. The produced situation  $A^+(H_2O)MX_2^-$  is almost the same as that of clay minerals. The interlayer cations in these complexes are exchangeable.

Summarizing all data for ion-exchanged intercalation compounds already reported, the formations of this type of intercalation compounds required that host layers and guest materials respectively have negative and positive charges. As for the ion-exchanged intercalation compounds, arise interesting problems whether the materials with negative charge enter into the interlayer region of the host layer having positive charge, and whether they are exchangeable or not. The present author finds another new type intercalation to clear this question.

Hydrotalcite-like compound  $Mg_6Al_2(OH)_{16}CO_3 \cdot nH_2O$  has anions in its interlayer region. Its carbonate is exchangeable with chloride, perchlorate, and sulfate with each acid treatment. The exchanged anions are easily replaced with carbonate. These anions are bonded to the host brucite-like octahedral layers mainly with electrostatic interaction to keep the total charge balance in the crystals. The ratio of divalent to trivalent cations in the host layer varies in the range of 2/1 - 5/1 changing the remained positive charge in the host layer. When more than one kinds of interlayer anions exist, they tend to segregate in different interlayer regions. These exchangeable anions are in the interlayer region with

some amounts of water. The water molecules are bonded to OH of the host layer with hydrogen bond and with the interaction between their dipole moments and interlayer anions. They are easily released from the interlayer region by heating. Thus this compound belongs to the anion-exchange type as well as to the sorption type.

Both type of sorption and ion-exchange release their intercalated substances without destructions of the host materials. In GRAFT TYPE complexes, intercalated materials react with the host layer and a part of the host layer is substituted with radicals formed from the intercalates. The produced complex has a structure derived from the original host material. The intercalated materials are firmly fixed to the host layer. They are not taken out without a destruction of the host. In the reaction product of  $\text{Zr}(\text{HPO}_4)_2$  with ethylene oxide,  $\text{CH}_2\text{CH}_2\text{OH}$  radicals substitute  $\text{H}^+$  in the interlayer surface of zirconium phosphate. They are linked to the oxygens in the host layer with covalent bond (19). The present study shows that methanol and ethylene glycol respectively replace chloride ions of  $\text{FeOCl}$  with monovalent  $\text{CH}_3\text{O}^-$  and divalent  $\text{C}_2\text{H}_4\text{O}_2^{2-}$ . These alkoxides are bonded to the host inorganic layer forming an ionic bond between the iron and the oxygen of alkoxide. In the viewpoint of the bonding characters between host layers and organic intercalates, the absorbed species are grafted more ionically in  $\text{FeOOR}$  than

in zirconium phosphate.

Present study showed that charge transfer interaction is the most important in  $\text{FeOCl}(\text{organic compound})_{1/n}$ . The drastic change of electrical conductivity with intercalations is characteristic of charge transfer type (66,67). The intercalations of pyridine derivatives into FeOCl much reduced electrical resistivities in the direction along the host layer. Graphite intercalates alkali metals as electron donors and halogens as acceptors (60,61). These intercalations improve electrical conduction in graphite layers. Ubbelohde explained the change of electrical properties due to an excess amount of electron transferred from the guest materials. This model is also applied to explain the properties of the intercalation compounds of transition metal dichalcogenides (9-14).

Charge transfer model in  $\text{FeOCl}(\text{organic compound})_{1/n}$  is also supported by the appearances of ESR signal and charge transfer band observed in ultraviolet spectrum. Correlation found in Table 2 between the properties of complexes and the basicities of intercalated bases also suggests that electrons transfer from the organic intercalates to FeOCl layer through the overlap of lone pair electron orbital and the interlayer surface of FeOCl layer. Bray and Sauer (41) found a similar correlation indicated in Fig. 37 between superconducting transition temperatures  $T_c$  of organic intercalated  $\text{TaS}_2$  and

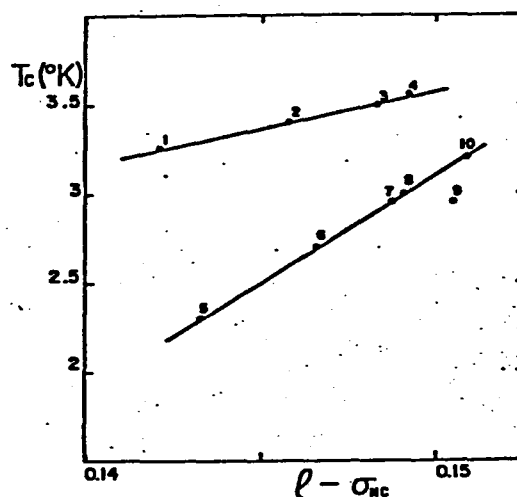


Fig. 37. Relation between the superconducting transition temperature ( $T_c$ ) and  $\rho - \sigma_{NC}$  in intercalation compounds  $TaS_2$ -pyridine derivatives (41).

1. 2-amino, 2. 4-amino, 3. 2,6-diamino,  
 4. none, 5. 4-dimethyl amino,  
 6. 4-methyl, 7. 2-methyl, 8. 2-ethyl,  
 9. 3-methyl, 10. 3-ethyl.

The compounds fall into two groupings having different numbers ( $n$ ) of intercalated molecules per  $TaS_2$  unit; the values of  $n$  are  $1/2$  (top line), and  $1/3$  (bottom line).

$l - \sigma_{NC}$  where  $l$  and  $\sigma_{NC}$  are respectively electron densities of lone pair electron on nitrogen atom and of  $\sigma$ -bond between nitrogen and carbon. The observed good linearity between these two parameters was assumed to suggest that electrons transfer from organic molecules to  $TaS_2$  layer through the overlap of the lone pair orbital of nitrogen and the sulfur atoms on the  $TaS_2$  surface.

The intercalation compounds are divided mainly into three groups as mentioned before. Unfortunately, since the previous works have been done on the limited research field, no systematic studies have been examined yet to understand what kinds of host materials form any kinds of intercalation compounds, what kinds of factor play important roles to make the intercalation compounds.

The present author has summarized his present experimental results on charge transfer type  $FeOCl(\text{organic compound})_{1/n}$ , ion-exchanged type  $Mg_6Al_2(OH)_{16} \cdot nH_2O$ , and grafted type  $FeOOR$  in order to find typical factor in preparation of each kind of intercalation compound in comparison with those on clay-organics.

There are some reports on the reactivity of clay minerals. The formations of sorption type clay-organics are seriously affected by the kinds of interlayer cations (69). Natural vermiculite containing  $Mg^{2+}$  as its interlayer cation does not react with organic compound. When the  $Mg^{2+}$  is exchanged

134

with  $\text{Na}^+$ , organic molecules are easily absorbed in the expanded interlayer region. Organic reactivity of clay minerals is also affected by stacking faults of silicate layers and by defects in tetrahedral or octahedral sites. One of the points is whether the origin of negative charge in the aluminosilicate layer is in octahedral or in the tetrahedral layer (70). Table 10 shows the results on reactivity of benzene with clay minerals containing  $\text{Cu}^{2+}$ . Benzene complex is obtained when the origin of the defect is in octahedral layer but not when in tetrahedral one.

Guest organic molecules are required to be polar in order to be intercalated in clay minerals. Table 11 shows the change of interlayer distance in montmorillonite with absorption of organic monomers. Blumstein estimated that acrylonitrile, methyl methacrylate, and vinyl acetate formed three, two, and two layers of these monomers (71). The results in this table suggest that monomers of large dipole moments are more absorbed than those of smaller ones.

The expansion of interlayer distance was important in absorption of alcohols of long alkyl chain into montmorillonite (72).  $\text{CH}_3\text{CH}_2\text{OH}$  was absorbed in advance to expand the interlayer distance to some extent and then it was substituted with longer alcohols  $\text{CH}_3(\text{CH}_2)_n\text{OH}$  ( $n \geq 2$ ).

Basicity of intercalate is very important for preparation and properties of charge transfer type intercalation compounds.



Table 10. Intercalation of benzene into clay minerals  
containing  $\text{Cu}^{2+}$  as their exchangeable cations (70).

Clay	Locality	Origin of negative charge <sup>a</sup> .	Intercalation <sup>b</sup> .
montmorillonite	Wyoming	octa.	+
montmorillonite	Arizona	octa.	+
hectorite	California	octa.	+
nontronite	Washington	tetra.	-
saponite	Scotland	tetra.	-
vermiculite	Montana	tetra.	-

a. octa : octahedral layer, tetra : tetrahedral layer

b. + and - stand for respectively the cases when benzene  
molecules are intercalated into clay or not.

Table 11. Absorption of monomers into montmorillonite (71).

Monomer	d (Å)	molecular thickness (Å)	number of intercalated layers	dipole moment (debye)
Acrylonitrile	8.7	2.8	3	3.88
Methyl metacrylate	7.6	3.8	2	1.7
Vinyl acetate	7.6	3.8	2	1.7
Stylene	0	3.5	0	0.37

It is qualitatively related to the ionization potential of the base. When an organic compound does not have a large basicity enough to donate electrons to the host layer compound, it is not intercalated as shown in Table 1. Molecular size is another factor. Too big molecules are not intercalated into FeOCl.

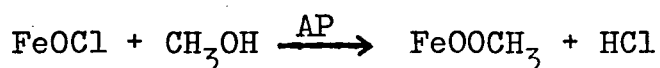
Pyridine is absorbed into TiOCl, VOCl, and FeOCl but not to CrOCl and InOCl. Ti, V, Fe in these compounds are trivalent. Oxides of these metals such as magnetite often show mixed valencies of divalent and trivalent (68). Thus these ions have possibilities to be in mixed valency states of lower valence with normal trivalent. Such kind of mixed valency state have not been observed on chromium compounds. Stable state of In is only trivalent. Whether the host materials have possibilities to be in mixed valency or not is important to intercalate organic molecules forming charge transfer bond. This can be applied to the charge transfer type intercalations in other systems. Valencies can change in metallic transition metal dichalcogenides such as TaS<sub>2</sub> and NbS<sub>2</sub> and layered bronzes such as MoO<sub>3</sub> and V<sub>2</sub>O<sub>5</sub>. All of them easily form charge transfer type intercalation compounds.

The present study shows that the reaction between FeOCl and pyridine is explained by nucleation followed by diffusion. These reaction processes showed two-dimensionality because of the layer structure of host crystal. The interlayer distance

of FeOCl extremely expands when it intercalates organic compounds. Strong elastic deformation of the layers starting at the edge of the crystals exerts a substantial stress on the inner sheet to be ruptured. The deformation is probably an important step in the nucleation. The nucleation process in the temperature below 60 °C follows the first-order rate law as observed in metal hydroxide intercalation into TaS<sub>2</sub> (27). In a higher temperature region than 70 °C, it follows the Avrami's equation of two-dimensional case. This means that the nucleation occurred very quickly at the two-dimensional phase boundary. Similar results were obtained on intercalation of ND<sub>3</sub> into TaS<sub>2</sub> at 25 °C by Riekel and Schüllhorn (30). Activation energy in the nucleation process is partly used to open the interlayer distance of the host layers. The observed values in the present study (~10kcal/mol) are comparable with the interlayer bonding energy in graphite (73). The intercalated materials diffuse into inner region of host crystal to complete the reaction when enough amount of nucleus is formed. The importance of diffusion processes have already been recognized by other researches, but it has not yet been expressed using equations. Jander's equation (74) is modified to two-dimensional case and is applied to the results in the present study. The two-dimensional diffusion explains well the results when the degree of the reaction is between 0.4 and 0.8. Absorbed pyridine molecules diffuse

into the inner region breaking the bond formed in the nucleation process. Activation energies in the diffusion process are evaluated to be reasonable to the bonding energy associated with charge transfer interaction. The observed activation energies of diffusion processes are  $\sim 15 \text{ kcal/mol}$ .

Methanol  $\text{CH}_3\text{OH}$  and ethylene glycol  $\text{H}_2(\text{O}_2\text{C}_2\text{H}_4)$  are grafted to  $\text{FeOCl}$  layer using the intercalation compound  $\text{FeOCl}(\text{AP})_{1/4}$  in the present study. The structural similarity between  $\text{FeOCl}$  and  $\gamma\text{-FeOOH}$  suggests a possibility of chloride substitution with alkoxide ion which is homologous to  $\text{OH}^-$  ion. Hagenmüller et al. reported the formation of  $\text{FeONH}_2$  by the reaction between  $\text{FeOCl}$  and ammonium (34). This reaction suggests a reactivity of chloride ion in  $\text{FeOCl}$ . However methanol and ethylene glycol molecules are not directly absorbed into the interlayer gap of  $\text{FeOCl}$ . The 4-aminopyridine intercalation expands the interlayer distance of  $\text{FeOCl}$  in advance. The expansion of the host interlayer distance makes it possible for alcohol molecules to be absorbed into  $\text{FeOCl}$ , and then the chloride ions on the interlayer surface are substituted with intercalated  $\text{CH}_3\text{O}^-$  or  $(\text{C}_2\text{H}_4\text{O}_2)^{-1/2}$ . This reaction can be written as follows;



and it reminds us Friedel-Craft's reaction in which organic compounds are grafted to benzene ring under the presence of small amount of  $\text{AlCl}_3$ .



The present reaction is an application of organic reaction into inorganic compounds.

The studies on intercalation have been limited to those using the host compounds having fixed composition and properties. The before mentioned cathodic reduction applied to  $\text{MX}_2$  and  $\text{MoO}_3$  is a technique to control the property of host layer. Present study proposed that substitution of cations in the host lattice is another method to modify the host property.  $\text{Mg}(\text{OH})_2$  can not intercalate anything, but a partial substitution of its  $\text{Mg}^{2+}$  with  $\text{Al}^{3+}$  leads to the intercalations of anions and water molecules. The amount and the kind of interlayer anions change with the quantity of charges in the host layer. Negatively charged host layer will be produced by using the opposite way of this case. These ion substitutions were sometimes applied to control properties of oxides, but they have not yet been done on hydroxides. The present study also shows that interlayer anions in hydrotalcite are exchangeable with some kinds of inorganic anions and that the amount of interlayer water easily changes with temperature and humidity.

The following points are important in preparation of intercalation compounds summarizing the present study.

- (1) It is required to expand the interlayer distance in advance in order to make intercalation easy. In intercalation of large molecules, it is useful to substitute a previously intercalated material having a small size.
- (2) Strong basicity of donor is required to obtain a charge transfer type intercalation compound. In order to accept transferred electrons from intercalated donors, host materials are required to have possibilities in mixed valency of the original and the lower valencies.
- (3) A presence of compound isostructural with the product (e.g. the relation between  $\gamma$ -FeOOH and FeOOR) is one of the guides to judge whether a graft type complex is obtained or not.
- (4) Formation of remaining charge in host layer is useful to obtain ion-exchange type compounds. Two techniques are introduced in the present study. One is the substitution of cation in the host layer with another cations having different valency from the former. The other is a partial reduction or an oxidation of host layer. These processes produce positive or negative charges in host layers. Anions or cations are respectively intercalated into the interlayer region to keep the total charge balance.

## ACKNOWLEDGMENTS

This work has been carried out at the Institute of Scientific and Industrial Research, Osaka University and in Material Research Laboratory of the Pennsylvania State University from April 1974 to March 1979.

I wish to express my sincere appreciation and gratitude to Professor M. Koizumi of Osaka University for his help and advice during the course of this investigation.

I am also indebted to Professor F. Kanamaru of Okayama University, Dr. M. Shimada of Osaka University and Professor G. W. Brindley of the Pennsylvania State University for many useful suggestions and comments.

I also thank all those who helped and encouraged me throughout this work.



## REFERENCES

- 1) Hannay, N.B., "Treatise on Solid State Chemistry", vol.3, Plenum Press (1973).
- 2) Huggins, R.A., "Annual Review of Materials Science", vol.3, pp.147, Annual Reviews Inc.(1973).
- 3) Grim, R.E., "Clay Mineralogy", 2nd ed., MacGraw Hill (1968).
- 4) van Olphen, H., "Clay Colloid Chemistry", 2nd ed., John Wiley & Sons (1977).
- 5) Mandelcorn, L., "Non-Stoichiometric Compounds", Chap.6, Academic Press (1964).
- 6) Farmer, V.C., Clay Minerals, 7, 373 (1968).
- 7) Deuel, H., Kolloid Z., 124, 164 (1951).
- 8) Lentz, C.W., Inorg. Chem., 3, 574 (1964).
- 9) Gamble, F.R., Osieki, J.H., and DiSalvo, F.J., J. Chem. Phys., 55, 3525 (1971).
- 10) Gamble, F.R., Osieki, J.H., Cais, M., Pisharody, R., DiSalvo, F.J., and Geballe, T.H., Science, 174, 493 (1971).
- 11) Toffield, B.C., and Wright, C.J., Solid State Commun., 22, 715 (1977).
- 12) Thompson, A.H., Gamble, F.R., and Koehler Jr., R.F., Phys. Rev.B, 5, 2811 (1972).
- 13) Ehrenfreund, E., Gossard, A.C., and Gamble, F.R., Phys. Rev. B, 5, 1708 (1972).
- 14) Bach, B., and Thomas, J.M., Chem. Commun., 1972, 301.
- 15) Wilson, J.A., and Yoffe, A.D., Advan. Phys., 18, 193 (1969).
- 16) Acrivos, J.V., and Salem, J.R., Phil. Mag., 30, 603 (1974).
- 17) Mulliken, R.S., J. Am. Chem. Soc., 74, 811 (1952).
- 18) Acrivos, J.V., Liang, W.Y., Wilson, J.A., and Yoffe, A.D., J. Phys., C4, 618 (1971).

- 19) Yamanaka, S., Inorg. Chem., 15, 2811 (1976).
- 20) Taylor, H.F.W., Mineral. Mag., 39, 377 (1973).
- 21) Allmann, R., Chimia, 24, 99 (1970).
- 22) Allmann, R., Acta Cryst., B24, 972 (1968).
- 23) Gastuche, M.C., Brown, G., and Mortland, M.M., Clay Minerals, 7, 177 (1967).
- 24) Brown, G., and Gastuche, M.C., Clay Minerals, 7, 193 (1967).
- 25) Miyata, S., Clays Clay Min., 23, 369 (1975).
- 26) Miyata, S., and Okada, A., Clays Clay Min., 25, 14 (1977).
- 27) Subba Rao, G.V., and Shafer, H.W., J. Phys. Chem., 79, 557 (1975).
- 28) Acrivos, J.V., Delios, C., Topsøe, N.Y., and Salem, J.R., J. Phys. Chem., 79, 3003 (1975).
- 29) Hancock, J.D., and Sharp, J.H., J. Am. Ceram. Soc., 55, 74 (1972).
- 30) Riekel, C., and Schüllhorn, R., Mat. Res. Bull., 11, 369 (1976).
- 31) Walker, G.F., Nature, 177, 239 (1956).
- 32) Reid, C., and Mulliken, R.S., J. Am. Chem. Soc., 76, 3869 (1954).
- 33) Lind, M.D., Acta Cryst., B26, 1058 (1970).
- 34) Hagenmüller, P., Portier, J., Barbe, B., and Bouclier, P., Z. Anorg. Allg. Chem., 355, 209 (1967).
- 35) Kanamaru, F., Shimada, M., Koizumi, M., Takano, M., and Takada, T., J. Solid State Chem., 7, 1 (1973).
- 36) Kanamaru, F., Yamanaka, S., Koizumi, M., and Nagai, S., Chemistry Letters, 1974, 373 (1974).
- 37) Schäfer, H., Wartenpfehl, F., and Weise, E., Z. Anorg. Allg. Chem., 295, 268 (1958).

- 38) Ehrlich, P., and Seifert, H.J., Z. Anorg. Allg. Chem., 301, 282 (1959).
- 39) Schäfer, H., and Wartenpfuhl, F., Z. Anorg. Allg. Chem., 308, 282 (1961).
- 40) Forsberg, H.E., Acta Chem. Scad., 10, 1287 (1956).
- 41) Bray, P.J., and Sauer, E.G., Solid State Commun., 11, 1239 (1972).
- 42) Stephensen, H.P., J. Chem. Phys., 22, 1077 (1954).
- 43) ed. Kotake, M., "Constants of Organic Compounds", Asakura Publishing Co., pp. 597 (1963).
- 44) Bijl, D., Kainer, H., and Rose-Innes, A.C., J. Chem. Phys., 30, 765 (1959).
- 45) Matsunaga, Y., and McDowell, C.A., Nature, 185, 916 (1960).
- 46) Feher, G., and Kip, A.F., Phys. Rev., 98, 337 (1955).
- 47) Sutton, D., "Electronic Spectra of Transition Metal Complexes", Chap. 1, McGraw-Hill Publishing (1968).
- 48) Lang, R.P., J. Am. Chem. Soc., 8, 1185 (1962).
- 49) Chaudhuri, J.N., and Basu, S., Trans. Faraday Soc., 55, 898 (1959).
- 50) Fuls, P.F., Rodrique, L., and Fripiat, J.J., Clays Clay Minerals, 18, 53 (1970).
- 51) Falk, M., and Whalley, E., J. Chem. Phys., 34, 1554 (1961).
- 52) Miyake, A., Bull. Chem. Soc. Japan, 32, 1381 (1959).
- 53) Guertin, D.L., Stephen, E.W., Bauer, W.H., and Goldenson, J., J. Phys. Chem., 60, 1018 (1956).
- 54) Hund, F., Naturwissenschaften, 46, 320 (1959).

- 55) Kanbayashi, U., and Nukada, K., Nippon Kagaku Zasshi, 84, 297 (1963).
- 56) Sawodny, W., Niedenzu, K., and Dawson, J.W., Spectrochim. Acta, 23A, 799 (1967).
- 57) Bish, D.L., Colloque sur la Minéralogie, Géochimie, et Géologie des Minéraux Nickelifères, Orléans, France, Abstracts, pp.35 (1978).
- 58) Bish, D.L., and Brindley, G.W., Am. Mineral., 62, 458 (1977).
- 59) Taylor, H.F.W., Mineral. Mag., 37, 338 (1969).
- 60) Ubbelohde, A.R., and Lewis, G., "Graphite and its Crystal Compounds", Oxford, Clarendon Press (1960).
- 61) Lieth, R.M.A., "Preparation and Crystal Growth of Materials with Layered Structures", vol.1, Reidel Publishing Co. (1977).
- 62) Campbell, L.E., Montet, G.L., and Perlow, G.L., Phys. Rev., B15, 3318 (1977).
- 63) Carver, G.P., Phys. Rev., B2, 2284 (1970).
- 64) Schüllhorn, R., and Meyer, H., Mat. Res. Bull., 9, 1237 (1974).  
Schüllhorn, R., Sick, E., and Lerf, A., Mat. Res. Bull., 10, 1005 (1975).
- 65) Schüllhorn, R., Kuhlman, R., and Besenhard, T., Mat. Res. Bull., 11, 83 (1976).
- 66) Ubbelohde, A.R., Proc. Roy. Soc., A327, 289 (1972).
- 67) Hermann, A.M., Somoano, R., Hadek, V., and Rembaum, A., Solid State Commun., 13, 1065 (1973).
- 68) Goodenough, J.B., "Magnetism and the Chemical Bond", Krieger (1976).

- 69) Weiss, A., Clays Clay Minerals, 10, 191 (1963).
- 70) Doner, H.E., and Mortland, M.M., Science, 166, 1406 (1969).
- 71) Blumstein, A., J. Polimer Sci., 3, 2653 (1965).
- 72) Brindley, G.W., and Satyabrata Ray, Am. Mineral., 49, 106 (1964).
- 73) Brennan, R.O., J. Chem. Phys., 20, 40 (1952).
- 74) Jander, W., Z. Anorg. Allg. Chem., 163, 1 (1927).

## LIST OF MANUSCRIPTS

- (1) Synthesis and Some Properties of  $\text{FeOOCCH}_3$   
S. Kikkawa, F. Kanamaru, and M. Koizumi  
Inorg. Chem., 15, 2195 (1976).
- (2) Preparation and Properties of  $\text{FeOCl}$ -Pyridine Derivative  
Complexes and Their Reactivities with Methyl Alcohol  
S. Kikkawa, F. Kanamaru, and M. Koizumi  
Proc. Int. Symp. 8th Reactivity of Solids, 725 (1977).
- (3) Formation of Mixed Mg, Al Hydroxides with Interlayer  
Nitrate and Carbonate Ions  
G. W. Brindley and S. Kikkawa  
Thermochimica Acta, 27, 385 (1978).
- (4) Intercalation Compounds  $\text{FeOCl}(\text{Pyridine derivatives})_{1/n}$   
and  $\text{FeOCl}(\text{n-Propylamine})_{1/4}$   
S. Kikkawa, F. Kanamaru, and M. Koizumi  
Bull. Chem. Soc. Japan, in press
- (5) A Crystal-Chemical Study of Mg, Al and Ni, Al  
Hydroxy-Perchlorates and Hydroxy-Carbonates  
G. W. Brindley and S. Kikkawa  
Amer. Mineralogist, under contribution
- (6) Kinetic Study on the System of  $\text{FeOCl}$  and Pyridine  
S. Kikkawa  
J. Solid State Chem., under contribution